UNIVERSITY OF OKLAHOMA

GRADUATE COLLEGE

APPLICATION OF 4D SEISMIC ATTRIBUTES TO MONITOR RESERVOIR FLUID MOVEMENT AND PRODUCTION DISCREPANCIES: MAUI FIELD, TARANAKI BASIN, NEW ZEALAND

A THESIS

SUBMITTED TO THE GRADUATE FACULTY

In partial fulfillment of the requirements for the

Degree of

MASTER OF SCIENCE

By

Evan Jowers

Norman, Oklahoma

2024

APPLICATION OF 4D SEISMIC ATTRIBUTES TO MONITOR RESERVOIR FLUID MOVEMENT AND PRODUCTION DISCREPANCIES: MAUI FIELD, TARANAKI BASIN, NEW ZEALAND

A THESIS APPROVED FOR THE
SCHOOL OF GEOSCIENCES

BY THE COMMITTEE CONSISTING OF

Dr. Heather Bedle, Chair

Dr. Matthew J. Pranter

Dr. Brett M. Carpenter

ACKNOWLEDGEMENTS

First and foremost, I would like to thank my friends and family for supporting and motivating me through my masters studies and the completion of this thesis. Additionally, I would like thank Dr. John Pigott for taking me on as a student at the University of Oklahoma and showing me a new perspective of geology. Dr. Pigott was truly an inspiration and will forever be missed. Furthermore, I would like to show thanks to Dr. Heather Bedle and the AASPI research group for bringing me into the group and exposing me to the world of geophysics.

TABLE OF CONTENTS

LIST OF TABLES

LIST OF FIGURES

ABSTRACT

4D timelapse seismic data is commonly implemented to monitor reservoir evolution associated with fluid changes over time. This research utilizes seismic attributes and machine learning to improve upon traditional 4D seismic workflows to better understand fluid movement in 4D time lapse seismic data within the C Upper Sand reservoir of the Maui Field off the western coast of New Zealand. This technique is unique as it implements attributes calculated on two separate 3D seismic volumes acquired in different years in the attempt to image changes in fluid types associated with concurrent hydrocarbon production. Additionally, a computed difference volume, looking at the variation between these two original seismic volumes, is analyzed with each attribute for further insights.

In particular, instantaneous, spectral, and geometric attributes are utilized to provide a better understanding of reservoir fluid movement in this 4D analysis. Instantaneous attributes, sensitive to frequency and amplitude variations are implemented to track movement of both reservoir gas and water associated with production. Spectral attributes are used to indicate facies heterogeneity throughout the reservoir that may affect fluid flow behavior. Geometric attributes are used to elucidate any previously overlooked reservoir baffles that could prohibit fluid movement through the reservoir as it is produced. Following these attribute calculations, attribute volumes were cross referenced with fluid saturation models and production maps to validate the accuracy of what each attribute is portraying in regards of fluid movement. Additionally, attributes that contribute to the overall understanding of reservoir fluid movement are combined in a principal component analysis (PCA) to accentuate reservoir heterogeneity and changes, spanning from lithologic facies to fluid alterations. After PCA computation, well logs were used to validate the interpretation of geologic reservoir heterogeneity for differential reservoir depletion among

zones, finding that baffles and facies that are prone to diagenetic cementation hinder fluid movement. The research concludes that employing a 4D attribute-based workflow aids in a more thorough comprehension of the geologic control of reservoir fluid movement during production in the Maui C Upper Sand over time.

INTRODUCTION

Monitoring the evolution of oil and gas reservoirs during production is vital for informing ongoing project development decisions for optimal production. This can be achieved through time-lapse 3D seismic surveying (4D seismic), comparing volumes acquired prior to production to repeat monitor surveys acquired years into maturity. After identical processing for consistency, differences in the baseline, monitor, and also the difference volume between the two surveys, aid in depicting fluid changes over time. Compartments, leaky seals, baffles, and water encroachment may become evident as reservoirs deplete in a heterogenous manner. Subtle changes in seismic data signifying complex reservoir fluid migration dynamics can be further enhanced via advanced seismic attributes, particularly those that are sensitive to amplitude and frequency. Though expensive, 4D seismic has proven valuable for engineering economically optimal plans and aiding long-term play management (Waal et al., 2003). While 4D seismic data alone is insightful, the addition of attributes that are sensitive to evolving reservoir fluid properties allows for a more thorough analysis of the data.

Rock physics plays a crucial role in altering seismic responses by elucidating the complex relationship between the physical properties of subsurface rocks and the corresponding seismic waves. Understanding the mechanical and elastic properties of rocks, such as porosity, density, fluid saturation, and mineral composition, enables geophysicists to interpret seismic data more accurately, particularly for the subtle changes that fluid discrepancies create in the seismic signal (King, 2008). As seismic waves travel through different rock layers, variations in these properties cause the waves to interact differently, leading to changes in amplitude, velocity, and frequency. With reservoir depletion, the rock properties, including density and velocities, of the reservoir will change drastically and can be observed through 4D timelapse data. Keeping rock physics in mind, geoscientists can model and analyze how target reservoirs impact seismic responses, aiding in reservoir monitoring and future development plans for bypassed hydrocarbons.

This integration of rock physics with seismic data enhances the precision of geological and reservoir characterizations, helping to facilitate these informed decisions regarding production and infill drilling. While the seismic amplitude volumes may show variations through time as production occurs, these variations are very subtle and can be difficult to interpret regarding insights into reservoir fluid changes **(Figure 1).** With the inclusion of seismic attributes, better imaging of these zones can be made to uncover subtle seismic variations, and thus previously overlooked aspects of the play. These aspects may include water infiltration, depletion, compartmentalization, and altered geophysical responses from the fluid changes over time.

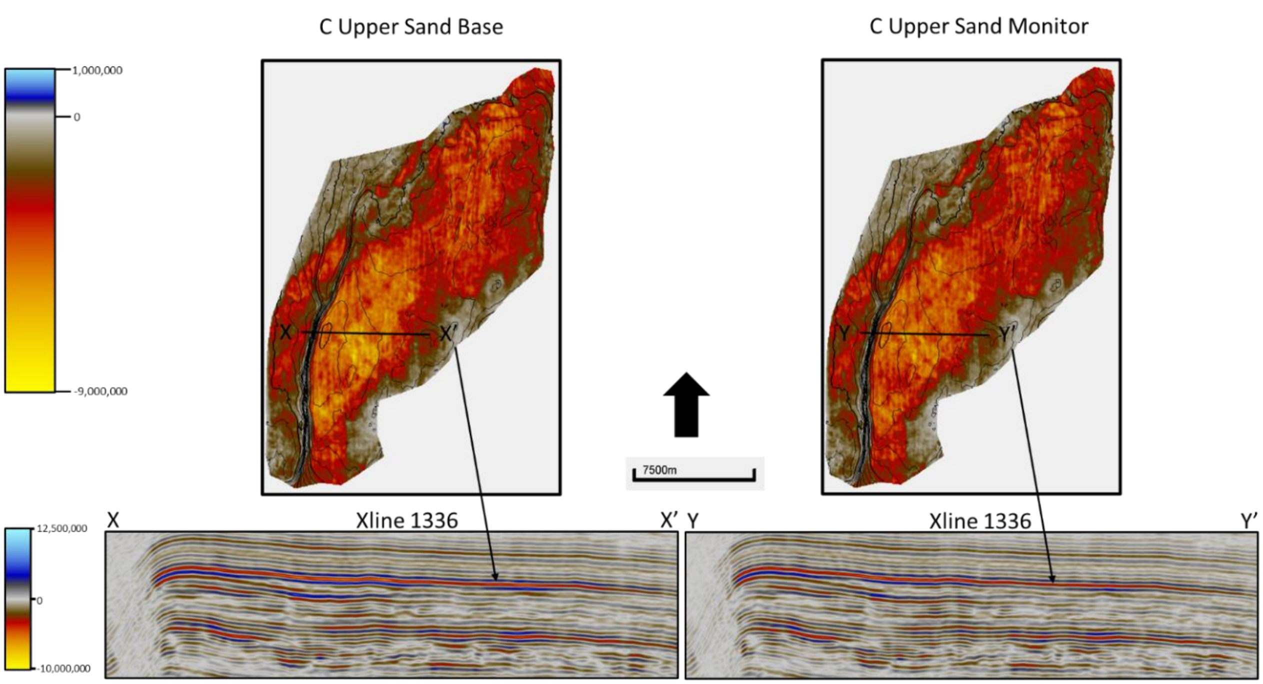

Figure 1. Seismic original amplitude of the base and monitor volumes on the C Upper Sand reservoir. xline views of original amplitude data of the base and monitor volumes are also displayed.

This attribute based 4D analysis was conducted using the 4D Maui seismic dataset acquired in the Maui Field located off the western coast of New Zealand. (**Figure 2)** More specifically, the area of focus herein is an Eocene age marginal marine sand termed the “Maui C Upper Sand.” This sand is recognized as the predominant gas saturated zone in the Maui Field. Produced zones of the Maui C Upper Sand will be searched in all volumes for seismic response variations through time. This study will focus on the Maui-B reservoir zone shown in **Figure 2** as detailed production and fluid saturation data was available in this area. Previous work implementing a few seismic attributes can be observed in work done by Hussein et al. (2021). Hussein’s study primarily homed in on the calculation of instantaneous attributes in relation to 4D data using the self organized maps machine learning algorithm. This research expands that work by including a broader range of seismic attributes than have been used before in fluid analyses that are sensitive to amplitude and frequency variations. After an effective group of attributes is determined, unsupervised machine learning techniques are used to categorize reservoir zones that show differing responses from the base to matched volumes. This technique utilizes instantaneous, spectral, and geometric attributes to highlight relationships between facies discrepancies, fluid changes, and possible reservoir baffles. With the inclusion of production data, clusters produced from machine learning techniques are analyzed to draw geological conclusions to what these attributes are revealing. The objective of this research is to establish an attribute-based 4D seismic analysis workflow utilizing unsupervised machine learning to guide future hydrocarbon development and enhanced insights into previously produced reservoirs. To do this, the previously characterized Maui field/data will be utilized as a baseline to determine effectiveness of the 4D reservoir fluid evolution workflow.

GEOLOGIC SETTING

To enhance the imaging of reservoir heterogeneities affecting non-uniform hydrocarbon production and fluid movement patterns in New Zealand's Taranaki Basin, this research combines 4D seismic attributes with machine learning techniques, focusing on the Maui C Upper Sand. To understand the non-uniform production possibly associated with reservoir heterogeneities, one must first understand the geologic history of the area of interest. This is done by taking previous work characterizing the geologic complexity of the Maui field into consideration to obtain insight of how this reservoir heterogeneity came to be.

Basin Evolution

The Taranaki Basin covers an area of approximately 330,000 square kilometers off the western coast of New Zealand (Coleman et al., 2018). Initial subsidence of the Taranaki Basin commenced with rifting of the southeastern portion of Gondwana during the late Cretaceous. This entailed divergence of the Australian and Pacific plates. With a decrease in rift activity in the early Paleogene, post rift cooling led to further subsidence until the early Eocene. Additionally, sediment loading of early Paleocene aged sediment contributed to gradual subsidence of the basin (Haque et al., 2016). Compressional stress originating from subduction of the Pacific Plate during the late Paleogene created regional anticlinal features and reverse faulting throughout the basin. Following this compressional event, it is thought that the Pacific plate experienced a rollback and retracted against the previous compression direction as subduction ceased (Giba et al., 2010). This rollback subjected the region to extensional stress which then reactivated some preexisting reverse faults into normal faults, as well as creating new ones (Reilly et al., 2015). These faults permeate the Taranaki Basin, creating structural highs and sealing faults that later allowed for the trapping of oil and gas in the Maui Field hydrocarbon province.

Maui Field

This field covers approximately 1,000 square kilometers off the western shore of the northern island of New Zealand. The field is segmented into the Maui A in the northeast, and Maui B to the southwest. These zones are separated by the occurrence of a saddle feature as a result of separate gentle anticlinal features created by compressional and extensional events of the Whitiki

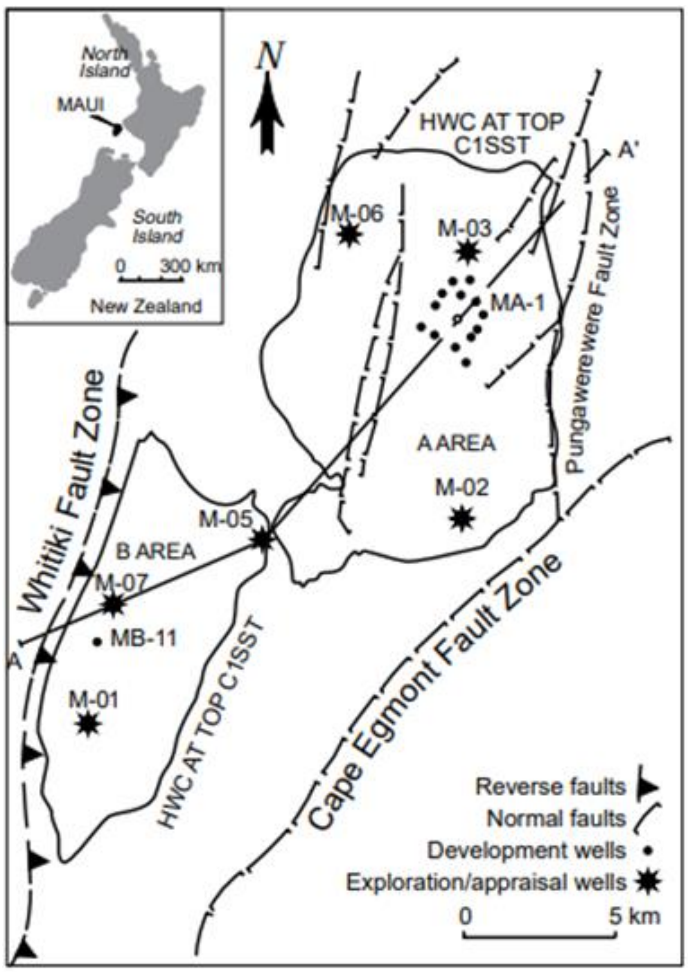

Figure 2. Location map of Maui Field illustrating the Maui C1 sand hydrocarbon accumulation in the Maui A and B segments. Well locations and faults are depicted as well (Modified from Bryant et al., 1995).

and Cape Egmont Fault zones shown in **Figure 2**. Events responsible for this deformation occurred in the late Miocene (Funnell et al., 2004).

The Maui Field hydrocarbon saturated sands reside in the Kapuni Group, which has been categorized as a retro gradational package consisting of shallow marine – coastal plain sediment deposited from the mid Paleocene through the Eocene (Bryant et al., 1995). These hydrocarbon saturated sands are recognized as the C-F Sands. Transgressive and regressive fluctuations in the

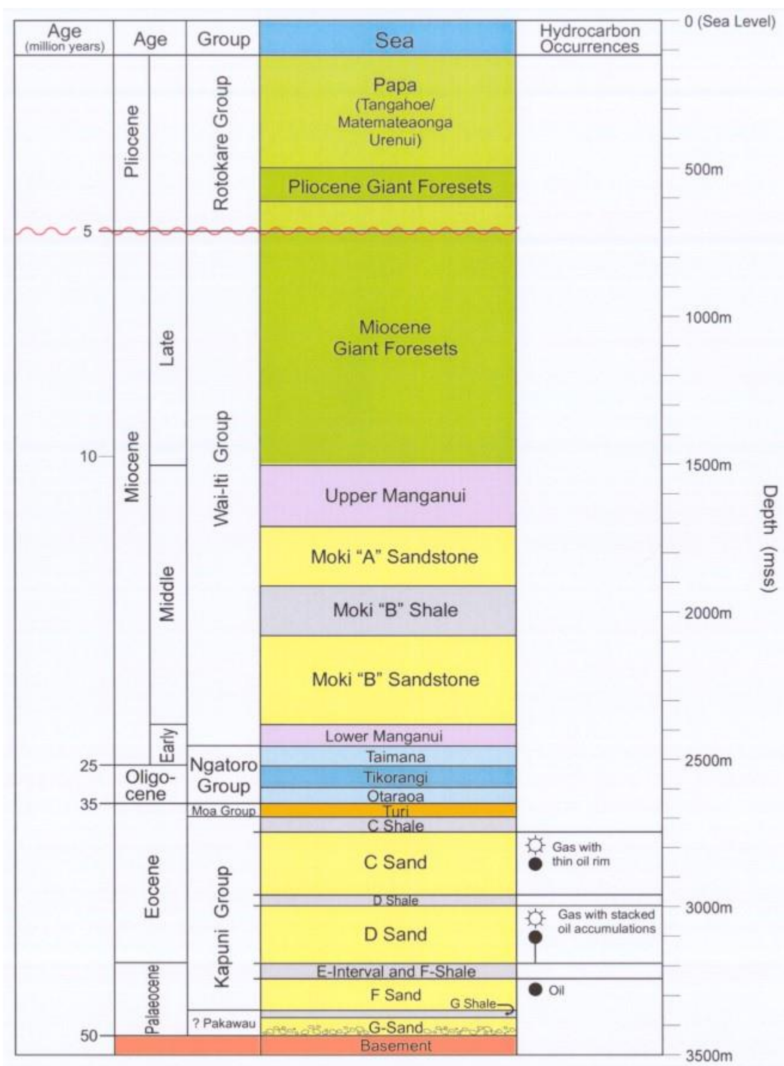

Kapuni Group are responsible for each sand body being encompassed in a shale layer. These

Figure 3. Stratigraphic column within the Maui Field illustrating Maui sand members (From New Zealand Petroleum and Mineral).

shales are the primary sealing mechanisms for the reservoirs. This study focuses on reservoir evolution of the Maui C Sand, as it is the predominant dry gas producer in the field (McBeath, 1977). Deposited in the mid to late Eocene, C Sand reservoirs in the Maui Field are recognized as northeast to southwest trending, laterally continuous marginal marine sands (Pannett et al., 2004). The lower portion of the C Sand was deposited in a coastal plain environment, and the upper portion is controlled by shoreface and tidal channel deposition (Funnell et al., 2004). Bryant et al., (1995) discusses minor calcite cementation of the C Upper Sand originating from the expulsion of pore waters of the overlying C Shale. Although the C Shale is considered to be primarily shale in lithology, there are some calcareous signatures that are thought to be the source of cementation in the C Sand. Both the C and D Shales encompass the C Sand interval that consist of inner shelf shales indicating transgressional events. The D Sand is categorized as being deposited in a fluvial-estuarine setting. Because of this, sand body architecture is much more complex than that of the C and F Sands (Funnell et al., 2004). This complex architecture type subdivides the D Sand reservoir and complicates hydrocarbon production. F Sands consist of simple layered sands of a paralic depositional environment. The D and F Sands have a higher oil saturation than that of the C Sand. However, the D Sand is the field's leading oil producer.

Maui C Sand Petroleum System Elements

Understanding the dynamics of hydrocarbon fluid movement in the Maui Field is crucial for effective optimal reservoir management. Here, we provide an overview into the significance of various geological factors influencing fluid behavior within the reservoir, including the source rock, migration pathways, reservoir characteristics, trap features, and sealing mechanisms. This understanding forms the basis of our investigation into utilizing 4D seismic analysis to monitor fluid movement over time.

Source Rock

Maui Sand hydrocarbons are thought to be sourced from late Cretaceous coals residing in the Rakopi formation. The depositional environment of the area during this time consisted of a swampy environment within the coastal plane. This type three terrestrial source rock is responsible for the abundant gas presence found in the Maui Sand intervals (Killops et al., 1994). Nearby hydrocarbon kitchens that are candidates for gas charging of the Maui C Sands include The Maui, Pihama, and Kahurangi sub basins illustrated in **(Appendix A. Figure 1.)** which provided the correct environment needed for thermal maturity of this source (Funnell et al., 2004). Of these, the Maui and Pihama sub-basins are considered to provide the majority of gas charge to the Maui Sand reservoirs as indicated in **(Appendix A. Figure 2.)**.

Migration Pathway

Migration pathways that charge the Maui C Sand reservoirs are very controversial due to the basin's complex tectonic history. As previously stated, possible kitchens that charged the Maui C Sand reservoirs include the Maui, Pihama, and Kahurangi sub basins. Of these, migration possibilities of the Maui and Pihama sub-basins during the late Miocene are more accepted to do the rather small volumes of predicted expelled gas from the Kahurangi sub-basin **(Appendix A. Figure2.)** (Funnel et al., 2004). In the Maui sub-basin it is thought hydrocarbon migration occurred in relation to multiple displacement events associated with the Cape Egmont Fault Zone. These displacement events lead to the juxtaposition of source and reservoir strata which created the necessary pathway for migration. Migration from the Pihama sub-basin is thought to be driven by smaller fault networks to the norther extent of the Cape Egmont Fault Zone (Funnell et al., 2004). Though primary migration to the Maui A portion of the C Sand interval was dominant, spillover of gas across the anticlinal saddle separating the Maui A from the Maui B did occur (Funnel et al., 2004).

Reservoir

Fluctuations in sea level during the Eocene provided baffle intervals that subdivide the Maui C1 Sand into the Maui C Upper, Middle, and Lower Sands. The Maui C Upper and Lower Sands are considered to be cleaner sands with higher porosity and permeability. These sands are also considered to be Arkosic Arenites originating from first cycle erosional processes of the up-dip potassium feldspar rich Karamea granite shown in **(Appendix A. Figure 3.)** (Bryant et al. 1995). The Maui C Middle Sand is a shalier interval that acts as a baffle separating the C Upper and Lower Sands. The Maui C Middle Sand was deposited during a time of very rapid small-scale sea-level changes giving it its interbedded shale presence (Funnell et al., 2004). The average thickness of the entire Maui C Sand interval is approximately 100 meters.

Trap

As previously stated, the Maui A and B regions of the field are separated by gentle anticlinal features. These features also play a role in the systems as a hydrocarbon trap for both the Maui A and B plays (Funnell et al., 2004). These features were created from compressional stress originating from subduction of the Pacific Plate during the late Paleogene (Reilly et al., 2015). Further aspects of Maui traps include the Pungawerewere normal fault that bounds the Maui A from the east, and the Whitiki reverse fault that bounds the Maui B from the west shown in **Appendix A. Figure 4.** (Holt et al., 1994). These faults juxtapose the C Sands with low permeability shale layers. Faulting plays more of a trapping role in the system in the Maui B area than that of the Maui A area. This is due to the gas to water contact depth that remains constant throughout the field.

Seal

The overlying, low permeability, C Shale provides a stratigraphic seal to the C Upper reservoir in both the Maui A and B region **(Appendix A. Figure 4.)**. Although the C Shale is considered to be primarily shale in lithology, there are some calcareous signatures that are to be noted. Completion reports of exploration wells in the Maui Field term this layer a shale/mudstone (New Zealand Petroleum and Minerals 1998).

Maui Field History

When observing 4D timelapse seismic data, understanding the fields exploration and production history is crucial. Pinpointing times of when seismic surveys were acquired and when production of gas both commenced and concluded plays a monumental role in interpreting reservoir fluid behavior. Without this information, interpretations would be made without validating evidence.

Timeline

Initial exploration of the Taranaki basin began in 1955 with a joint project with Shell, BP, and the native Todd hydrocarbon company. The Kapuni Group was discovered in 1959 with the drilling of exploration wells that proved promising hydrocarbon potential (Abbott, 1990). This same team later discovered the giant Maui Field with the further drilling of exploration wells in 1969 and estimated that 5.3 tcf – 8.4 tcf of gas resided within the Maui Sands. With promising findings, development of the field commenced in 1978 (Abbott, 1990). With successful hydrocarbon production, came the need to acquire seismic data of the region. The first 3D seismic survey was performed in 1991 encompassing the Maui Field. As production commenced in 1993, water breakthrough became more of a problem in producing wells. An attempt to understand this occurrence was made by acquiring a separate 3D volume encompassing the Maui Field in 2002 (Pannett et al., 2004). Recently, ownership of this field was transferred from Shell to OMV New Zealand in 2018. As of 2023, the Ministry of Business, Innovation, and Employment estimated that the field held a remaining accumulation of approximately 4,014 bcf of recoverable gas reserves and approximately 236 mmbbls of recoverable oil reserves. (Ministry of Business, Innovation, and Employment, 2023)

Well History within 4D Timeframe

Wells drilled in the Maui C Upper sand within the base to monitor survey timeframe include vertical wells MB-02, MB-09, and MB-10. Production of wells MB-09 and MB-10 commenced in 1993, and well MB-02 later began production in 1994. Well MB-09 was a good gas producer for 6 years until it was watered out in the year 2000. Well MB-10 produced gas for 8 years until 2002 when it was also watered out. Well MB-02 was a good gas producer for 13 years until 2007 when the well watered out (New Zealand Petroleum and Minerals, 2018). Maui wells are considered to be "watered out" when the production gas water ratio falls below 40%, and they become economically unproductive. With wells MB-09 and MB-10 watering out in a relatively short timeframe, a 3D monitor survey was acquired in 2001 to evaluate reservoir fluid behavior in a 4D seismic analysis (Pannett et al., 2004).

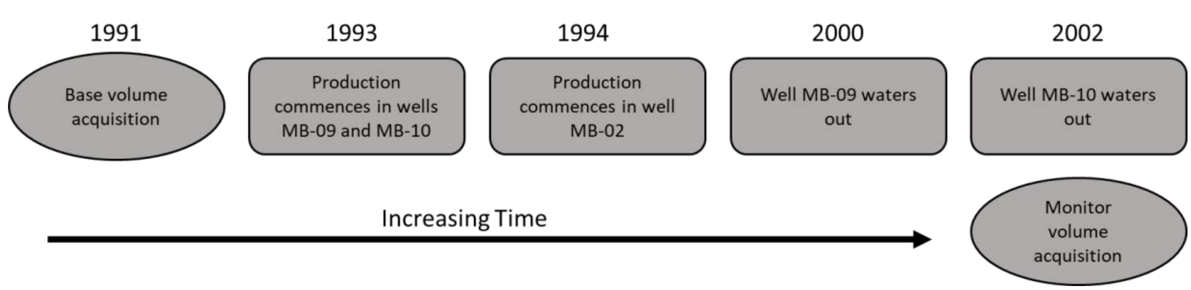

Figure 4. Timeline of seismic acquisition and production milestones within 4D timeframe.

DATA

Seismic

Seismic data provided by New Zealand Petroleum and Minerals consisted of a base (collected in 1991) and monitor (2002) 3D volume. For each attribute included in the 4D analysis a difference volume was calculated. This process consisted of subtracting the monitor attribute volume from the base attribute volume to highlight the variation of each attribute through time. These volumes encompass an area of approximately 700 square kilometers, and completely include the focus area. (Data boundaries shown in **Figure 4**) Processing of the monitor volume, as well as reprocessing of the base volume occurred in 2003 to eliminate any potential seismic signal variations due to processing techniques. These are full stack volumes with a normal SEG polarity, meaning that a decrease in acoustic impedance is represented by a trough in the seismic data. The original record length of these volumes was approximately 5 seconds, but this was cropped to 1,949 - 2,451 milliseconds in the analysis to focus on the specific reservoir. Both volumes are in the minimum phase. These volumes have a sample rate of 2 milliseconds and a bin size of 30x30 meters as noted in **Table 1**.

Polarity	Normal SEG
Phase	Minimum
Bin Size	25x25 m
Sample Interval	2 ms
Time Interval	Cropped to 2,080 – 2,240 ms

Table 1. Table illustrating seismic data parameters.

Wells

Seven vertical exploration well logs within the field were provided by New Zealand Petroleum and Minerals. Provided logs consist of gamma ray, density, neutron, resistivity, and spontaneous potential. Except for well "Maui – 4", all wells intersect the C Upper Sand within the Maui_4D seismic volume boundary. The Maui – 4 well was drilled further south of the seismic boundary and showed poor hydrocarbon recovery potential. These wells are used to examine reservoir

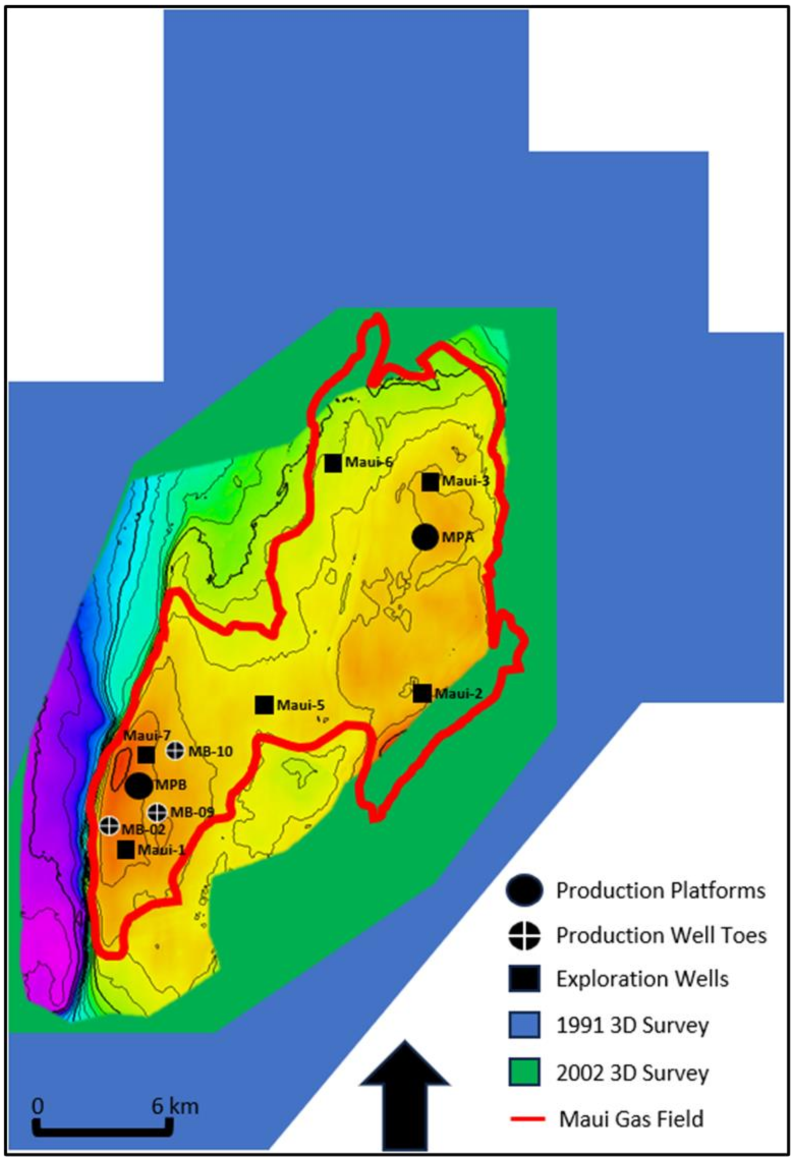

Figure 5. Location map illustrating well locations incorporated in study. Base and monitor survey boundaries, Maui gas field extent, and C Upper Sand depth structure map are illustrated as well (Adapted from Hussein et al., 2021).

thickness, draw lithological confirmations of zones of interest, and examine reservoir petrophysical properties. Along with these exploration wells, three gas producing wells of the C Upper Sand that were drilled within the 4D timeframe are available. These wells are named MB-02, MB-09, and MB-10, and were drilled at the MPB production platform shown in **Figure 5.** These logs were provided by New Zealand Petroleum and Minerals in the form of scanned TIF images. These scanned images were then digitized to be imported into the well log analysis software. Replicted log types of producing wells align with that of the exploration wells. Since these wells share a common production platform and are deviated, well toe locations are represented for depletion analyses purposes.

Production/Fluid Saturation Maps

Maps with information regarding production fluid type were provided by New Zealand Petroleum and Minerals. This timeline of production maps provides data at each year of production between the base (1991) and monitor (2002) surveys. Each well indicates whether it was producing gas in the current year, or if the well had been watered out. These maps provide data points to cross reference when interpreting fluid changes through time in 4D seismic attributes. Production maps were also provided following the 4D timeframe up until 2014. While these maps cannot be directly compared to the 4D seismic volumes, reservoir zones that have proven to be either successful or unsuccessful producers can still be observed, to help validate or invalidate the seismic interpretation. Additionally, reservoir fluid saturation models were also provided. This provides a visual to track the gas water contact for the Maui C reservoir through time. This data is crucial to ensure the interpreted presence of either hydrocarbons or water based off attributes are accurate. Furthermore, water saturation values at 8 wells within the Maui-B reservoir zone during 1993 were provided. Since these gas saturations were obtained before production commenced, these saturation values were linked attribute values at the borehole to add backing evidence as to what fluid type certain attributes are portraying.

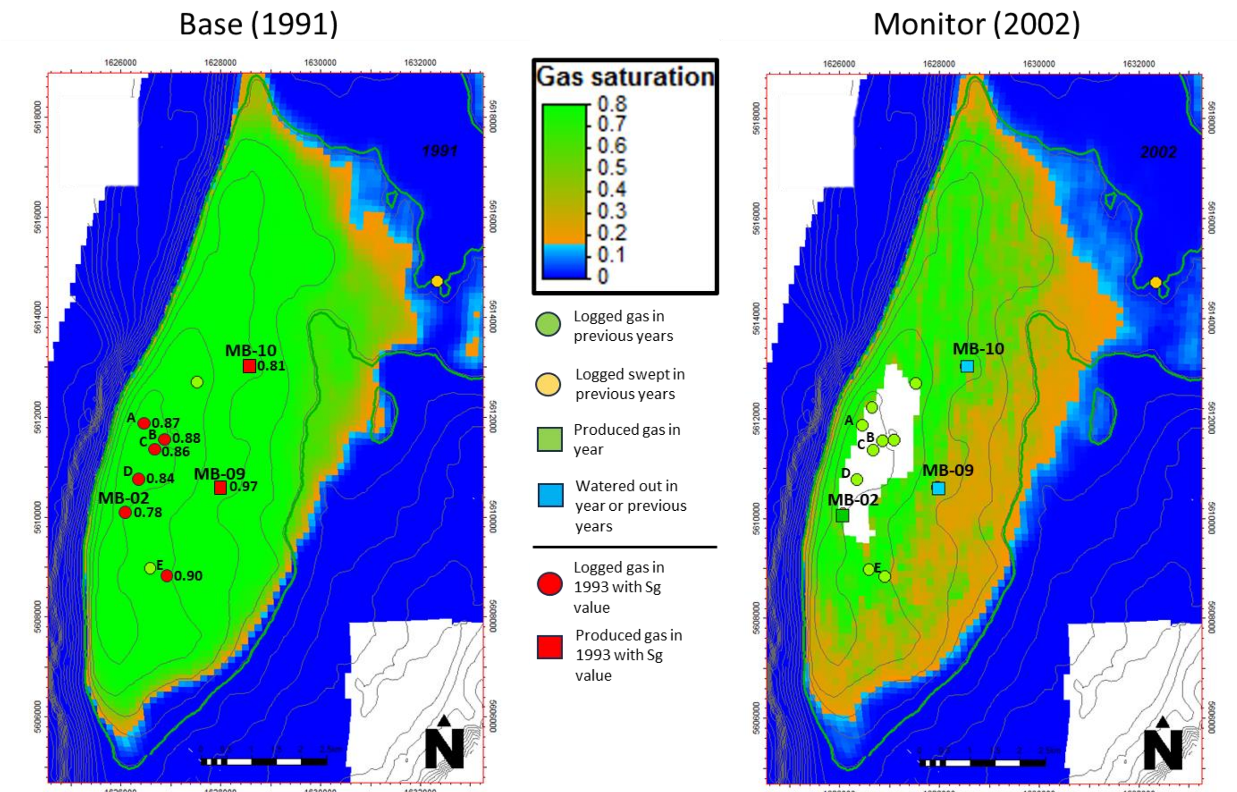

Figure 6. Production/fluid saturation maps of the Maui C Upper Sand. Zones that have a gas water ratio of greater than 40% are illustrated in green. Zones within the 18-40% gas water ratio zone are considered to be swept and are illustrated in orange. All zones below 18% gas water ratio are illustrated in blue (Modified from New Zealand Petroleum and Minerals).

METHODS

To ensure accurate interpretation of reservoir fluid behavior, the following workflow shown in **Figure 7** was performed. This process is subdivided into data preparation/mapping, attribute calculation, hydrocarbon depletion analysis, and machine learning. Every subsection of this workflow shares an equal importance in analyzing reservoir fluid behavior through time.

Workflow:

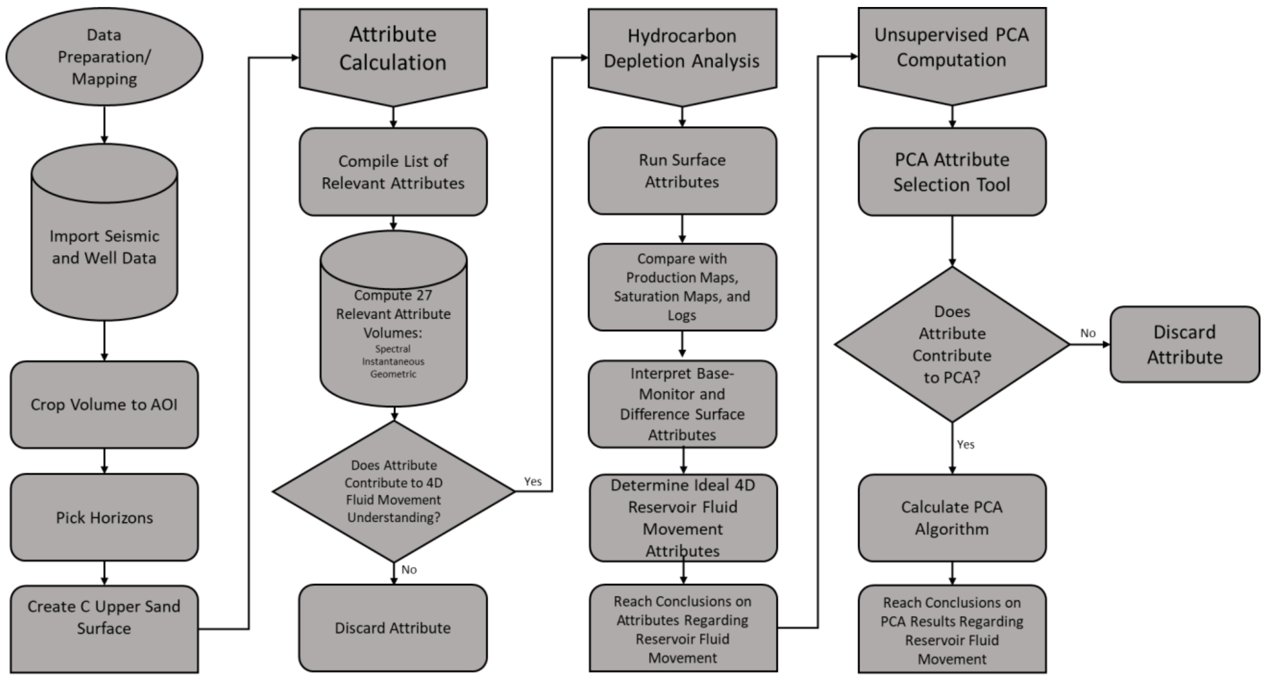

Figure 7. Workflow of 4D fluid movement analyses.

Primary data conditioning was performed in the manner of cropping the seismic volume to the area of interest and immediate neighboring strata. This was done to reduce both attribute and machine learning calculation time of the base, monitor, and difference volumes. A horizon was mapped and used to create a surface for the C Upper Sand interval. Reservoir zones showing varying responses from the base and matched surveys, as well as the difference volume, where then observed and noted. These zones represent the focal point of varying properties when compiling relevant attributes. From here, a list of fluid sensitive attributes is compiled for testing and attributes of the base, monitor, and difference seismic volumes were calculated. Following these calculations, all attribute volumes were examined for fluid movement and geologic significance. This examination was performed by running surface attributes on the C Upper Sand surface. A narrowed list of attributes was chosen and decisions were made to which attributes complement one another to reveal additional insight regarding fluid movement.

Attribute Selection

Attribute	Attribute Description	Study Implication
Sweetness	Calculated by dividing instantaneous amplitude by the square root of the instantaneous frequency	Identifying gas accumulations
Envelope	Displays positive and negative acoustically strong events	Identifying gas accumulations
Relative Acoustic Impedance	Increases low frequencies and decreases high frequencies	Identifying fluid discrepancies
Mean Frequency	Average frequency	Identifying fluid discrepancies/facies identification
Spectral Bandwidth	the frequency distance between the lowest and highest half-magnitude frequency components	Identifying facies discrepancies
Sobel Filter Similarity	Displays laterally homogenous seismic waveforms and amplitudes	Identifying structural reservoir baffles

Table 2. Table showing attribute descriptions and study implications.

Initially 27 attributes were computed as candidates to elucidate fluid movement from the base to monitor surveys, as well as reservoir properties. These attributes consisted of both spectral and instantaneous attributes that are sensitive to alterations in amplitude and frequency. After all attributes were analyzed, the list was narrowed down to 6 attributes that most effectively portrayed and explain fluid movement in the reservoir. These attributes include sweetness, envelope, relative acoustic impedance, mean frequency, spectral bandwidth, and Sobel filter similarity. Descriptions of these attributes and their relevance can be viewed in **Table 2.**

Attribute Implications

Prior to delving into the interpretation of 4D attributes, it is crucial to establish a fundamental comprehension of the calculations underlying each attribute. Furthermore, examining prior research relevant to the study and identifying the specific attributes that effectively conveyed geological information is beneficial. Replicated attributes computed in work done by Chenin, (2020) proved to be successful in identifying gas accumulations in clastic reservoirs. Recognition of successful attributes in analogous studies such as this enhances confidence in interpreting 4D attributes, providing a valuable context for the analysis at hand. Furthermore, water saturation values of provided wells were used to calculate gas saturation by subtracting the water saturation from 1. Gas saturation was then cross plotted with the attribute value at the intersection of the well bore and the C Upper Sand surface. Cross plots of fluid detecting attributes were created to add backing evidence as to what fluids these attributes are portraying.

Sweetness

The sweetness attribute is calculated by dividing instantaneous amplitude by the square-root of instantaneous frequency. This is further explained by dividing the trace envelope by the square root of average frequency (Kosen et al., 2014). This attribute is particularly good at identifying lithology discrepancies and indicating hydrocarbon accumulations. This sweetness equation does just this in providing a high value when high amplitude and low frequency events occur (Radovich et al., 1998). The sweetness attribute value at the intersection of the well bore and the C Upper surface was crossplotted with the gas saturation percentage of the well **(Figure 8.)**. This was process validated the correlation between a high sweetness value and high gas saturation.

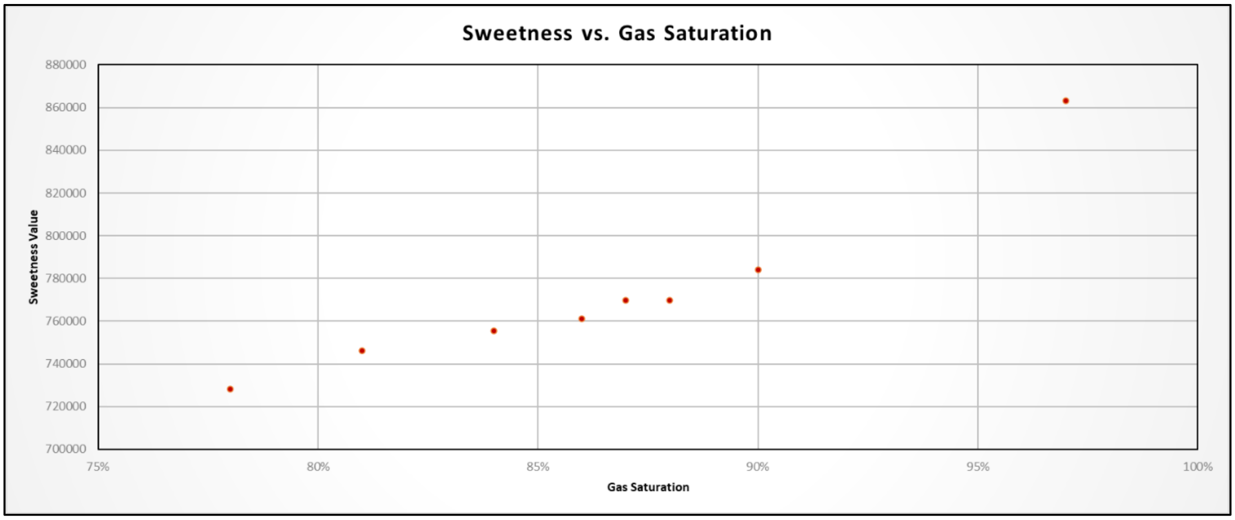

Figure 8. Cross plot illustrating the relationship between gas saturation values and sweetness attribute values at the well bore. Attribute value is shown on the Y-axis and gas saturation percentage is shown on the x-axis.

Envelope

The envelope attribute portrays the wavelet's energy of the signal, which is equivalent to the magnitude of the walvelets reflection coefficient. The attribute displays acoustically bright positive and negative events and can often represent gas presence (Kosen, 2014). In this study, the attribute is used to portray reservoir zones of high gas saturation. The envelope attribute value at the intersection of the well bore and the C Upper surface was crossplotted with the gas saturation percentage of the well **(Figure 9.)**. This was performed to validate the correlation bewtween a high envelope value and high gas saturation.

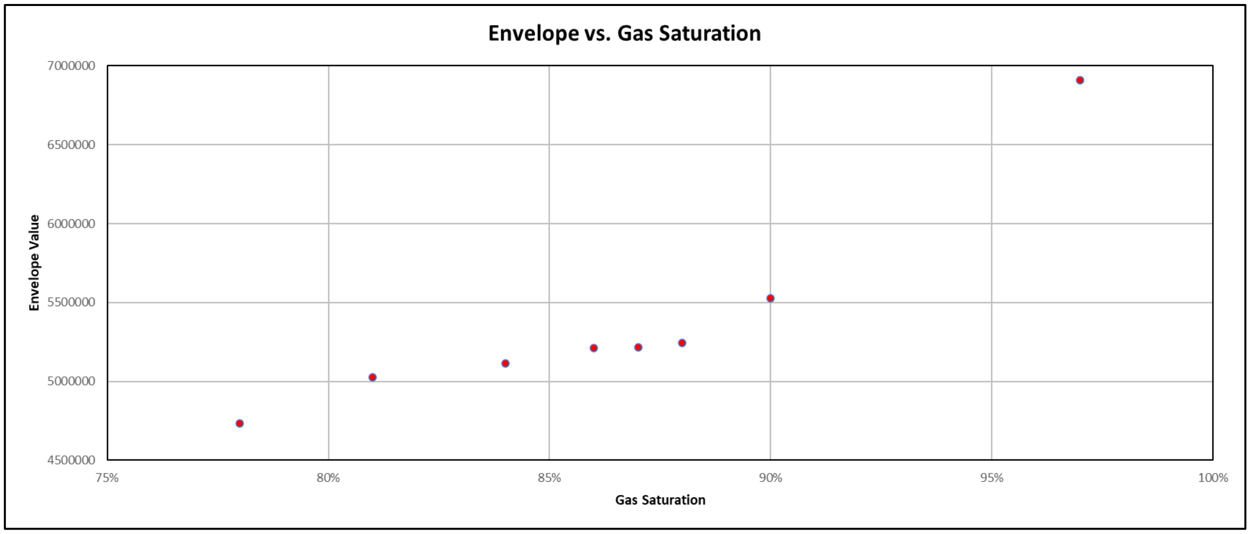

Figure 9. Cross plot illustrating the relationship between gas saturation values and envelope attribute values at the well bore. Attribute value is shown on the Y-axis and gas saturation percentage is shown on the x-axis.

Mean Frequency

The mean frequency attribute is calculated by obtaining the magnitude-weighted average frequency of a wavelet at a certain time (Chopra et al., 2024). Korneev at al. (2004) explains how observing subtle frequency discrepancies can provide insight into reservoir fluid presence and fluid type. By indicating fluid types of differing densities and frequencies, water encrochment associated with production can be better understood.

Relative Acoustic Impedance

The relative acoustic impedance attribute increases extreme low frequencies and increases extreme high frequencies. Simultaneously, the attribute rotates the data by 90 degrees (Chopra et al., 2024). This calculation provides an output that is useful in identying discrepancies in acoustic impedance. Acoustic impedance variations can indicate contacts of differeing fluid types and aid in monitoring depletion and water encroachment associated with production through time. A study conducted by Ashraf et al. (2020) explores the uses of the relative acoustic impedance attribute to delineate gas saturated zones in a similar manner.

Spectral Bandwidth

A paper written by Chopra et al. (2024) defines the spectral bandwidth attribute as "the frequency distance between the lowest and highest half-magnitude frequency components", and also explains that the attribute is particulary good at facies identification. Since this attribute is not particulary good at subsurface fluid identification, spectral bandwidth was only calculated on the base volume as the rock itself did not change within the 4D timeframe.

Sobel Filter Similarity

The Sobel filter similarity attribute is a geometric attribute that measures similarities throughout a volume by detecting laterally homogenous seismic waveforms and amplitudes (Qi et al., 2017). While the attribute is searching for similarities, it also detects dissimilarities in the absence of similarity. These dissimilarities can indicate subsurface features such as faults and channels (Mirkamali et al., 2016). Since sobel filter similarity is a geometric attribute, the attribute was only calculated on the base volume as these geometries did not change within the 4D timeframe. For this study, this attribute will be used to rule out any possible baffles that could hinder reservoir fluid movement.

Next, fluid saturation models and production data were incorporated into the study to link attribute findings to ongoing gas production and water sweeping throughout the 4D timeframe. Following this process, hypotheses were drawn based of relevant attribute findings regarding fluid movement in response to ongoing production, as well as reservoir properties that either hinder or improve fluid movement. To obtain a better understanding of these hypotheses, varying unsupervised machine learning principal component analyses were carried out.

Principal Component Analysis

While making observations on single attribute volumes is insightful, observing how these attribute volumes interact with one another in a machine learning algorithm takes the analysis one step further. The unsupervised principal component analysis machine learning algorithm extracts patterns found in the input data volumes and organizes them (Wold et al., 1987). This computation includes 3 principal components in order to display the multidimensional attribute data in a two-dimensional visualization. In this case the end goal is to utilize PCA to elucidate patterns that can be interpreted to better understand the interaction of reservoir rock properties and differential fluid movement within the reservoir over time. This method of performing a PCA with seismic attributes has previously been used to identify free gas (Lubo-Robles et al., 2020). In this study, we adopt a similar approach, utilizing unsupervised PCA to monitor both gas depletion and the subsequent water encroachment in 4D data. By employing PCA in this manner, we uncover nuanced patterns and relationships within the seismic facies, enhancing our understanding of reservoir dynamics.

PCA Attribute Selection

To ensure optimal machine learning outputs, the user must first ensure the input attribute's relevance to the research. This is done by utilizing the PCA attribute selection tool, which determines the overall contribution each attribute is making to the machine learning computation. Several relevant attributes were chosen for this selection tool process with two separate test runs. These separate tests included a small and broader range of attributes to determine the ideal combination for identifying lithologic and fluid patterns in the resultant clusters.

PCA Test 1

Test 1 included the attributes sweetness, envelope, mean frequency, relative acoustic impedance, and spectral bandwidth. Eigenvector bar graphs were then analyzed and the most relevant fluid and facies indicating attributes were determined **(Appendix C. Figure 1.)**. Both the base and monitor sweetness attribute volumes as well as the base spectral bandwidth volume were chosen as inputs for the machine learning computation. Only the base volume was used as an input for the spectral bandwidth attribute volume as it is not a fluid detecting attribute and showed no variations from the base to monitor volume. This first principal component analysis test was termed “PCA 3”, as it included three relevant attribute volumes.

PCA Test 2

Test 2 included the attributes sweetness, mean frequency, relative acoustic impedance, Sobel filter similarity, and spectral bandwidth. The geometric attribute Sobel filter similarity was included in this test in an attempt to identify any possible baffles that could prohibit reservoir gas flow. Eigenvector bar graphs portrayed each attribute to have an impactful presence in the computation **(Appendix C. Figure 2.)**. A broader range of input attributes were incorporated into this test to determine if a more complex computation either improved or hindered the output. Therefore, the base and monitor volumes of all input attributes were selected for this test, excluding spectral bandwidth and Sobel filter similarity, which used only the base volume. This second principal component analysis test was termed “PCA 8”, as it included eight input attribute volumes.

RESULTS

Following attribute calculations of the base, monitor, and difference volumes, results of these volumes were observed, and notes were taken. Analyzing these attributes individually through time is crucial to interpret exactly what the attribute is portraying in regard to reservoir fluid movement and rock properties. Following this attribute analysis, results of the PCA computation were observed as well. Finally, interpretations of the PCA outputs are made to make sense of differential depletion across the Maui-B reservoir zone of the C Upper Sand.

Attribute Analysis

Sweetness

High sweetness values were observed in the same areas in which the gas water ratio was greater than 40% in the provided saturation models (New Zealand Petroleum and Minerals, 2018). The comparison of base to monitor surveys including the sweetness attribute highlighted major depletion of reservoir zones neighboring producing wells (**Figure 10**). The difference volume showed an accumulation of high values around producing well locations. This is interpreted to indicate the area of gas that had been depleted from the reservoir between the 4D seismic timeframe. Furthermore, a linear feature portrayed in the difference volume seems to show a lack of depletion in the northwestern portion of the Maui-B reservoir zone. This is indicated by an abrupt cutoff of high to low sweetness responses.

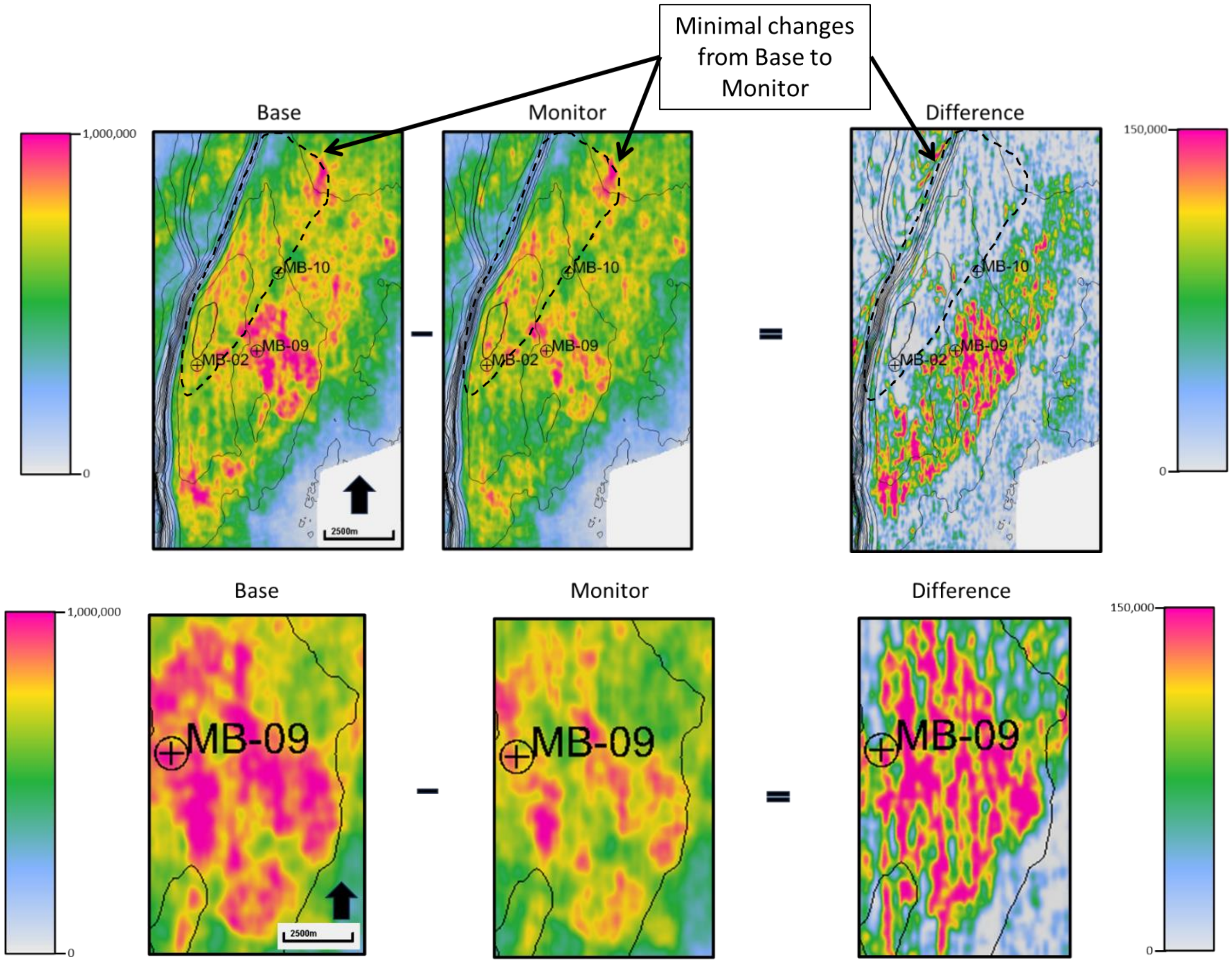

Figure 10. Results of the sweetness attribute along the C Upper Sand surface. Base, monitor, and difference attribute volumes are shown, as well as production wells MB-02, MB-09, and MB-10. Additionally, images zoomed to focus on the production zone of the MB-09 well are provided.

Mean Frequency

The mean frequency attribute seems to capture the sweeping of water throughout the reservoir (**Figure 11**). This is inferred because water has a higher density than gas, so it would be expected that reservoir zones with greater water saturation would produce a higher mean frequency value. Since it is expected for mean frequency values to increase over time due to water encroachment, the difference volume was claculated by subtracting the monitor volume from the base volume.

From the base to monitor surveys it is evident that higher mean frequency values occur in accordance with the gas water saturation percentage decreasing. Frequencies increase up to approximately 10 hz within the 4D timeframe of the C Upper Sand in the Maui B reservoir zone.

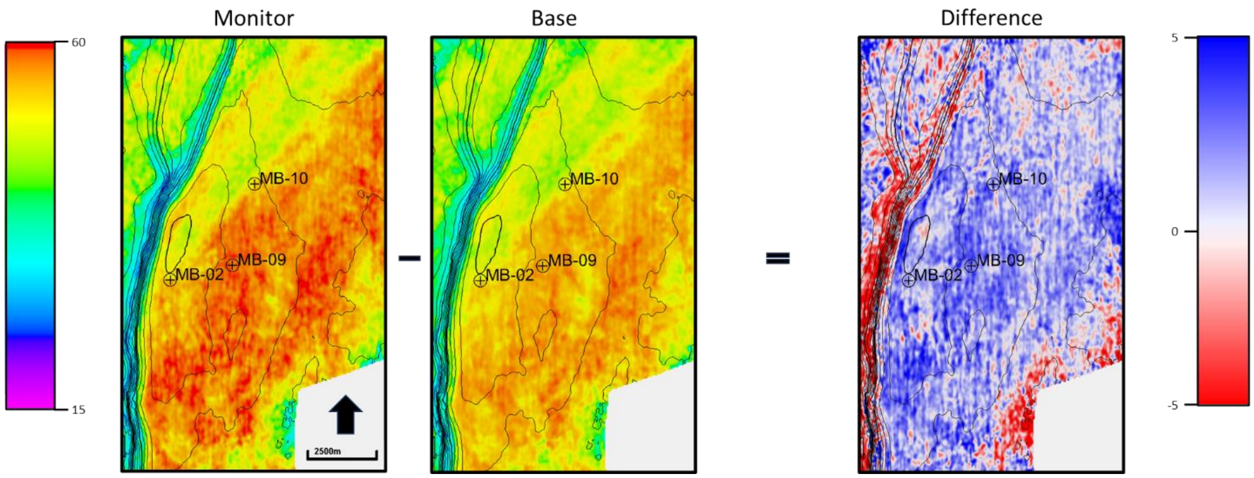

Figure 11. Results of the mean frequency attribute along the C Upper Sand surface. Base, monitor, and difference attribute volumes are shown, as well as production wells MB-02, MB-09, and MB-10.

Envelope

High envelope values are observed in areas that yield a gas water ratio higher than 40% in the provided saturation models. Gas depletion is shown by the comparison of base to monitor volumes incorporating the envelope attribute (**Figure 12**). Depletion seems to occur surrounding producing wells of the reservoir. The difference volume clearly shows high envelope values surrounding producing wells indicating the area of produced gas. A linear feature portrayed in the difference volume seems to show a lack of production in the northwestern portion of the Maui-B reservoir zone. This is indicated by an abrupt cutoff of high to low envelope responses trending northwest. The outputs of this attribute are similar to that of the sweetness attribute.

However, there are some noted discrepancies in interpreted gas saturation areas, such as accumulation densities of high gas saturation reservoir zones. The envelope attribute seems to segment these zones into smaller subsections.

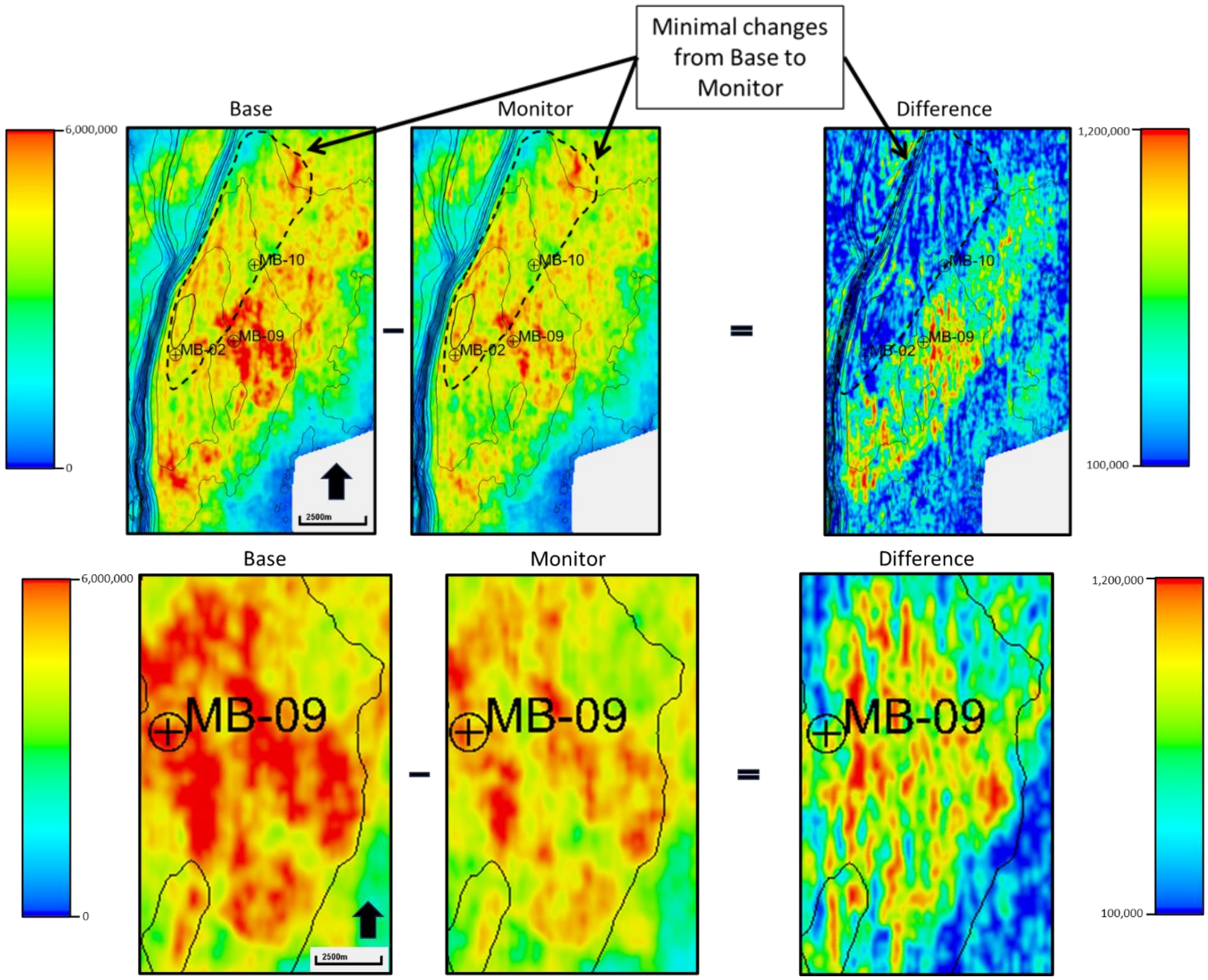

Figure 12. Results of the envelope attribute along the C Upper Sand surface. Base, monitor, and difference attribute volumes are shown, as well as production wells MB-02, MB-09, and MB-10. Additionally, images zoomed to focus on the production zone of the MB-09 well are provided.

Relative Acoustic Impedance

Extreme low relative acoustic impedance values are observed in the base volume surrouding the gas to water contact (**Figure 13**). This in interpreted to indicatate the presence of the gas water ratio being greater than 40% (New Zealand Petroleum and Minerals, 2018). The monitor volume still shows this initial contact, although it is dimmed significanlty with a lesser abundance of extreme low relative acoustic impedence values. Apart from previously mentioned attributes, the monitor volume showed an accumulation of extreme low relative acoustic impedance. This negative response occurs within the linear boundary that shows an interpretted lack of gas depletion in previously mentioned attributes.

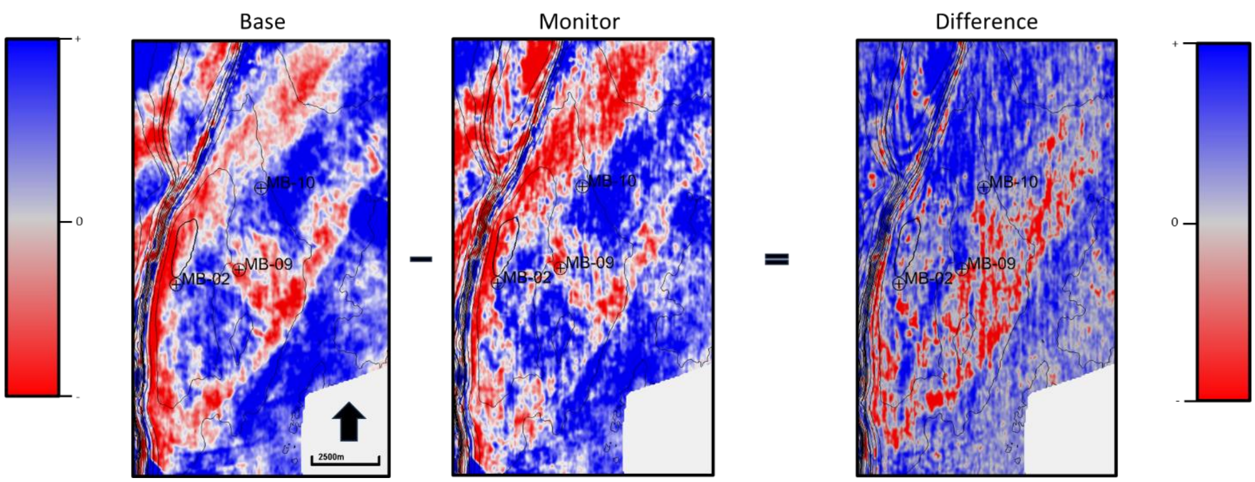

Figure 13. Results of the relative acoustic impedance attribute along the C Upper Sand surface. Base, monitor, and difference attribute volumes are shown, as well as production wells MB-02, MB-09, and MB-10.

Spectral Bandwidth

When the spectral bandwidth attribute was ran on this study's dataset it revealed a northeast to southwest trending lineation of the C Upper Sand surface (**Figure 14**). Production well MB-02 produces from the C Upper Sand just outside of this lineation, but gas detecting attributes do not show evidence of gas depletion across the zone though time. Furthermore, gas saturation models during the year of the monitor seismic survey illustrate that this lineation was yielding a gas water ratio of greater than 40% (New Zealand Petroleum and Minerals, 2018).

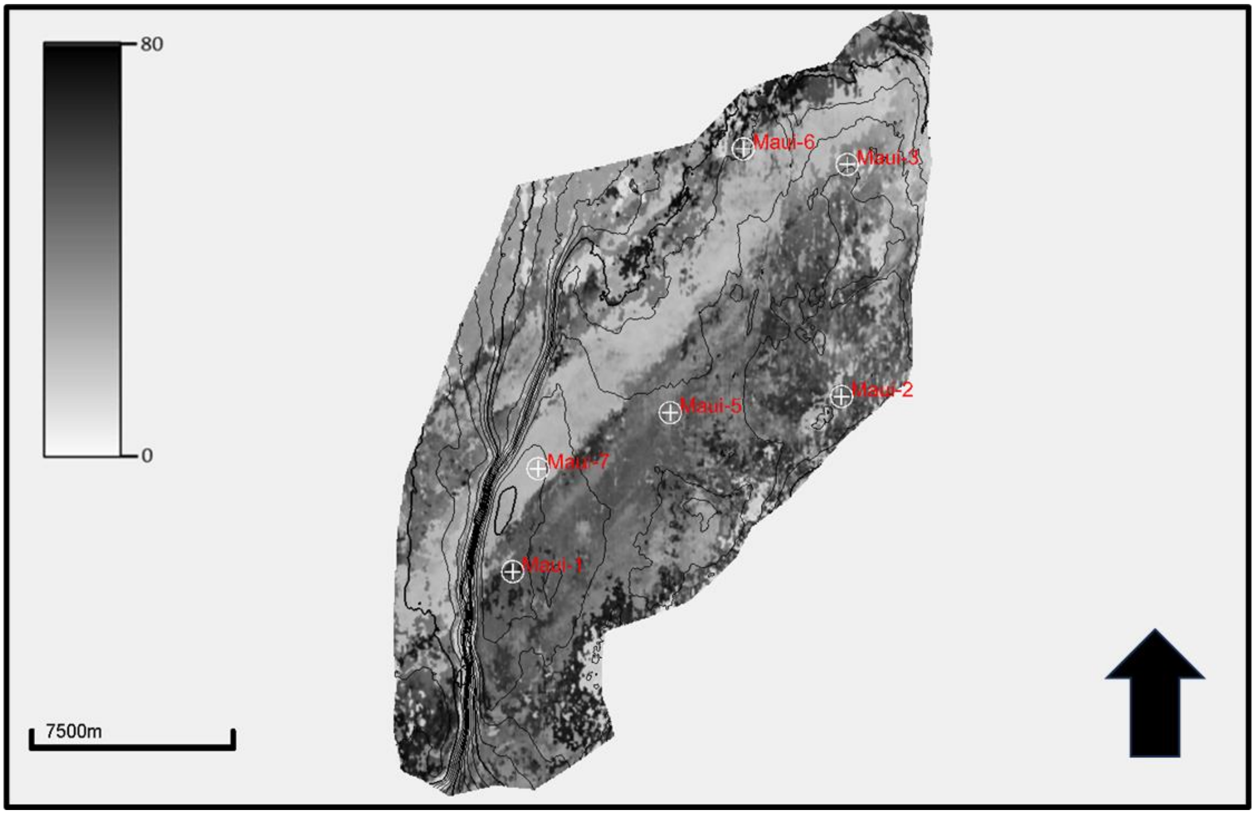

Figure 14. Results of the spectral bandwidth attribute along the C Upper Sand surface. Associated vertical exploration well locations are included as well.

Sobel Filter Similarity

The Sobel filter similarity attribute was ran on the base seismic volume in an attempt to uncover any previous small scale baffles that could be responsible for differential gas depletion of the Maui C Upper sand in the Maui-B reservoir zone. After observing results of this attribute (**Figure 15)**, it is evident that there was not a seismically detectable baffle present in this zone. However, the attribute was successful in detecting the Whitki Fault Zone as well as minor faults within the Maui-A reservoir zone. While the attribute failed to portray any Maui-B reservoir baffles, this observation is crucial to rule out all differential depletion possibilities.

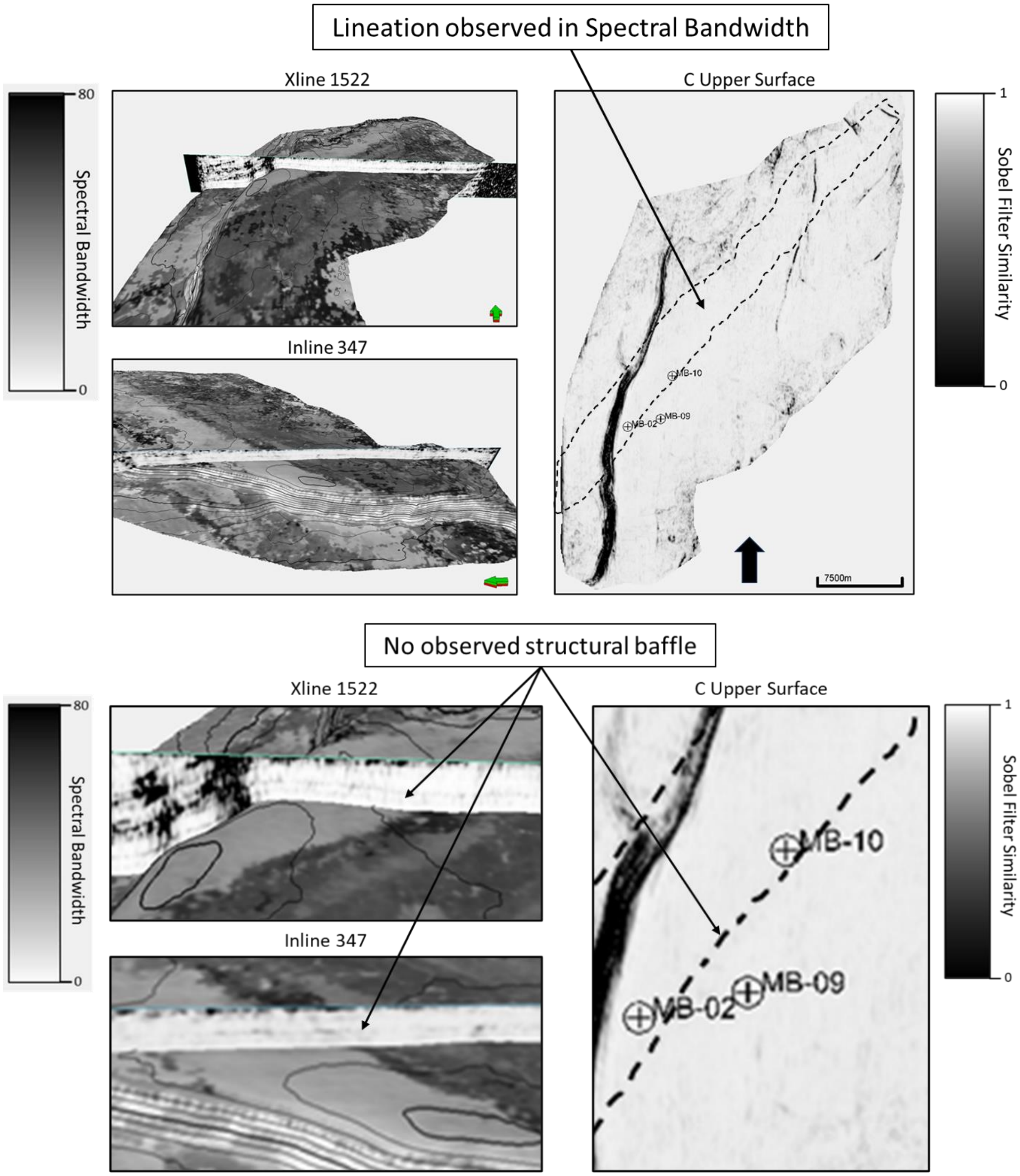

Figure 15. Results of the Sobel filter similarity base attribute volume along the C Upper Sand surface extracted spectral bandwidth attribute. Production wells MB-02, MB-09, and MB-10 are shown as well. Xline and inline slices of the Sobel similarity attribute volume are shown to rule out and faulting of the reservoir zone. The lineation observed in the spectral bandwidth attribute is illustrated with a dashed line. Zoomed images focusing on the lineation observed in the spectral bandwidth attribute are provided as well within the Maui-B zone.

PCA Results

After analyzing the seismic attributes, PCA is utilized to merge insights of the different attributes, from lithology to fluid movement into one map. These results provide valuable insights into understanding differential depletion across the Maui-B reservoir zone of the C Upper Sand.

PCA 3

As previously stated, this PCA computation included both the base and monitor sweetness volumes, as well as the base spectral bandwidth volume. The output of this computation does a fairly good job of relating the facies discrepancy to differential depletion in the reservoir. The interpreted linear shoreface zone is shown in light green, trending northeast to southwest in the seismic boundary (**Figure 16**). The zone that had yielded a high gas saturation percentage but

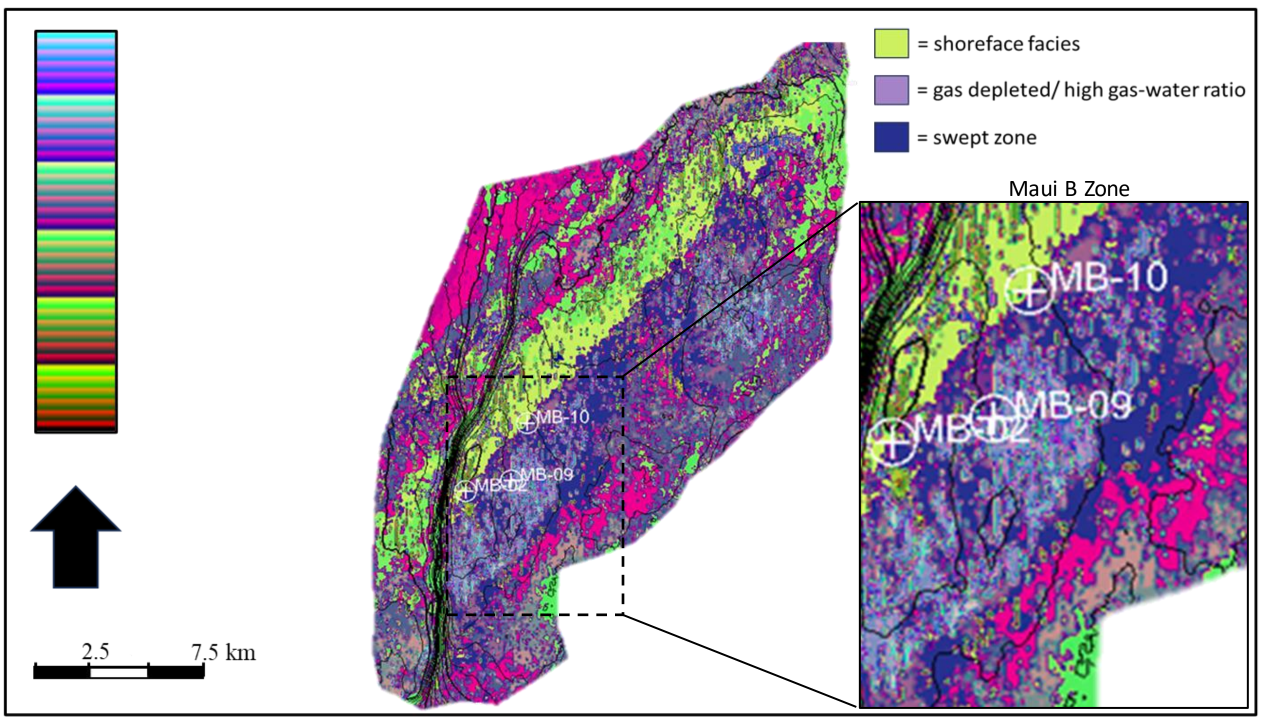

Figure 16. Output of the PCA 3 machine learning test including the base and monitor attribute volumes of sweetness and the base attribute volume of spectral bandwidth.

was subsequently swept due to gas depletion, here yields a high water saturation percentage and is represented by a dark purple color. Zones where gas was depleted but still obtain a high gas saturation percentage are indicated by a light purple color.

PCA 8

This PCA computation includes base and monitor attribute volumes of sweetness, mean frequency, relative acoustic impedance, and the base volumes of spectral bandwidth and Sobel filter similarity. This result seems to portray the facies discrepancy and initial high gas saturation zone quite well (**Figure 17**). However, it struggles in clearly revealing the swept and gas depleted zones. Gas depleted zones seem to only be indicated where a substantial change in gas water ratios occurred though time. The interpreted linear shoreface zone is shown in forest green, trending northeast to southwest in the seismic boundary. The initial gas saturated zone is shown

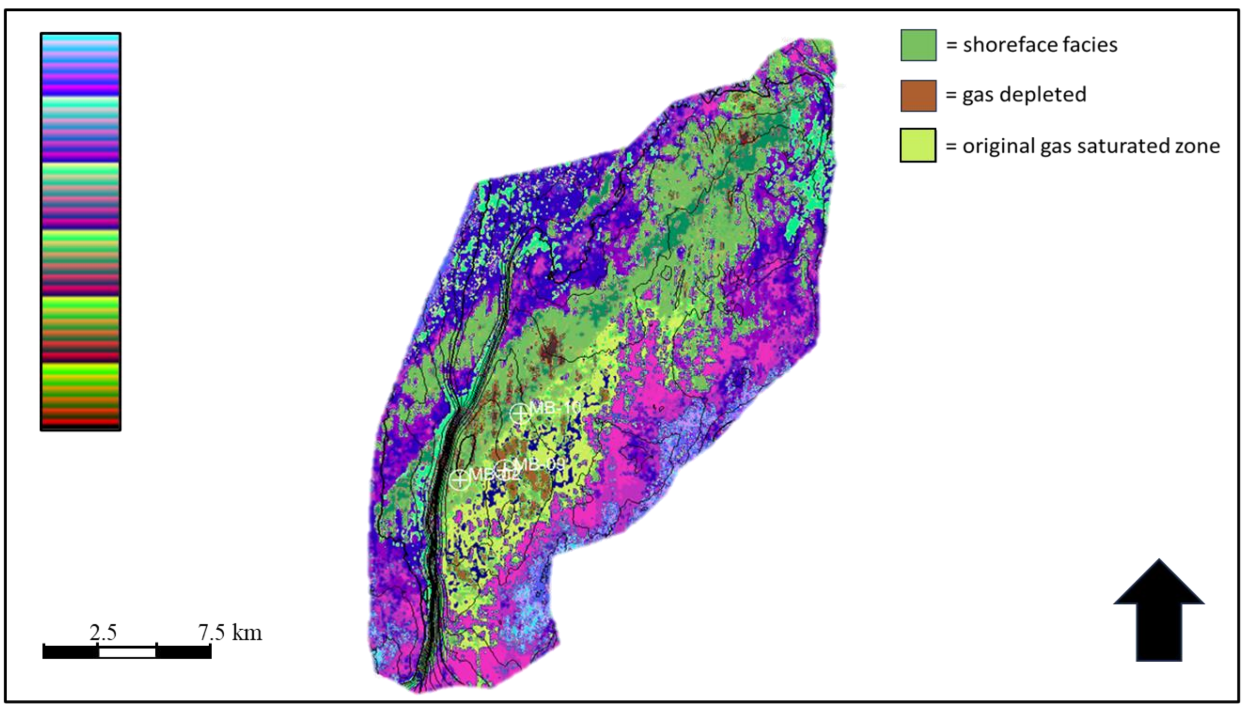

Figure 17. Output of the PCA 8 machine learning test including the base and monitor attribute volumes of sweetness, mean frequency, relative acoustic impedance, and the base volumes of spectral bandwidth and Sobel filter similarity.

in a lime green, and the interpreted swept zone does not seem to be captured in this computation. Zones where gas was depleted but still obtain a high gas to water ratio are modestly indicated by a light brown color.

DISCUSSION

Attributes

It is apparent that among the selected attributes, each contributes significantly to our understanding of reservoir fluid movement in 4D seismic data. Notably, the sweetness and envelope attributes emerge as particularly similar, with both effectively identifying areas of high gas saturation within the reservoir. The presence of low-density gas attenuates frequency readings and in turn produces a higher sweetness and envelope reading. Consequently, both of these seismic attributes can be used for effectively monitoring reservoir gas movement associated with production over time. Reservoir zones obtaining higher sweetness and envelope values tend to indicate elevated gas-water ratios, making them particularly promising for production. Additionally, the mean frequency attribute adeptly captures water sweeping into the reservoir zone, which can be linked to gas production. Reservoir zones with lower gas-water ratios manifest higher response values in the mean frequency as the water does not attenuate the seismic signal as much as when a higher gas-water ratio is present. As the gas-water ratio decreases, the mean frequency increases as the higher frequencies are not being attenuated.

The delineation of the gas-to-water contact was most effectively depicted through the calculation of the relative acoustic impedance attribute. This stems from the density contrasts that exist when the pore space is filled with gas versus water. A higher gas-water ratio corresponds to a slower event, leading to a more negative acoustic impedance response, while a lower ratio results in a faster event and a more positive response. Analysis of this attribute on the base volume revealed a distinct gas-to-water contact characterized by a high gas-water ratio within the gas zone, presenting a sharp boundary. However, in the monitor volume, this boundary exhibited a softer response, indicative of and increase in water associated with production. One possible explanation for this could be some residual gas of the initial contact still being present, but the gas water ratio on the gas side of the contact has drastically decreased.

Analysis of the spectral bandwidth attribute across all volumes revealed a distinct northeast-southwest trending linear feature interpreted as a paleoshoreface. This lineation on the C Upper surface shown by the spectral bandwidth attribute was interpreted to be the wave base associated to the shoreface of the depositional environment of this time. The wave base zone would expose sediment to a high energy environment with better sorting, which would lead to higher porosity and permeability of sandstones in the zone. With this abrupt horizontal change in petrophysical properties, it is evident that seismic responses could differ also across these zones. This feature was also noted by Bryant et al. (1995), whom concluded from integrated seismic, well log, and core data, this linear seismic pattern marks the transition from shoreface to offshore depositional environments. Interestingly, multiple seismic attributes had a negligible change, suggesting a lack of fluid movement within the shoreface over the 4D monitoring period, despite Well MB-10 penetrating the C Upper Sand just landward of this feature. The apparent barrier to lateral gas flow could reflect permeability compartmentalization arising from depositional facies changes across the paleoshoreline.

PCA Analysis

PCA facilitates the visualization of complex multi-dimensional seismic attribute analyses in a simplified 2D space, thereby aiding in the visual clustering of seismic facies for improved interpretability. Notably, the outcomes derived from PCA 3 exhibit significantly more promise when compared to any single original input attribute volumes. This finding underscores the significance of leveraging PCA techniques in uncovering insights into reservoir dynamics using 4D seismic data. Of particular note is the incorporation of both base and monitor sweetness volumes in the PCA 3 computation for fluid changes, along with the base spectral bandwidth volume which is pivotal for facies variations. This approach allows for a more nuanced understanding of facies dynamics, effectively highlighting the discrepancy in lithologic facies, revealing differential depletion patterns across the reservoir. We note that an interpreted linear shoreface zone, depicted in light green and trending northeast to southwest **(Figure 16)**, emerges prominently in PCA 3. The swept reservoir zone, previously characterized by high gas saturation percentages, has undergone significant changes due to gas depletion and now yields a high water saturation percentage and is represented by a dark purple color. Conversely, areas where gas depletion has occurred but still maintain relatively high gas saturation percentages are denoted by a light purple color. Overall, the insights gleaned from PCA 3 underscore its utility in elucidating complex reservoir dynamics that require insight from multiple seismic attributes from both the base and monitor volumes. It is noted that when including attribute volumes of both the base and monitor surveys, a majorly narrowed list of input attributes yields better results as shown by PCA 3. When compiling a greater number of similar attributes volumes of the base and monitor surveys for the PCA input, it seemed that attributes counteracted one another and provided less than desirable results as shown in PCA 8. With this being said, it has been determined that when deciding upon input attributes for 4D PCA it is of better interest to choose a simplified list of attributes.

Reservoir Depletion Discrepancies

With the observation of this linear reservoir zone that seems to prohibit fluid flow (**Figure 14**), the question as to what is causing this lack of fluid flow causing differential production across the linear zone is brought forth. Baffles that could be causing this differential depletion across the observed lineation could possibly be in the form of structural, petrophysical, or deformational anomalies such as faulting, reservoir heterogeneity, and deformation banding. The Sobel filter similarity attribute was calculated in an attempt to explain the phenomena by identifying the presence of a structural baffle that may explain lack of production across this lineation. After observing results of this attribute, it was determined that there wasn't a presence of a seismically detectable structural baffle that may prohibit gas flow in this region of the Maui-B reservoir zone. However, it is still possible that a structural baffle or baffles may be present, but below the volume's vertical resolution of ~30 feet. If this is the case, this small-scale feature could interfere with the reservoir enough to create fluid movement complications. This raises the question as to whether or not this baffle prohibiting fluid flow could be in the form of a permeability barrier rather than a structural barrier.

Another hypothesis that could explain this differential production across this linear feature could be the cementation of sands within the feature. A study performed by Bryant et al. (1995) discusses the idea that pore water expelled from the overlying C Shale could have been the source of calcite cementation occurring in the C Upper Sand. As previously stated, this lineation was interpreted to be the presence of a shoreface deposit. Depositional environments of shoreface deposits tend to produce sandstones of high permeability and porosity. With this in mind, cementation caused by water flow through this highly porous and permeable sand is more probable. This occurrence of cementation would drastically decrease the permeability of the reservoir zone, thus prohibiting fluid movement out of the zone (Dutton et al., 2002). For this theory to hold true, gas migration to the C Upper Sand would have taken place prior to this cementation event. Both fluid saturation models and selected attributes indicate there was a high gas water ratio present within the lineation in both the base and monitor surveys. The sweetness and envelope attributes showed relatively high values within the lineation, but no change in gas saturation in the difference volume. This could be portraying the presence of trapped gas due to flow restriction from calcite cementation. A pronounced negative relative acoustic impedance response was noted in the lineation of the monitor volume. This phenomenon may stem from the declining gas-water ratio throughout the reservoir during production, while the ratio within the lineation remains relatively constant due to limited flow. If this hypothesis holds true, the trapped gas within this lineation could represent the lowest negative value observed within the sampled volume. Density porosity logs of well Maui-7 within the shoreface seem to indicate a slightly lesser porosity of 2.21 g/cm3 than that of well Maui-1 outside of the shoreface of 2.03 g/cm3, but overall porosity values are similar. However, resistivity logs of the interval vary drastically with Maui-7 having a peak resistivity of ~560 ohms, and Maui-1 having a peak resistivity of ~200 ohms. Well locations in relation to the shoreface boundary are shown in **Figure 14.** A study conducted by Bunch, (2019) explored wireline well log responses of carbonate cementation in clastic sandstones, where they discuss the possibility that high resistivity readings in a porous sand reservoir could be an indication of carbonate cementation and lower permeability. Cementation of this sand could be minor and primarily affect pore throats of the sand, decreasing the permeability and prohibiting flow, but only minimally affecting porosity. This could explain the presence of a similar porosity reading accompanied by drastic variations in resistivity as shown in **Figure 18**. As this theory seems plausible, adequate well data and core samples would be needed to fully prove the theory. With this uncertainty, the question arises as to what other factor could be possibly responsible for prohibiting fluid movement in the C Upper Sand reservoir.

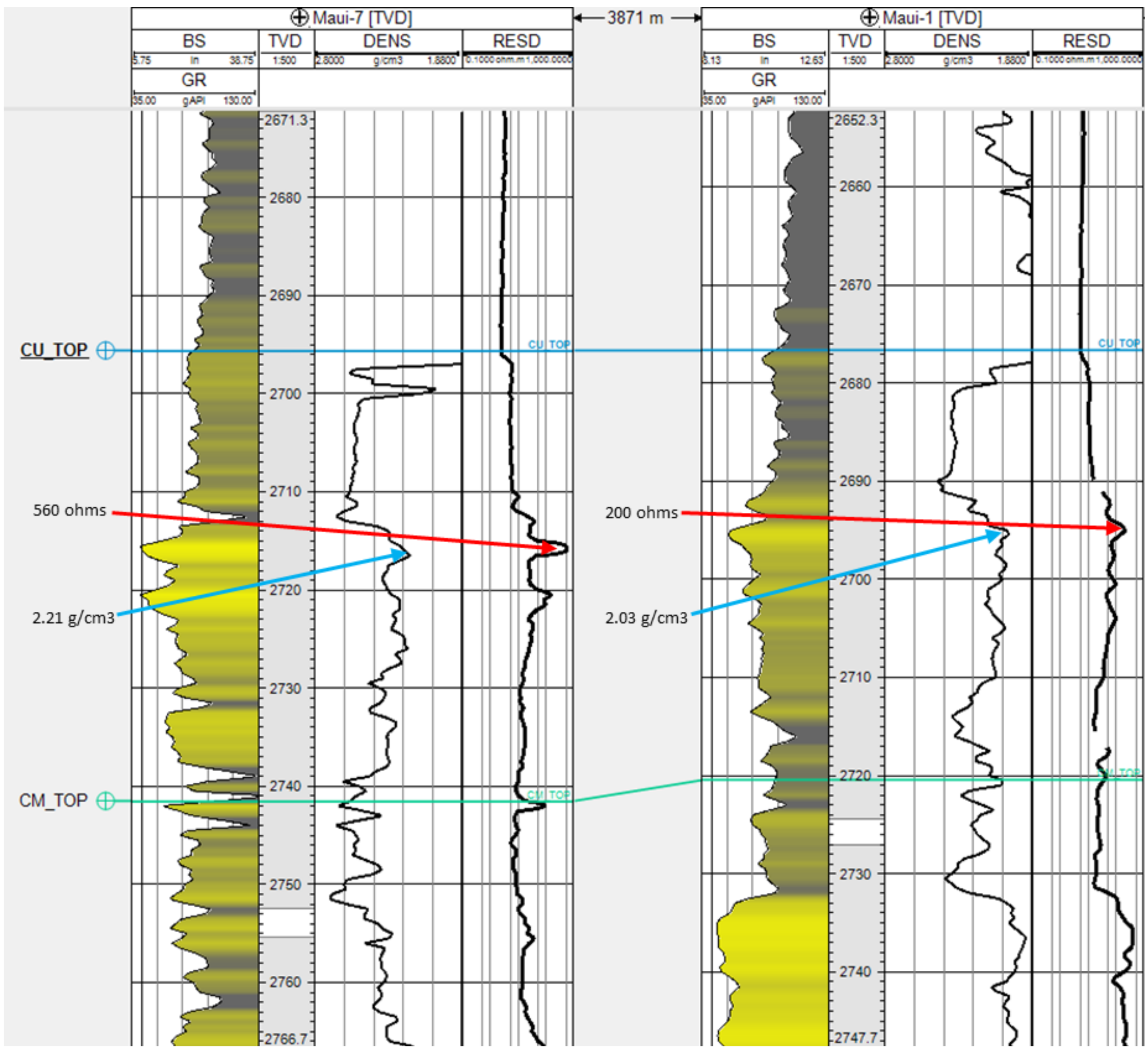

Figure 18. Well logs of Maui-7 (within interpreted shoreface) and Maui-1 (outside interpreted shoreface) portraying the gamma ray log in track 1, density porosity in track 2, and resistivity deep log in track 3. Well tops of the C Upper (CU_TOP) and C Middle (CM_TOP) are provided as well. Red arrows are pointing to max resistivity readings and blue arrows are pointing to max density porosity readings.

A study conducted by Parnell et al. (2004) discusses how the process of post depositional deformation bands can create reservoir compartmentalization and restrict hydrocarbon flow, especially in porous fluvial and shoreface sand deposits. Grains incorporated within deformation bands have been reorganized in the manner of sliding, rotating, or fracturing as the result of differing forces such as compaction, shearing, or dilation (Fossen et al. 2007). With the reorganization of these grains, permeability could be affected within these deformation bands. Compartmentalization caused from these deformation bands could have occurred following hydrocarbon migration to the reservoir, thus not allowing hydrocarbons to be produced across compartments. However, given the small scale of deformation banding, the provided data used in this study is inadequate to neither prove nor disprove this possibility. In research such as this, it is important to not rule out any theories unless disproven by substantial supporting data.

Production Following 4D Timeframe

Following observations of attributes and machine learning results, the question arises of whether future production of Maui-B reservoir zone may have been improved if these techniques were implemented. Following the 4D timeframe, numerous wells were drilled within the previously mentioned linear shoreface zone that proved to be unsuccessful. One of these wells was drilled within the lineation in 2006 and was watered out by 2007 **(Appendix D. Figures 18-19.)**. Another well drilled within the lineation in 2008 watered out within the year (**Appendix D. Figure 20.)**. While it may have been understood that the reservoir zone had proved to yield unsuccessful wells, the extent of this zone may not have been understood due to the absence of a vast well log data set of the area. By incorporating facies indicating attributes with 4D fluid sensitive attributes, the extent of this reservoir lineation with unfavorable production properties may have been elucidated. With a better understanding of the lateral extent of this unfavorable reservoir zone, future production of the reservoir with vertical wells could be planned around it accordingly. If the previously mentioned theory about trapped gas due to calcite cementation is correct, the use of horizontal drilling and hydraulic fracturing could lead to a more successful production outcome. Hydraulic fracturing could increase the permeability of this possibly cemented sand and permit the flow of gas and water.

Limitations

When reaching conclusions regarding reservoir fluid movement it is important to first realize the limitations of the study. Factors that can ultimately play a monumental role in manipulating the course of reservoir fluid movement may not be visible in seismic imaging. With conventional seismic resolution, while these fluid movement behaviors may be captured, seismic data alone cannot prove or disprove the cause of the behavior. At the reservoir scale, a broader well dataset would be needed in order to reach conclusions as to exactly why the fluids are behaving the way they are. However, the purpose of this research is not to prove or disprove theories related to reservoir fluid movement, but to use an attribute-based method to elucidate behaviors of this fluid movement. Additionally, the absence of well-specific production data precludes the assignment of quantitative values to production within the designated 4D timeframe. While we assume a decrease in gas saturation surrounding producing wells is indicating gas production, this cannot be proven without the individual well production data. Consequently, the evaluation of 4D attribute volumes in this study remains predominantly qualitative. This qualitative assessment encompasses the integration of attribute volumes and gas saturation models corresponding to the year of the 4D survey acquisition. Furthermore, a qualitative examination of individual well productivity is conducted based on the provided production history within the gas saturation models. These models delineate the initiation of production for each well and the duration until the well is watered out. Despite the qualitative nature of these attribute observations, it is essential to understand that the computation of the attributes themselves is inherently quantitative. Therefore, qualitative inferences are derived from quantitative outcomes, highlighting the interplay between the two facets of analysis. Another limitation of the study is the absence of pressure data. Since changing reservoir pressures associated with ongoing production can alter seismic responses, minor discrepancies of 4D attributes due to pressure changes cannot be ruled out.

CONCLUSIONS

In summary, the attribute-based seismic analysis conducted on the movement of reservoir fluids in the Maui C Upper Sand reservoir has provided valuable insights into both gas depletion and water encroachment dynamics. The comparison between base and monitor volumes, along with the difference volume analysis, has proven effective in illustrating gas depletion and water encroachment behaviors in unique manners. The base-monitor comparison offers a clear before-and-after perspective, facilitating the observation of fluid movement within the 4D timeframe, particularly useful for identifying reservoir compartmentalization and potential barriers to fluid flow. On the other hand, the difference volume analysis highlights reservoir zones where substantial gas depletion has taken place, providing a qualitative representation of reservoir zones that have experienced a drastic decrease in gas saturation, which is especially valuable for assessing hydrocarbon depletion intensity across different zones.

There was additional insight with the addition of attribute analysis performed on both the base and monitor survey. Attributes such as sweetness and envelope have demonstrated their efficiency in indicating zones with high gas saturation, with observable depletion evident when comparing base and monitor surveys. Mean frequency analysis has effectively highlighted water encroachment trends where an increase in mean frequency was observed through the 4D timeframe, as the frequency attenuating gas moved out of this area.

The spectral bandwidth attribute also facilitated the recognition of facies changes within the reservoir, revealing a northeast to southwest trending lineation interpreted as a shoreface depositional setting. This lineation, while hindering gas flow as evidenced by the absence of depletion within it, also indicates the theorized presence of calcite cementation, likely induced by water expelled by the overlying C Shale. This cementation was hypothesized to primarily affect pore throats of the sandstone, decreasing permeability and restricting gas flow.

Finally, the utilization of the unsupervised principal component analysis has facilitated the effective portrayal of differential depletion across reservoir zones with facies discrepancies. Particularly, the PCA 3 computation, with both the base and monitor sweetness attribute volumes, successfully delineated zones exhibiting varying gas-water ratios through time, thereby elucidating the interaction between these zones and the interpreted shoreface facies. What sets PCA analysis apart is its ability to amalgamate attribute analysis from both the base and monitor surveys to understand fluid changes, alongside seismic attributes that emphasize facies alterations. Rather than relying on multiple seismic analyses, PCA results accentuate reservoir heterogeneity and changes, spanning from lithologic facies to fluid alterations.

Concluding this 4D analysis method, insight was provided in regards to reservoir fluid movement and factors that may influence this movement. The most probable theory to explain restricted flow across the interpreted shoreface lineation was the presence of a permeability barrier formed from diagenetic calcite cementation. While this theory seems likely, adequate well log data, core samples, and quantitative production data would need to be accessible to fully prove the theory. The need for future studies extending this 4D attribute and machine learning approach with adequate data in similar reservoir settings is apparent.

In conclusion, this attribute-based reservoir fluid movement analysis workflow has significantly enhanced our understanding of reservoir fluid behaviors over time. The findings suggest a complex interplay of factors, including facies variations and cementation effects, influencing fluid flow dynamics within the Maui C Upper sand reservoir.

REFERENCES

Abbott, W. O. (2010). Maui Field Occidental exploration and production company Bakersfield, California. *International Law Reports*, *138*, 35–91. https://doi.org/10.1017/cbo9780511760464.002

Ashraf, U., Zhang, H., Anees, A., Ali, M., Zhang, X., Shakeel Abbasi, S., & Nasir Mangi, H. (2020). Controls on reservoir heterogeneity of a shallow-marine reservoir in Sawan gas field, Se Pakistan: Implications for reservoir quality prediction using acoustic impedance inversion. *Water*, *12*(11), 2972. https://doi.org/10.3390/w12112972

Bryant, I. D., Greenstreet, C. W., & Voggenreiter, W. R. (1995). Integrated 3-D geological modeling of the C1 Sands Reservoir, Maui Field, offshore New Zealand. *AAPG Bulletin*, *79*. https://doi.org/10.1306/8d2b152a-171e-11d7-8645000102c1865d

Bunch, M. (2019). Quantified detection of carbonate cementation in sandstones using standard Wireline Log Data. *ASEG Extended Abstracts*, *2019*(1), 1–7. https://doi.org/10.1080/22020586.2019.12073185

Chenin, J. (2020a). *Examining seismic amplitude responses of gaseous media using unsupervised machine learning* (thesis).

Chopra, S., & Marfurt, K J. (2024). *Essentials of Seismic Attributes and Impedance Inversion*: SEG

Coleman, R. D., & Trudgill, B. (2018). *The tectonic evolution of Taranaki Basin, offshore New Zealand* (thesis). ProQuest LLC.

Dutton , S. P., White, C. D., Willis, B. J., & Novakovic, D. (2002). Calcite cement distribution and its effect on fluid flow in a deltaic sandstone, Frontier Formation, Wyoming. *AAPG Bulletin*, *86*. https://doi.org/10.1306/61eedde6-173e-11d7-8645000102c1865d

Fossen, H., Schultz, R. A., Shipton, Z. K., & Mair, K. (2007). Deformation bands in Sandstone: A Review. *Journal of the Geological Society*, *164*(4), 755–769. https://doi.org/10.1144/0016-76492006-036

Funnell, R. H., Stagpole, V. M., Nicol, A., McCormack, N., & Reyes, A. G. (2004). Petroleum generation and implications for migration: a Maui Field charge study, Taranaki Basin. *New Zealand Petroleum Conference Proceedings*.

Giba, M., Nicol, A., & Walsh, J. J. (2010). Evolution of faulting and volcanism in a back-arc basin and its implications for subduction processes. *Tectonics*, *29*(4). https://doi.org/10.1029/2009tc002634

Haskell, T., 1991, An analysis of Taranaki Basin hydrocarbon migration paths; some questions answered: Petroleum Exploration New Zealand News, Jan., p. 19–25

Haque, A. E., Islam, MD. A., & Ragab Shalaby, M. (2016). Structural modeling of the Maui Gas Field, Taranaki Basin, New Zealand. *Petroleum Exploration and Development*, *43*(6), 965–975. https://doi.org/10.1016/s1876-3804(16)30114-8

Holt, W. E., and T. A. Stern, 1994, Subduction, platform subsidence, and foreland thrust loading: The late Tertiary development of Taranaki Basin, New Zealand: Tectonics, 13, 1068–1092, doi: 10.1029/94TC00454.

Hussein, M., Stewart, R. R., Sacrey, D., Johnston, D. H., & Wu, J. (2021). Unsupervised machine learning for time-lapse seismic studies and Reservoir Monitoring. *Interpretation*, *9*(3). https://doi.org/10.1190/int-2020-0176.1

Hussein, M., Stewart, R. R., & Wu, J. (2021). Which seismic attributes are best for subtle fault detection? *Interpretation*, *9*(2). https://doi.org/10.1190/int-2020-0068.1

Killops, S. D., Woolhouse, A. D., Weston, R. J., & Cook, R. A. (1994). A geochemical appraisal of oil generation in the Taranaki Basin, New Zealand. *AAPG Bulletin*, *78*. https://doi.org/10.1306/a25ff21f-171b-11d7-8645000102c1865d

King, M. S. (2009). Recent developments in seismic rock physics. *International Journal of Rock Mechanics and Mining Sciences*, *46*(8), 1341–1348. https://doi.org/10.1016/j.ijrmms.2009.04.008

Korneev, V. A., Goloshubin, G. M., Daley, T. M., & Silin, D. B. (2004). Seismic low-frequency effects in monitoring fluid-saturated reservoirs. *GEOPHYSICS*, *69*(2), 522–532. https://doi.org/10.1190/1.1707072

Koson et al., 2014. Seismic attributes and seismic geomorphology. Vol. 6, No. 1, 1-9

Lubo-Robles, D., Bedle, H., Marfurt, K. J., & Pranter, M. J. (2023). Evaluation of principal component analysis for seismic attribute selection and self-organizing maps for seismic facies discrimination in the presence of gas hydrates. *Marine and Petroleum Geology*, *150*, 106097. https://doi.org/10.1016/j.marpetgeo.2023.106097

McBeath, D. M. (1977). Gas-condensate fields of the Taranaki Basin, New Zealand. *New Zealand Journal of Geology and Geophysics*, *20*(1), 99–127. https://doi.org/10.1080/00288306.1977.10431594

Mirkamali, M. S., Keshavarz F.K., N., & Bakhtiari, M. R. (2016). Evolution analysis of miocene channels and faults in offshore area of Strait of Hormuz (eastern part of Persian Gulf) using seismic meta-attributes. *Journal of Petroleum Science and Engineering*, *147*, 116–128. https://doi.org/10.1016/j.petrol.2016.05.012

New Zealand Petroleum and Minerals. (2018). *Geodata catalogue*. https://www.nzpam.govt.nz/maps-geoscience/geodata-catalogue/

Pannett, S., S. Slager, G. Stone, and S. Dekker, 2004, Constraining a complex gas-water dynamic model using 4D seismic: Presented at the Annual Technical Conference and Exhibition, 209–225, SPE.

Parnell, J., Watt, G. R., Middleton, D., Kelly, J., & Baron, M. (2004). Deformation band control on hydrocarbon migration. *Journal of Sedimentary Research*, *74*(4), 552–560. https://doi.org/10.1306/121703740552

Petroleum Reserves Data. Ministry of Business, Innovation, and Employment. (2023, January). https://www.mbie.govt.nz/building-and-energy/energy-and-natural-resources/energy-statistics-and-modelling/energy-statistics/petroleum-reserves-data/

Radovich, B. J., & Oliveros, R. B. (1998). 3-D sequence interpretation of seismic instantaneous attributes from the gorgon field. *The Leading Edge*, *17*(9), 1286–1293. https://doi.org/10.1190/1.1438125

Reilly, C., Nicol, A., Walsh, J. J., & Seebeck, H. (2015). Evolution of faulting and plate boundary deformation in the southern Taranaki Basin, New Zealand. *Tectonophysics*, *651–652*, 1–18. https://doi.org/10.1016/j.tecto.2015.02.009

Qi, J., F. Li, and K. J. Marfurt. 2017, Multiazimuth coherence: Geophysics, 82, o83-o89.Lyu, B., J.

Waal, H. de, & Calvert, R. (2003). Overview of global 4D seismic implementation strategy. *Petroleum Geoscience*, *9*(1), 1–6. https://doi.org/10.1144/1354-079302-531

Wold, S., Esbensen, K., & Geladi, P. (1987). Principal component analysis. *Chemometrics and Intelligent Laboratory Systems*, *2*(1–3), 37–52. https://doi.org/10.1016/0169-7439(87)80084-9

APPENDICES

Appendix A. Petroleum System Elements

Understanding the dynamics of hydrocarbon fluid movement in the Maui Field is crucial for effective reservoir management and production optimization. Figures illustrating crucial petroleum system components are shown below.

Appendix A. Figure 1. Cross section view of stratigraphy illustrating the source rock to reservoir relationship (from Killops, 1994).

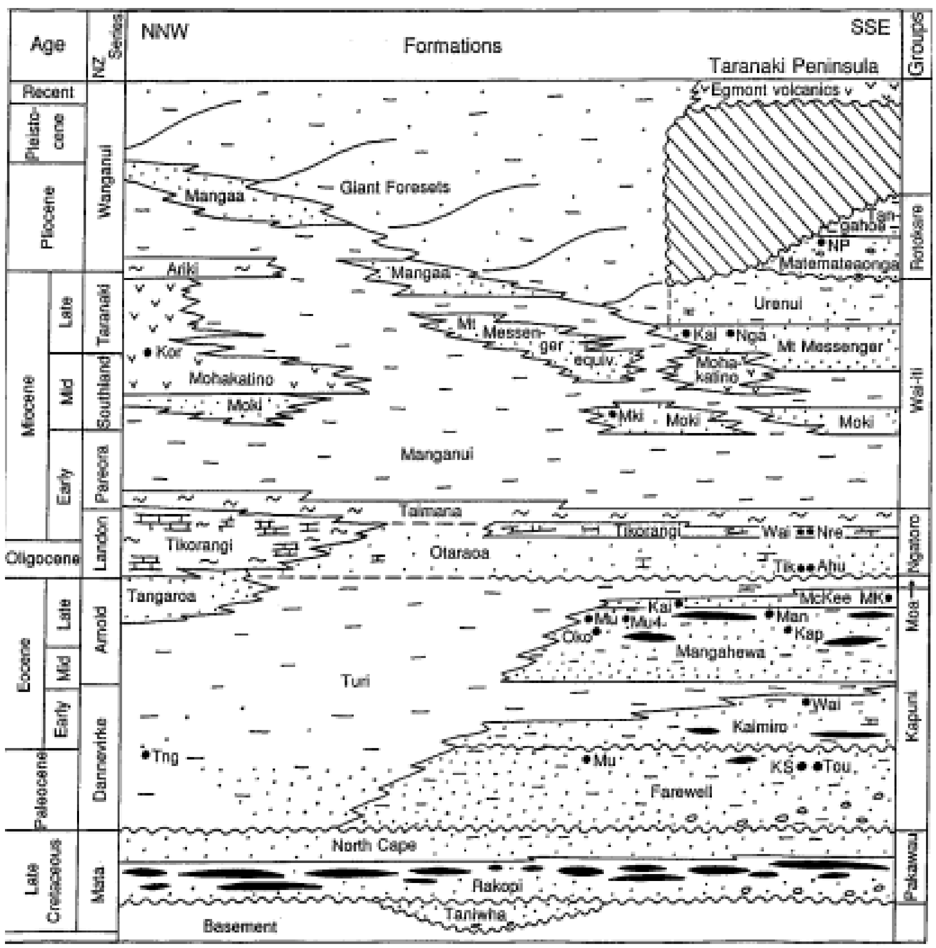

Appendix A. Figure 2. Illustrating possible migration pathways from sub-basin kitchens to Maui sand reservoirs. Map of predicted gas expelled from sub-basin kitchens is depicted as well (Modified from Funnell 2001).

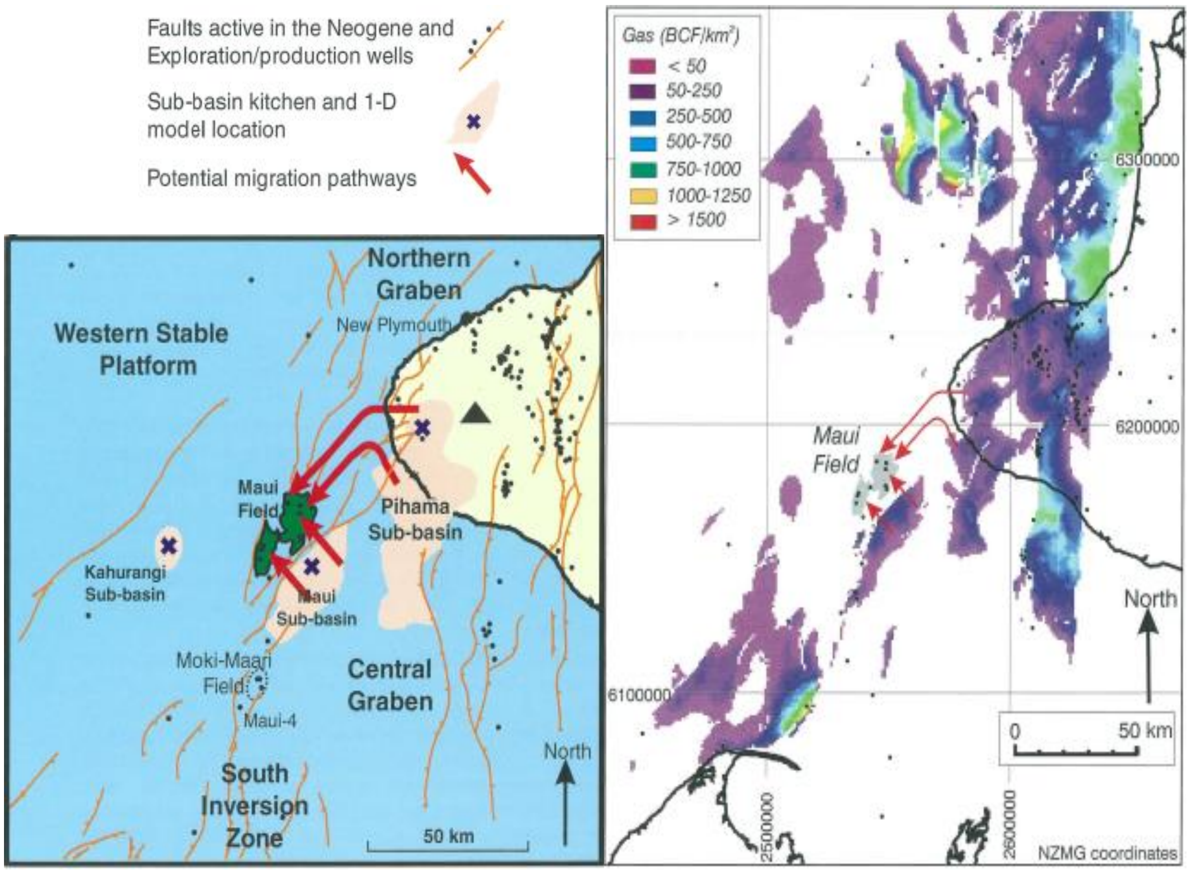

Appendix A. Figure 3. Paleo depositional environment in relation to present day Maui Field. Up dip sediment source location is highlighted (From Bryant et al., 1995).

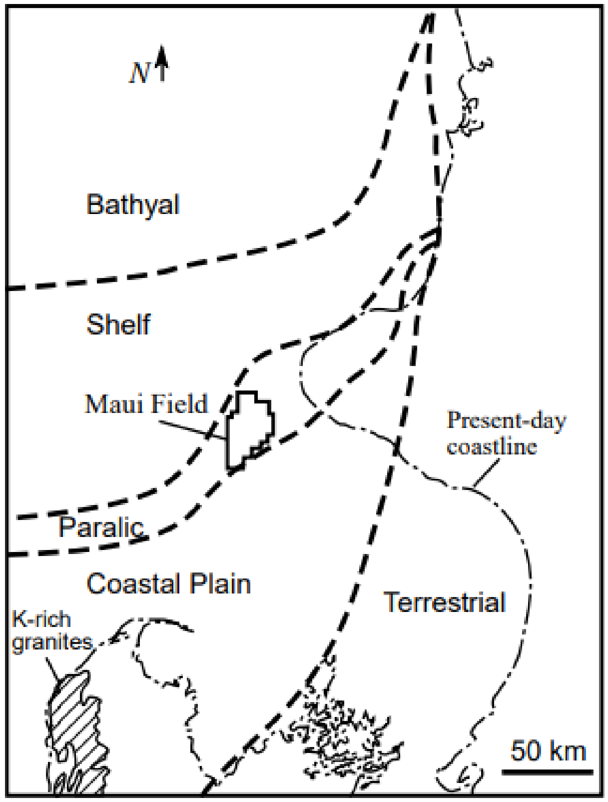

Appendix A. Figure 4. Cross section view illustrating the hydrocarbon trap of the Maui C1 Sand reservoir and underlying strata. (C 1-4 Sands are equivalent to C Upper, Middle, and Lower) (From Bryant et al., 1995).

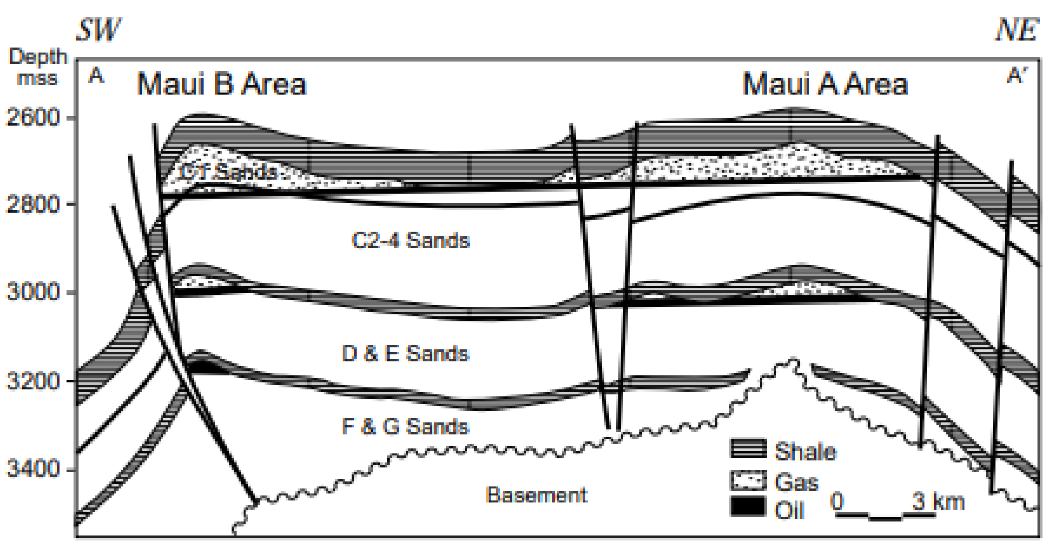

Appendix B. Gas Saturation vs. Attribute Value Cross Plots

While the visual comparison of fluid detecting attributes to fluid saturation models provides a predicted idea the fluid type the attribute is portraying, it is important to correlate borehole saturation percentages to attribute values at the borehole to increase confidence in attribute findings regarding fluid type. Cross plots linking gas saturation to attribute values are shown below.

Appendix B. Figure 1. Cross plot illustrating the relationship between gas saturation values and sweetness attribute values at the well bore. Attribute value is shown on the Y-axis and gas saturation percentage is shown on the x-axis.

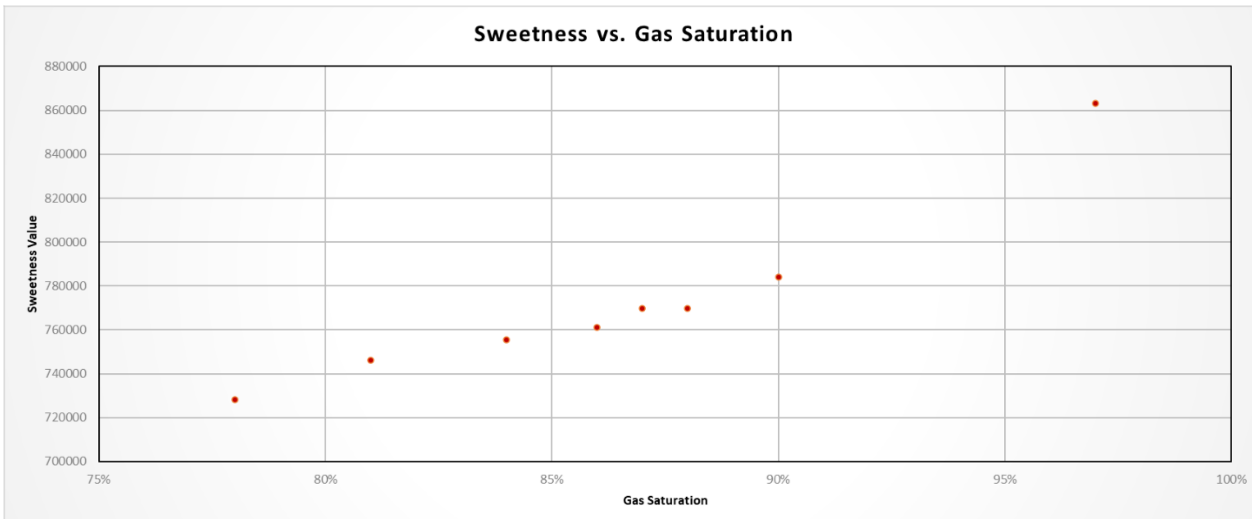

Appendix B. Figure 2. Cross plot illustrating the relationship between gas saturation values and envelope attribute values at the well bore. Attribute value is shown on the Y-axis and gas saturation percentage is shown on the x-axis.

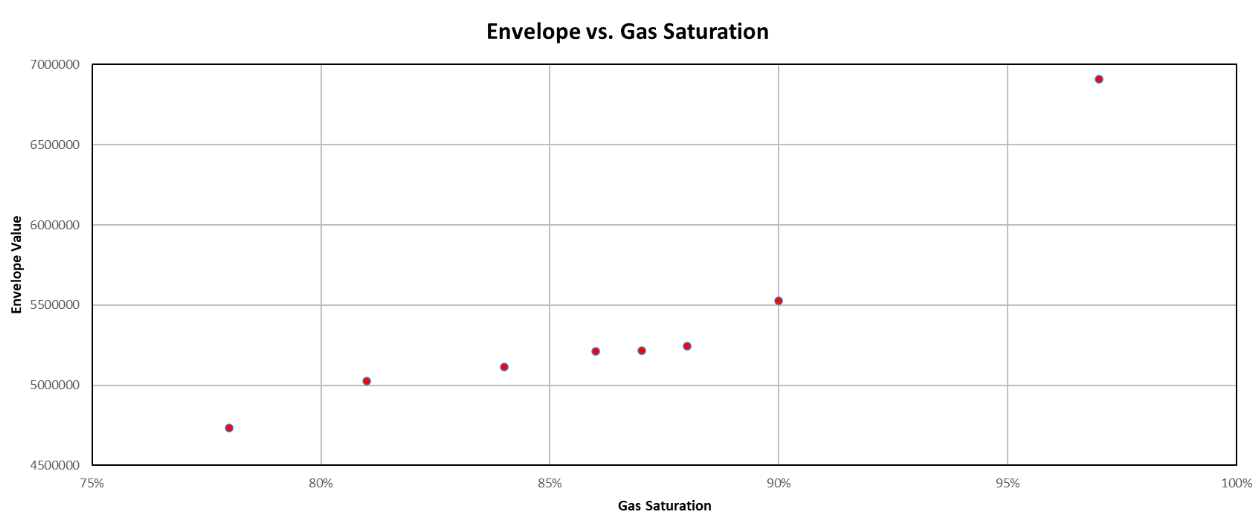

Appendix C. Eigenvector Bar Graphs

The PCA attribute selection tool was used to determine which attribute were most relevant in the different machine learning computations. 3 Eigenvector bar graphs were produced for each machine learning tests to gauge relevancy. Figures illustrating these eigenvector bar graphs are shown below.

Appendix C. Figure 1. Eigenvector bar graphs created by the PCA attribute selection tool of the PCA test 1. Eigenvector graphs 1-3 are shown below with the % involvement on the y-axis and attribute name on the x-axis.

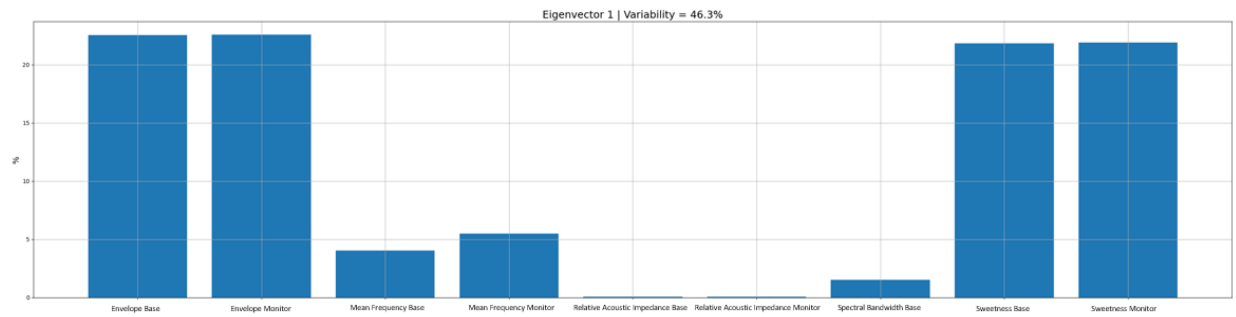

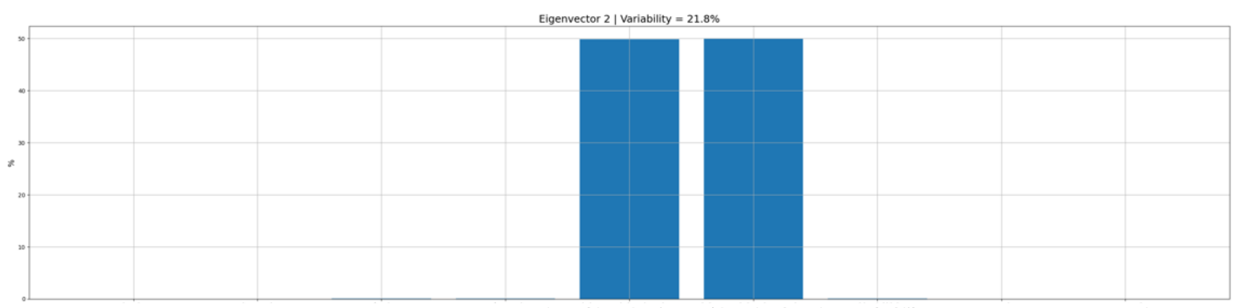

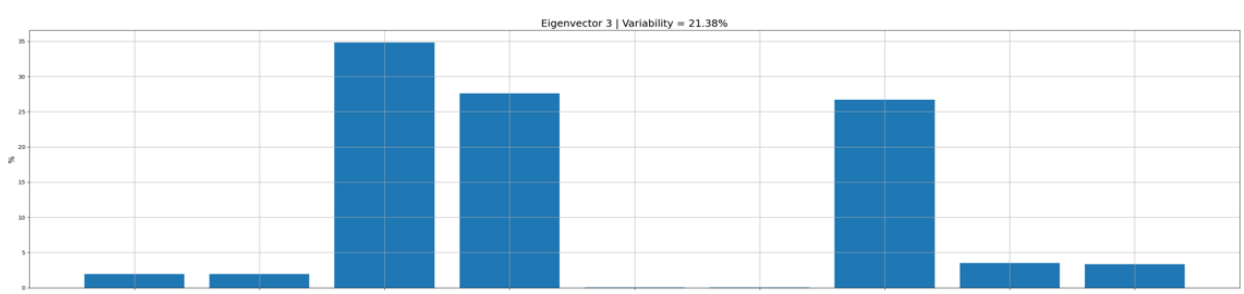

Appendix C. Figure 2. Eigenvector bar graphs created by the PCA attribute selection tool of the PCA test 2. Eigenvector graphs 1-3 are shown below with the % involvement on the y-axis and attribute name on the x-axis.

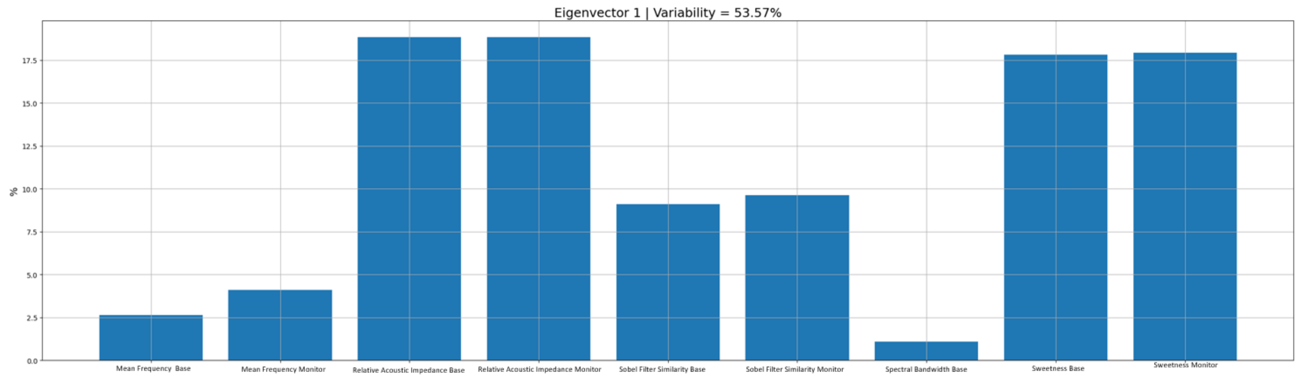

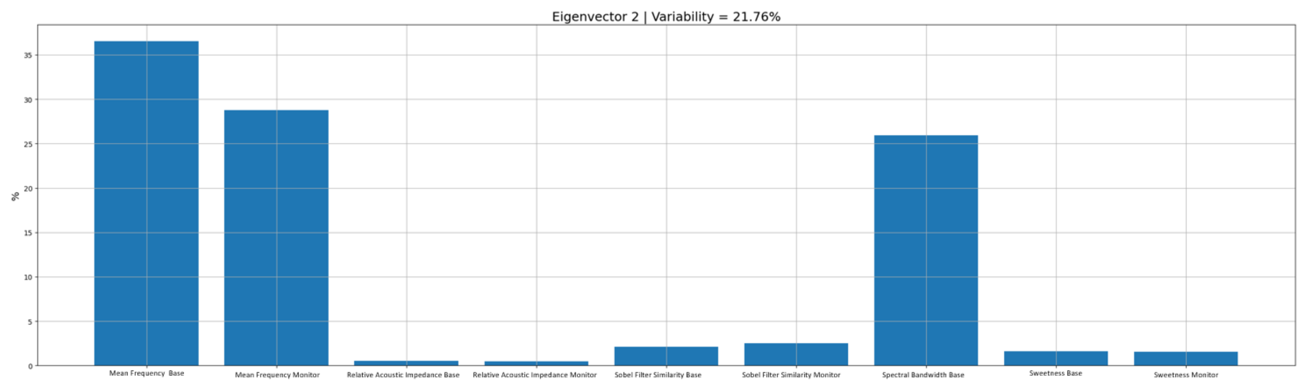

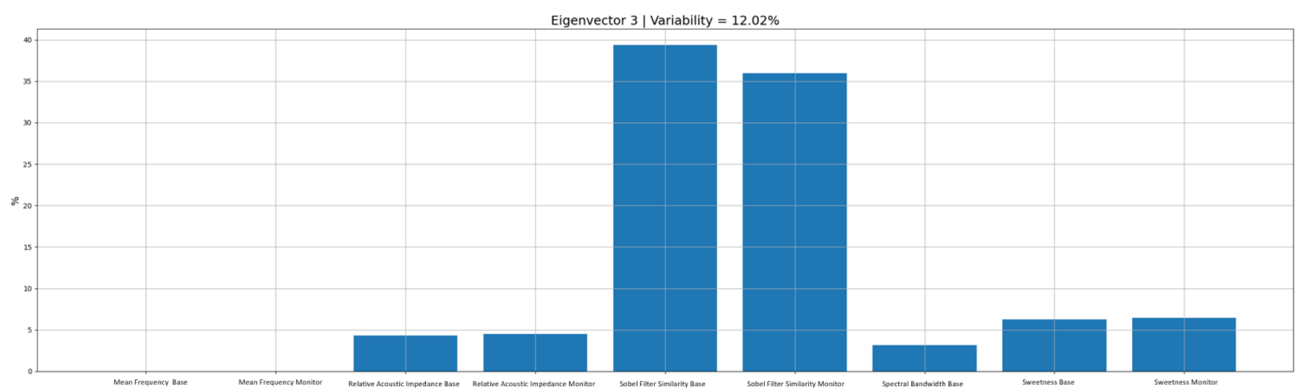

Appendix D. Fluid Saturation Models/Well Information Maps Through Time

Maps including gas saturation models, well productivity, and logging were shown in the text for the exact years of the base and monitor surveys (1991 and 2002). Since production plans following the 4D timeframe were discussed, maps of saturation models, well productivity, and logging for all years of exploration and production are shown below.

Appendix D. Figure 1. Map of well paths of producing wells and vertical exploration well location of the C Upper Sand in the Maui-B zone (New Zealand Petroleum and Minerals, 2018).

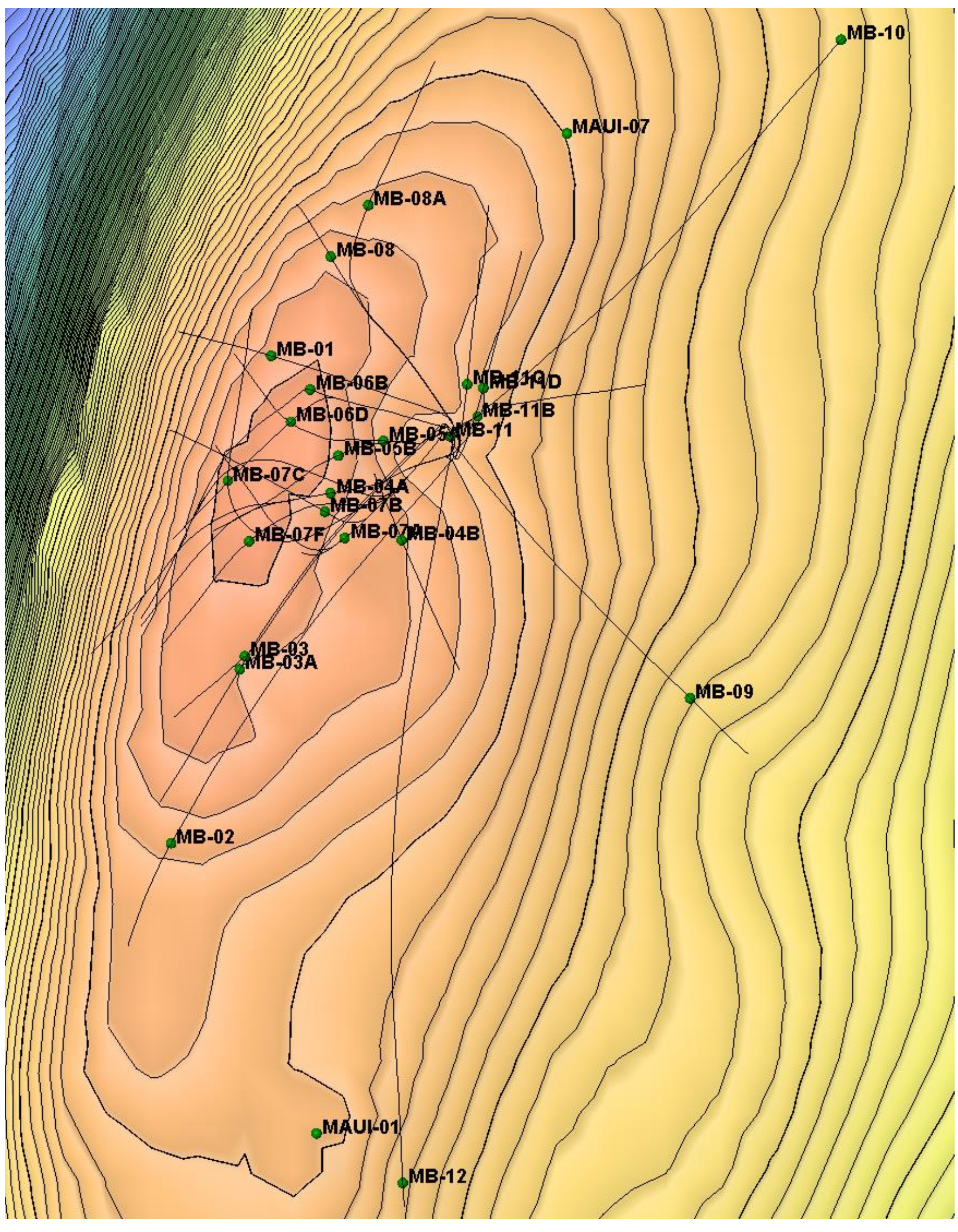

Appendix D. Figure 2. Legend for Fluid Saturation Models/Well Information Maps (New Zealand Petroleum and Minerals, 2018).

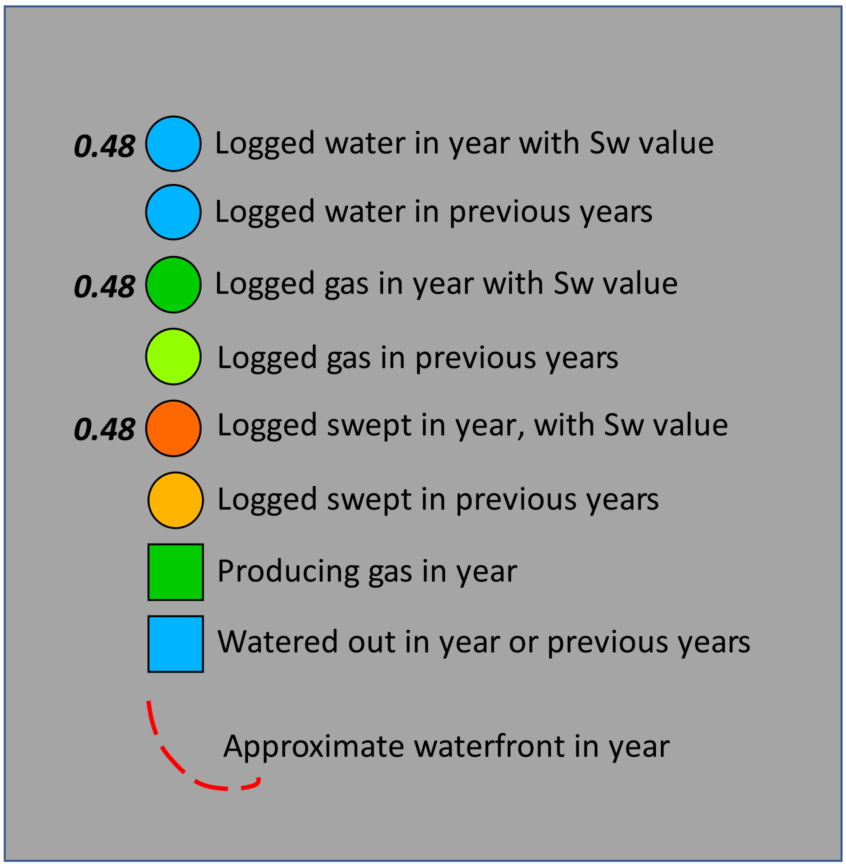

Appendix D. Figure 3. Fluid Saturation Model/Well Information Map ***(1991)*** (New Zealand Petroleum and Minerals, 2018).

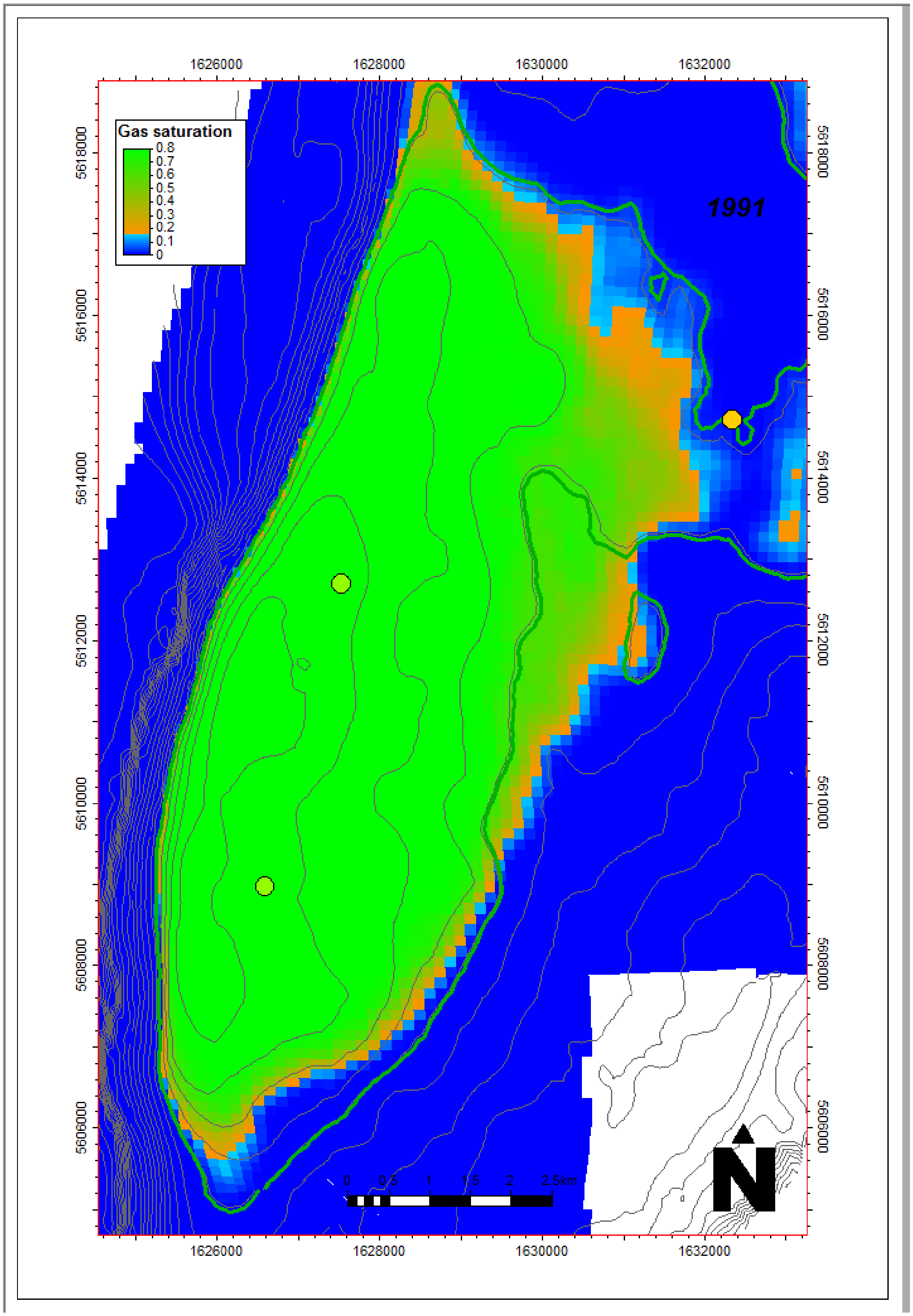

*Appendix D. Figure 4. Well Information Map **(1992)*** (New Zealand Petroleum and Minerals, 2018).

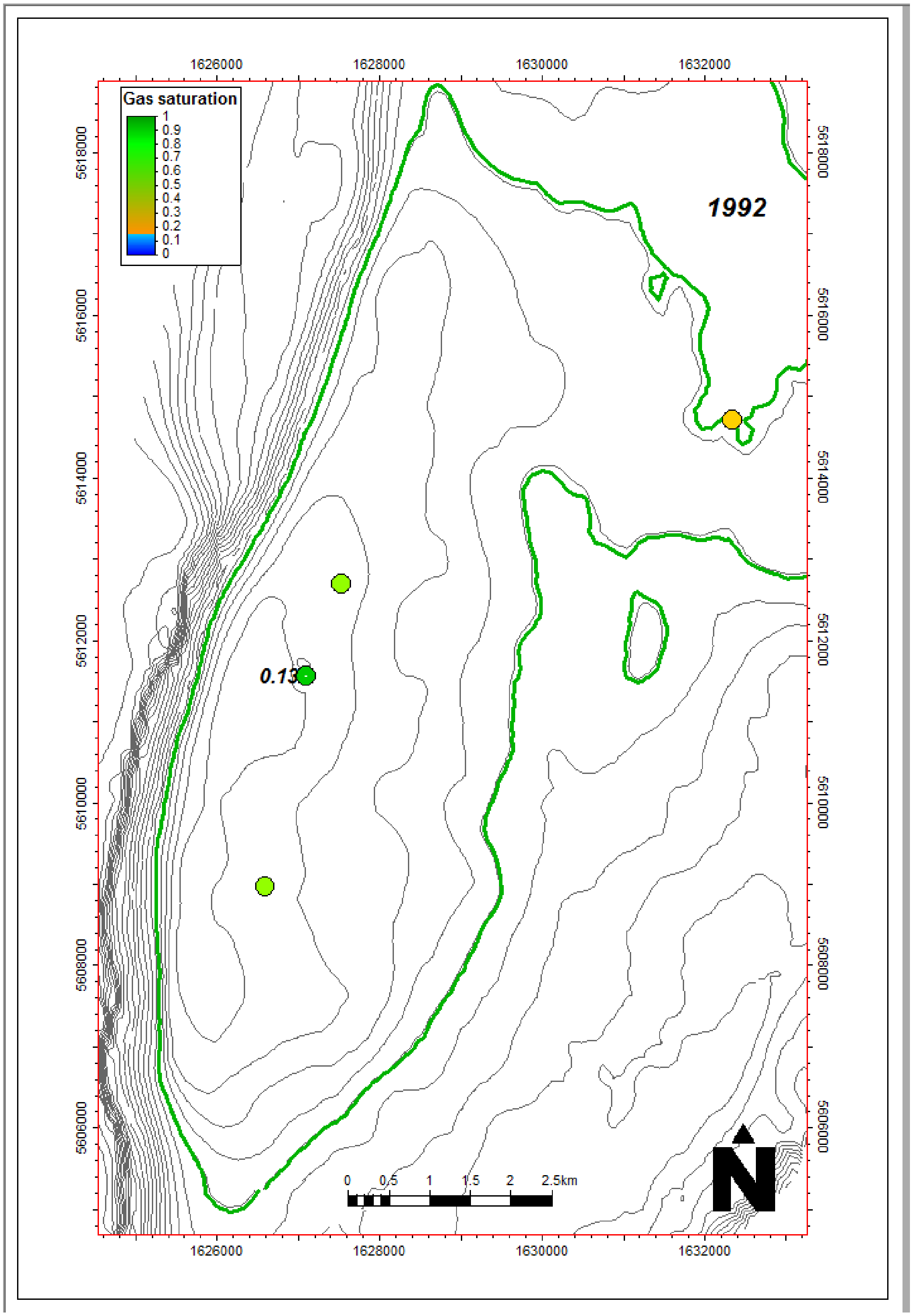

Appendix D. Figure 5. Well Information Map ***(1993)*** (New Zealand Petroleum and Minerals, 2018).

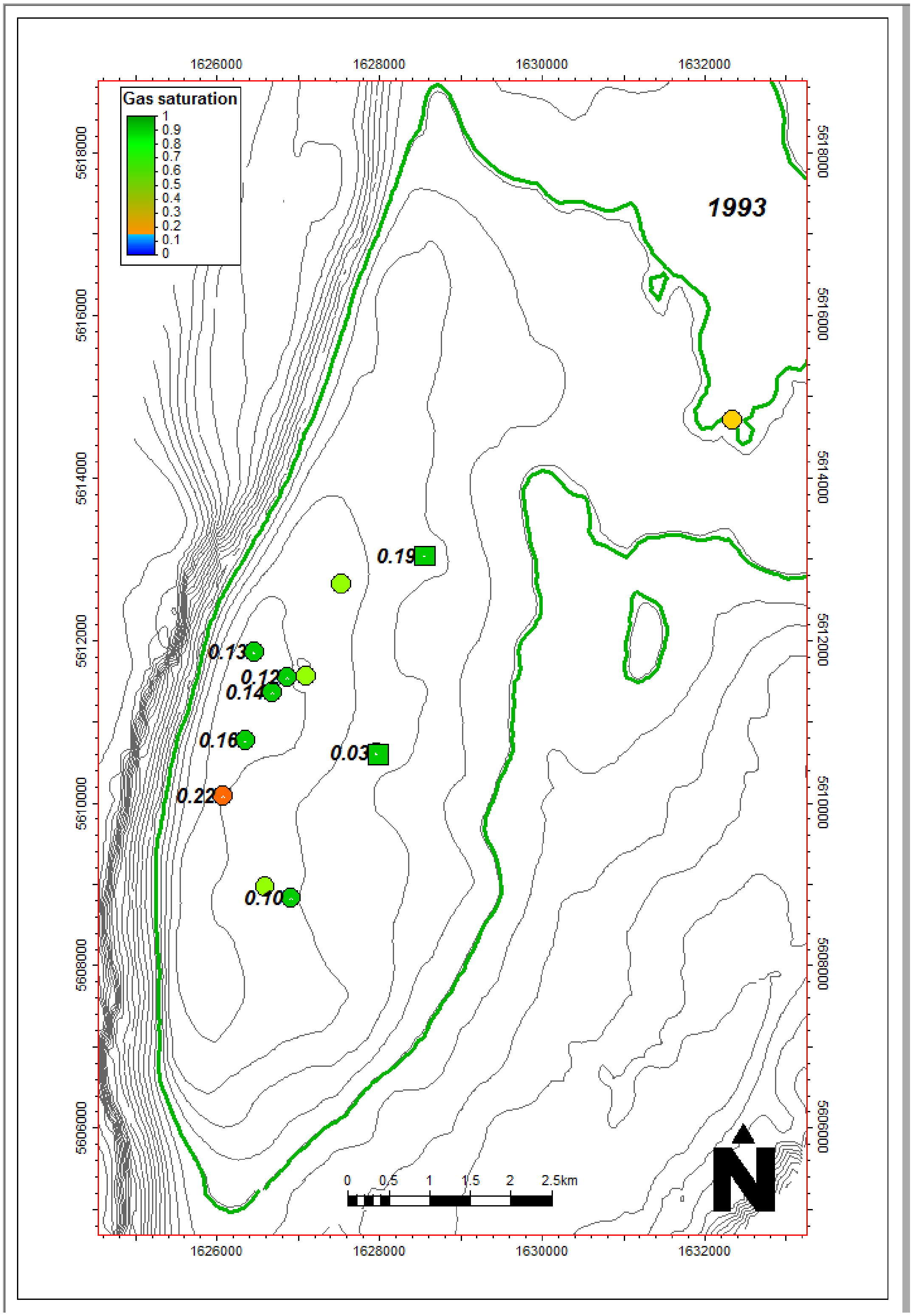

Appendix D. Figure 6. Well Information Map ***(1994)*** (New Zealand Petroleum and Minerals, 2018).

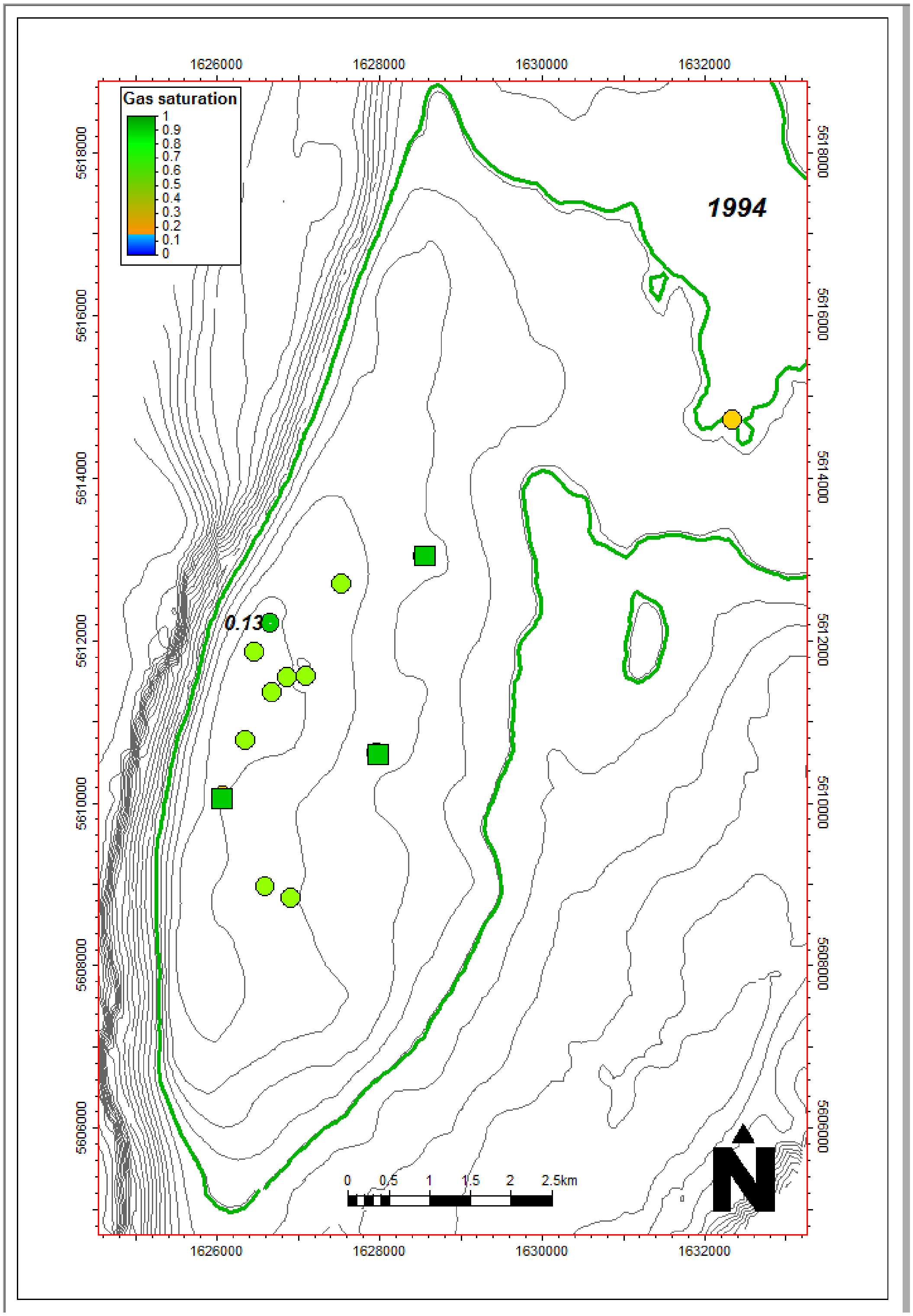

Appendix D. Figure 7. Well Information Map ***(1995)*** (New Zealand Petroleum and Minerals, 2018).

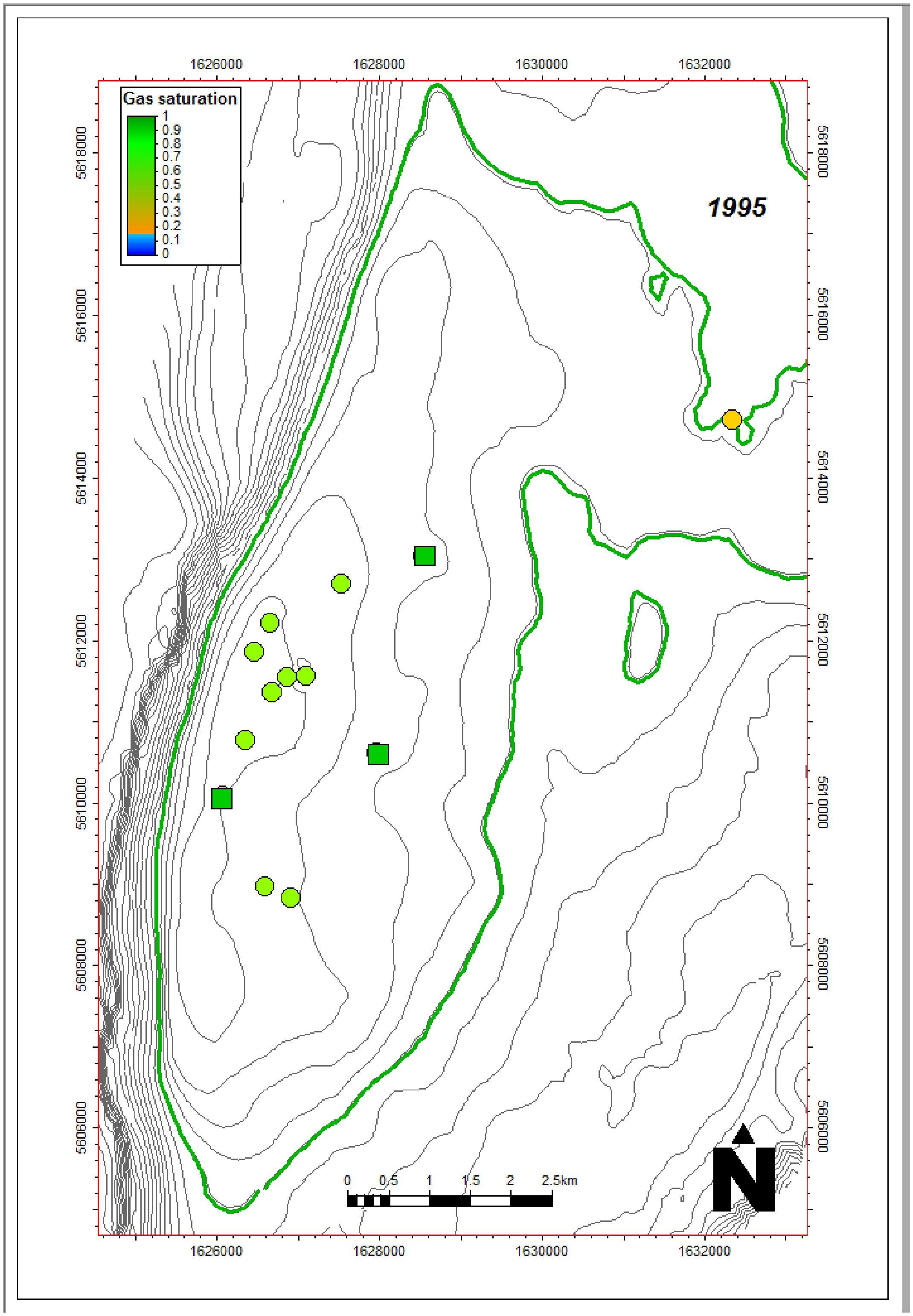

Appendix D. Figure 8. Well Information Map ***(1996)*** (New Zealand Petroleum and Minerals, 2018).

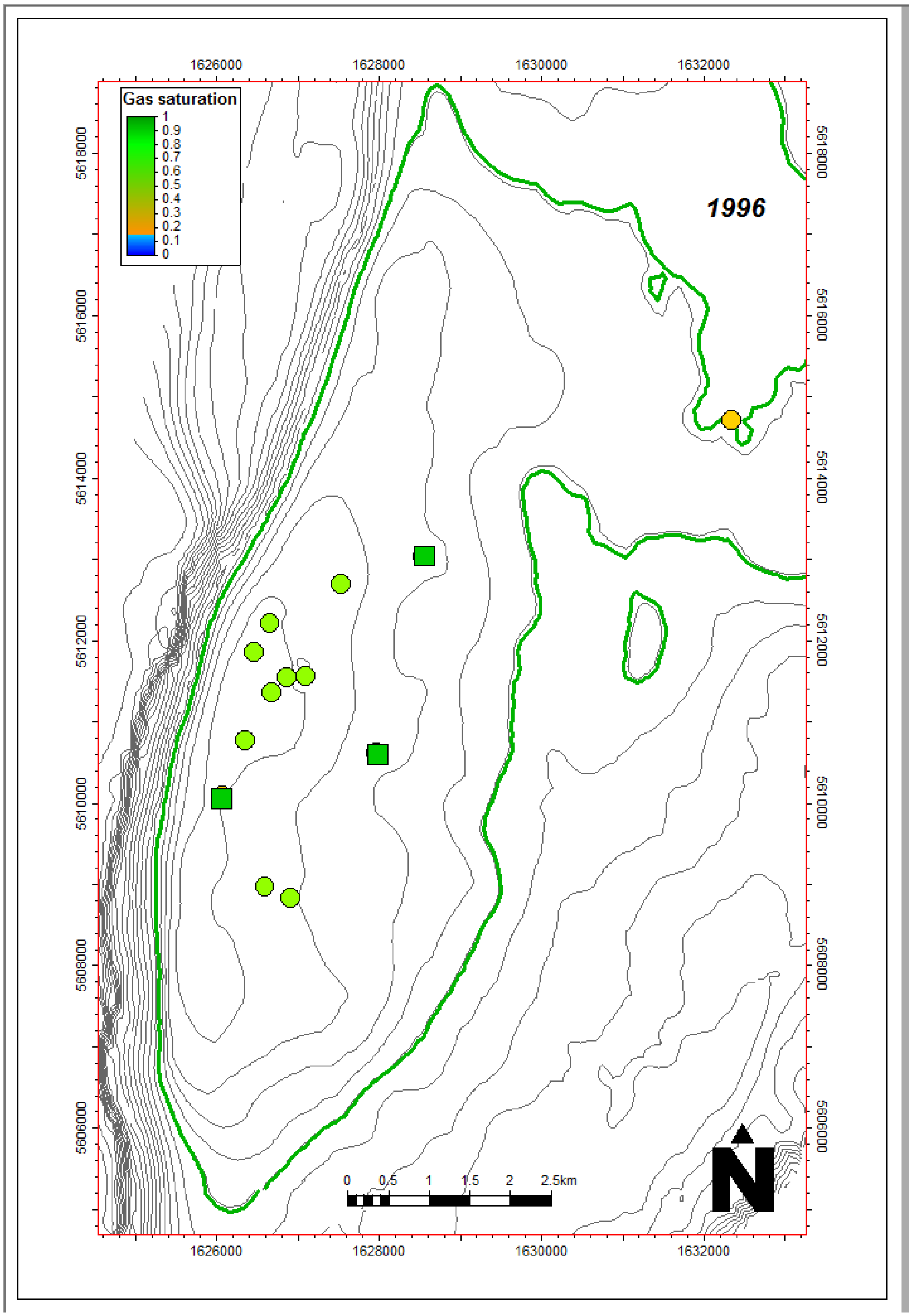

*Appendix D. Figure 9. Well Information Map **(1997)*** (New Zealand Petroleum and Minerals, 2018).

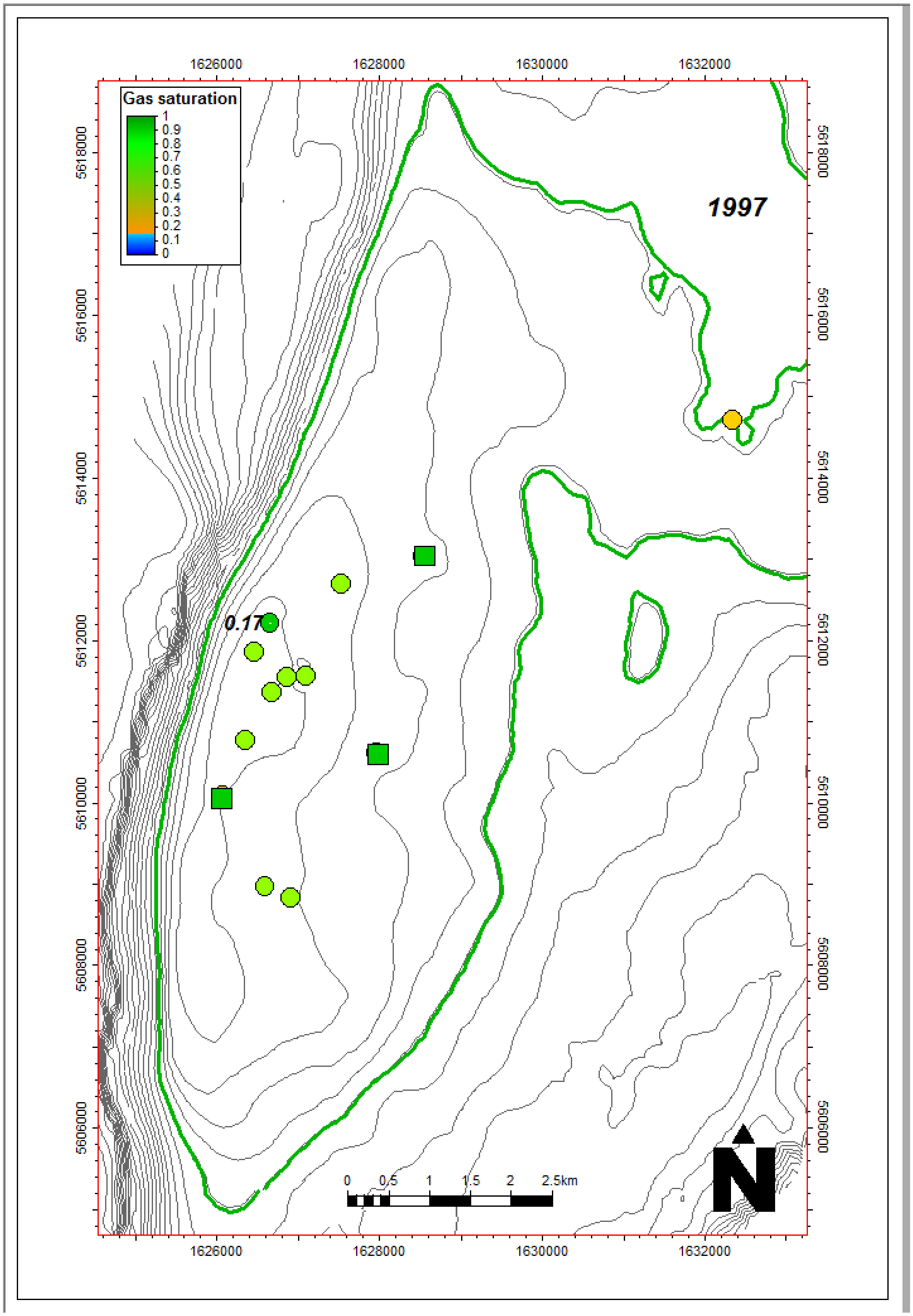

Appendix D. Figure 10. Well Information Map ***(1998)*** (New Zealand Petroleum and Minerals, 2018).

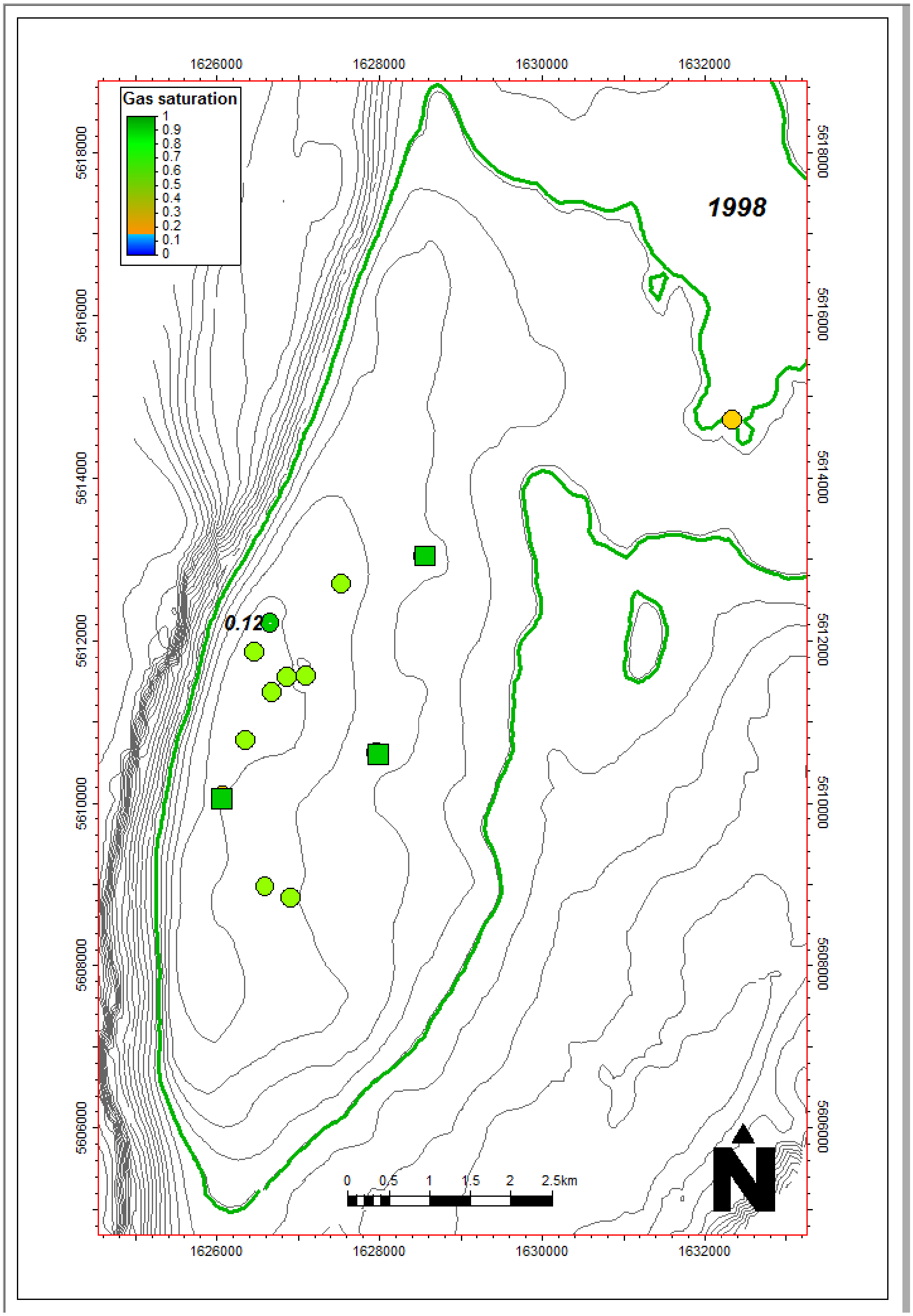

Appendix D. Figure 11. Well Information Map ***(1999)*** (New Zealand Petroleum and Minerals, 2018).

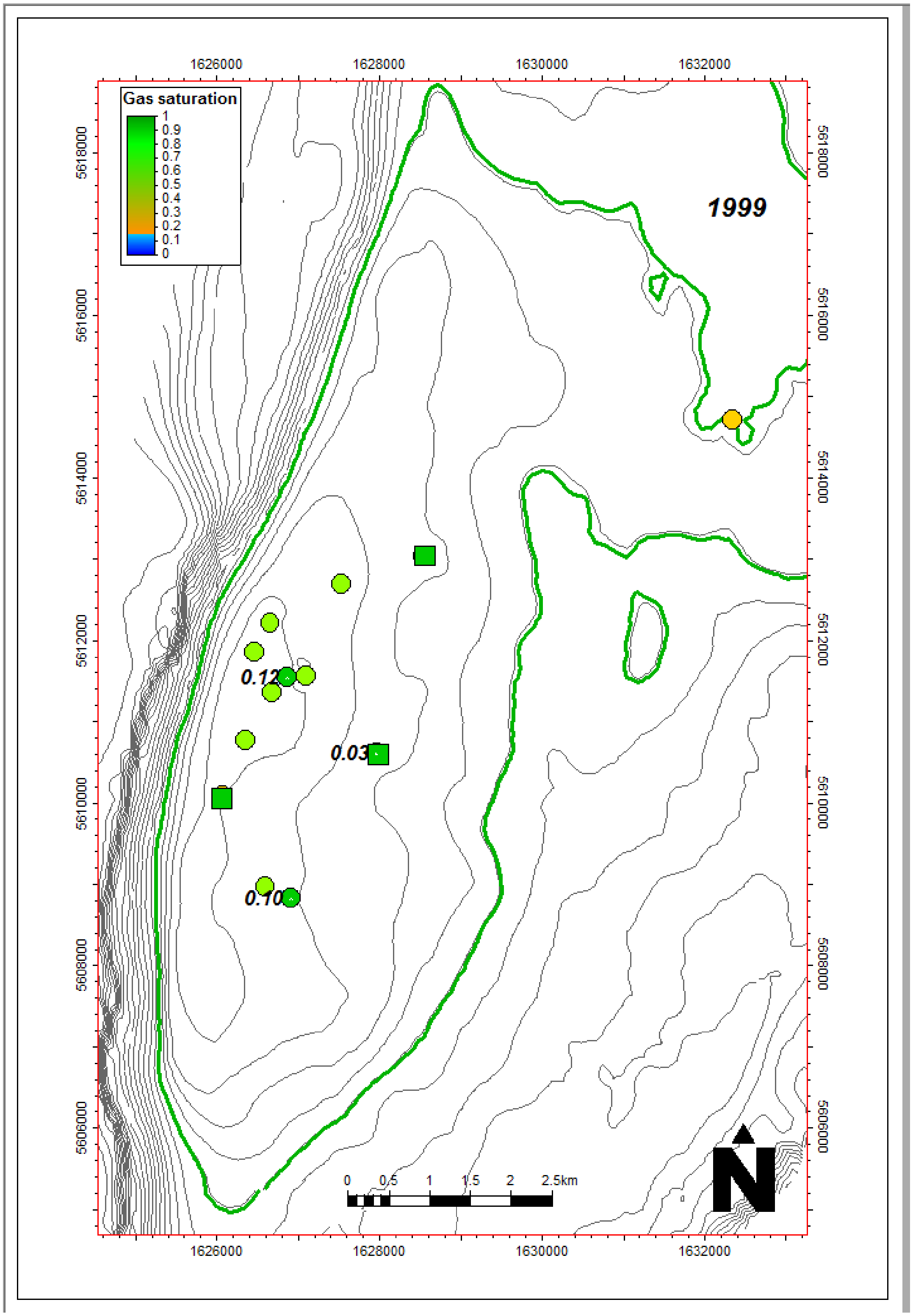

Appendix D. Figure 12. Well Information Map ***(2000)*** (New Zealand Petroleum and Minerals, 2018).

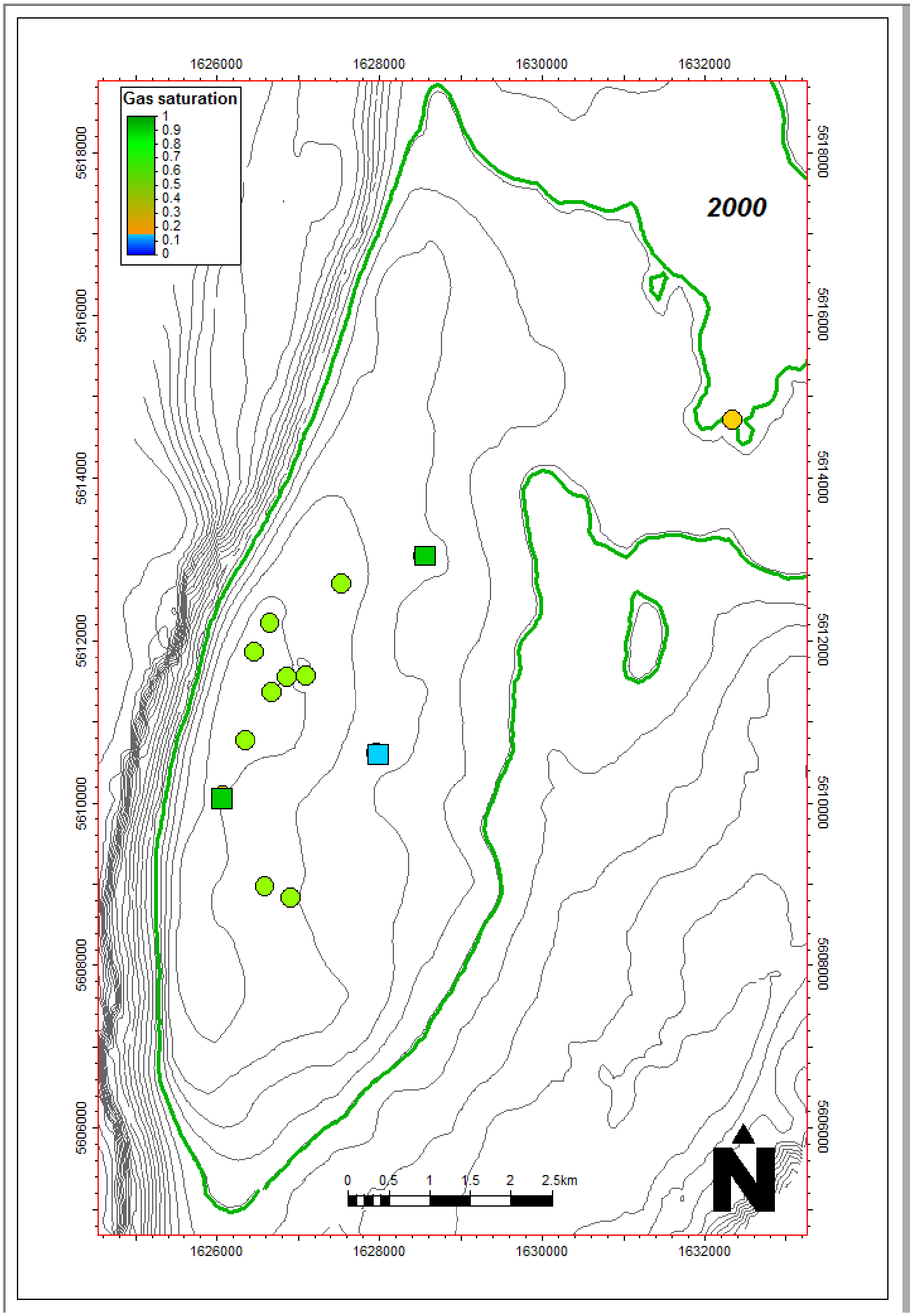

Appendix D. Figure 13. Well Information Map ***(2001)*** (New Zealand Petroleum and Minerals, 2018).

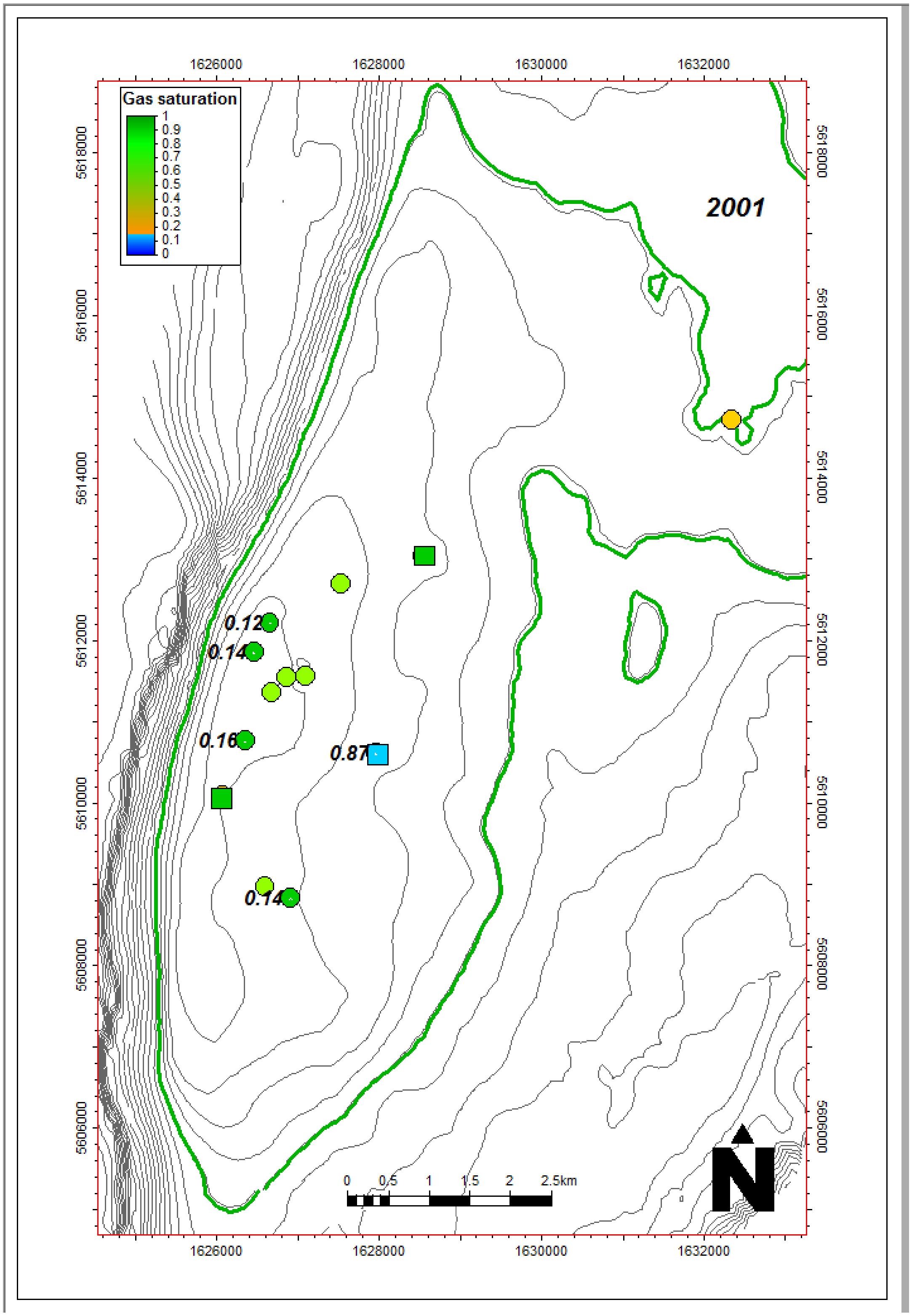

Appendix D. Figure 14. Fluid Saturation Model/Well Information Map ***(2002)*** (New Zealand Petroleum and Minerals, 2018).

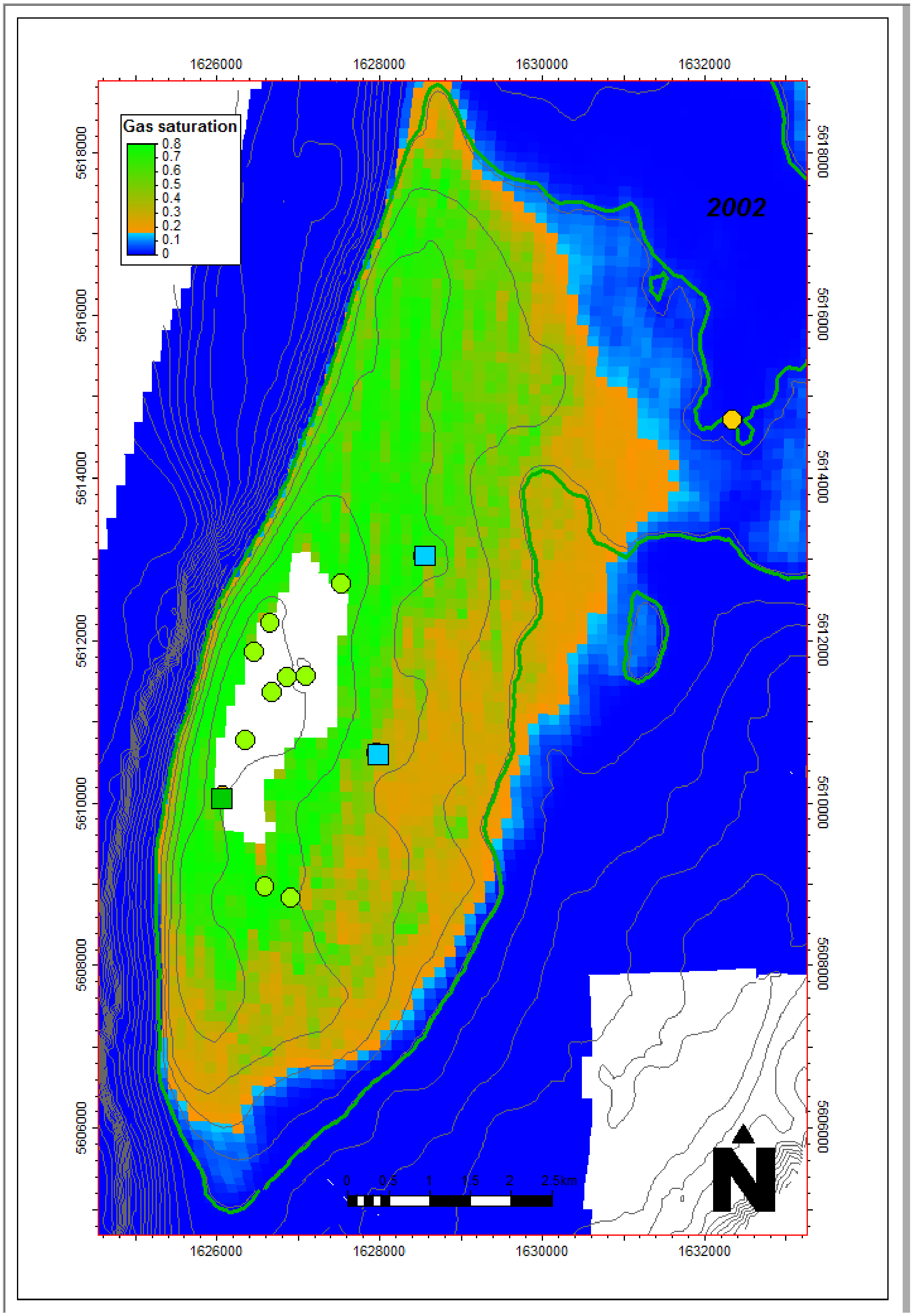

*Appendix D. Figure 15. Well Information Map **(2003)*** (New Zealand Petroleum and Minerals, 2018).

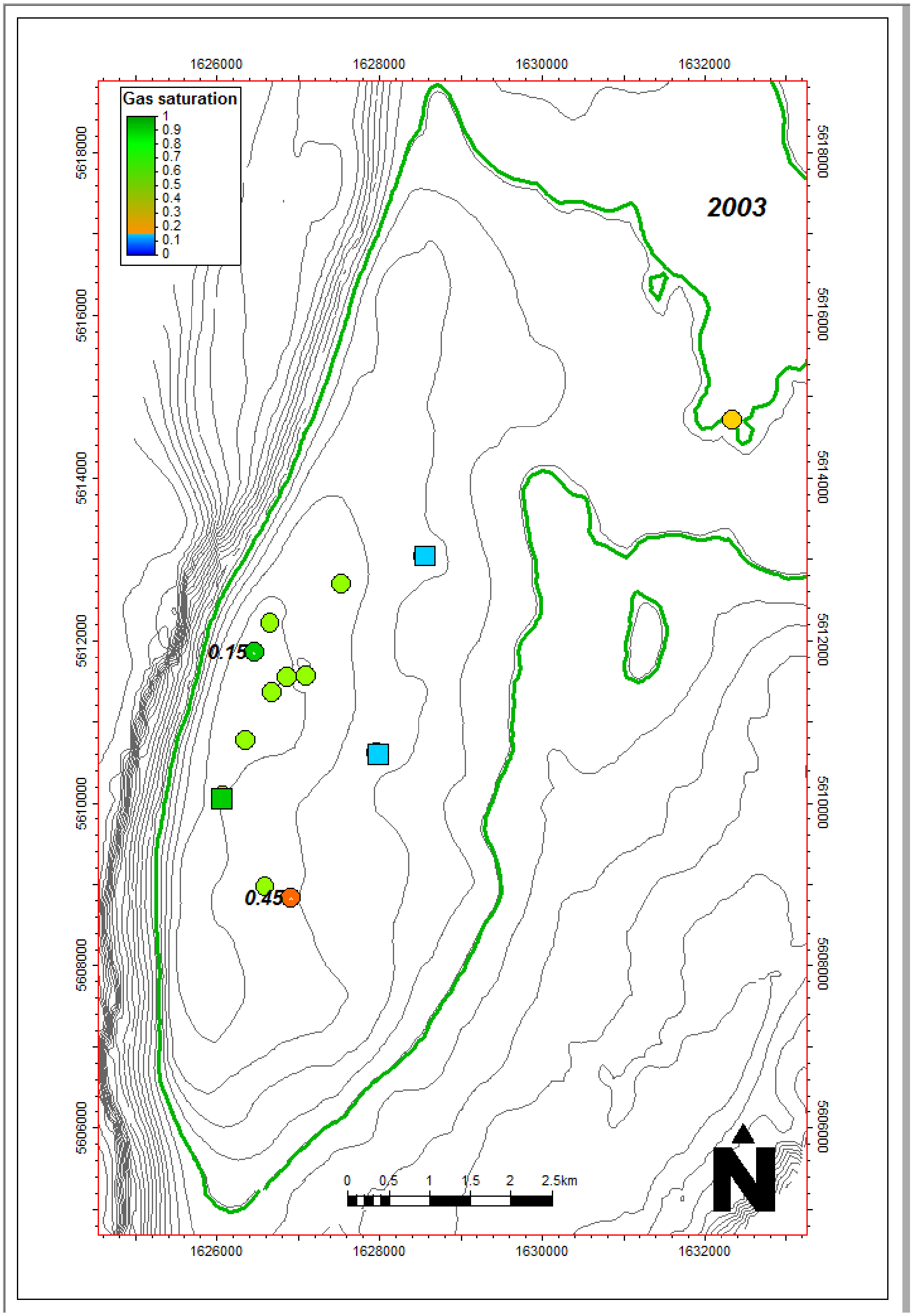

Appendix D. Figure 16. Well Information Map ***(2004)*** (New Zealand Petroleum and Minerals, 2018).

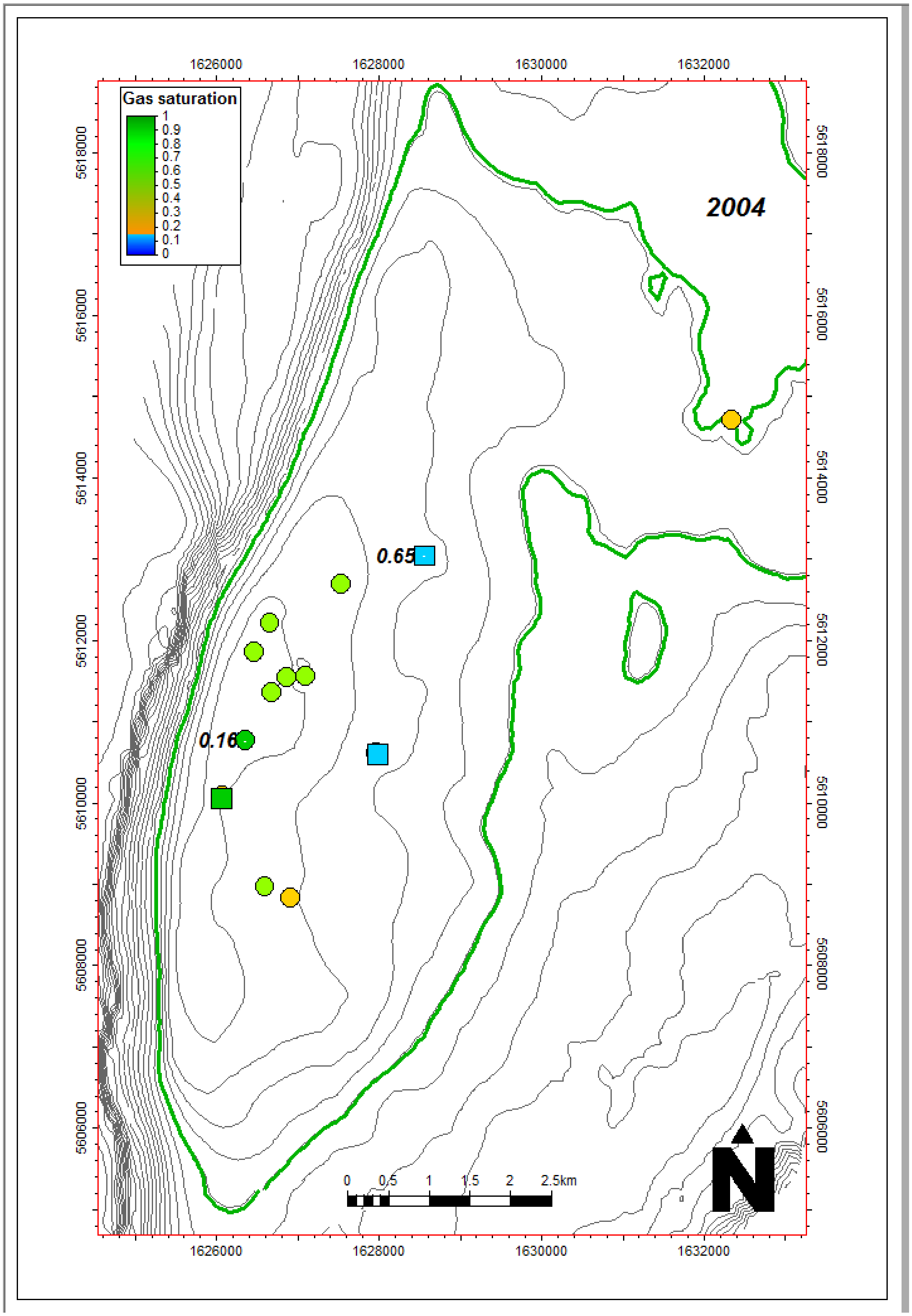

Appendix D. Figure 17. Well Information Map ***(2005)*** (New Zealand Petroleum and Minerals, 2018).

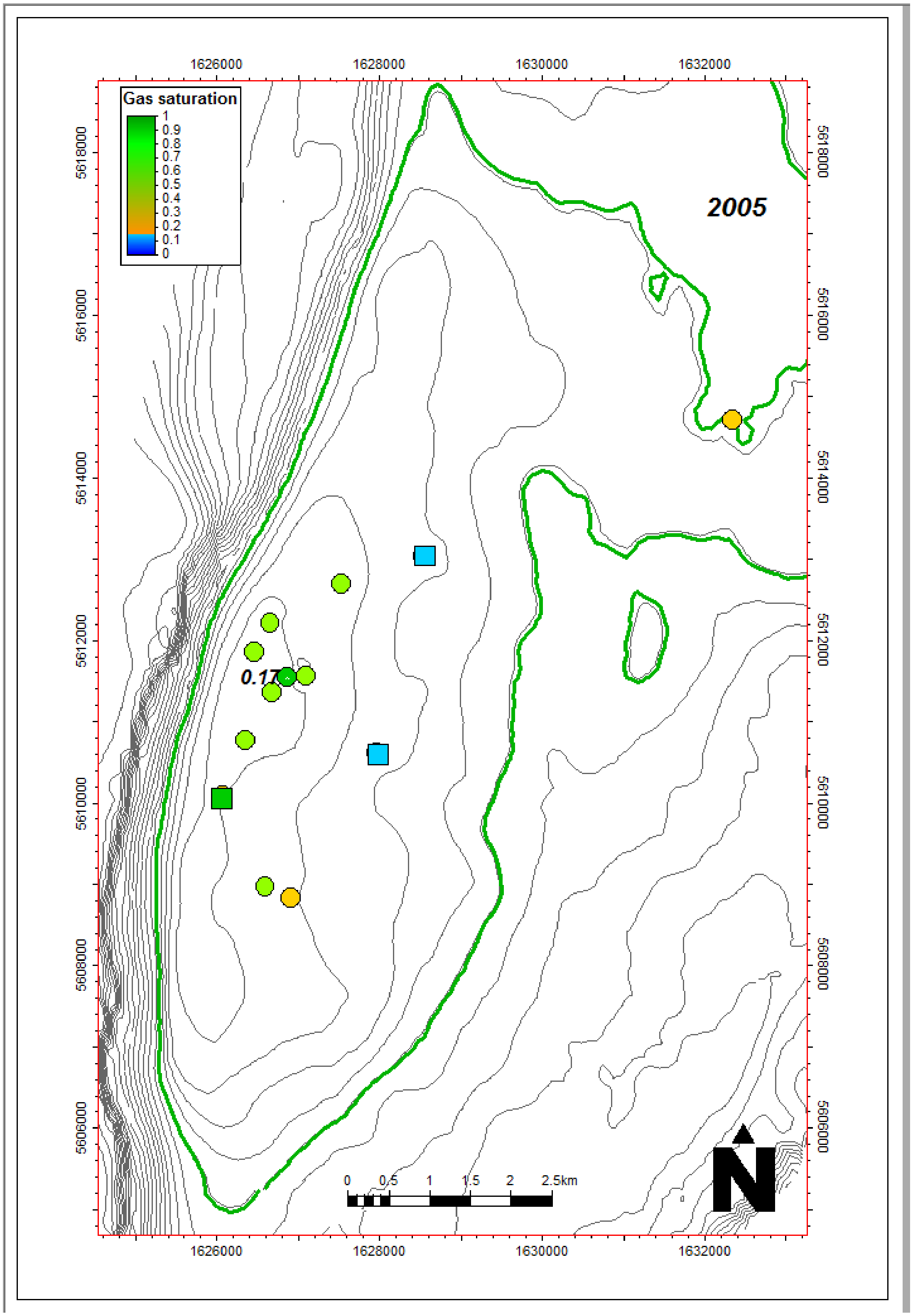

Appendix D. Figure 18. Well Information Map ***(2006)*** (New Zealand Petroleum and Minerals, 2018).

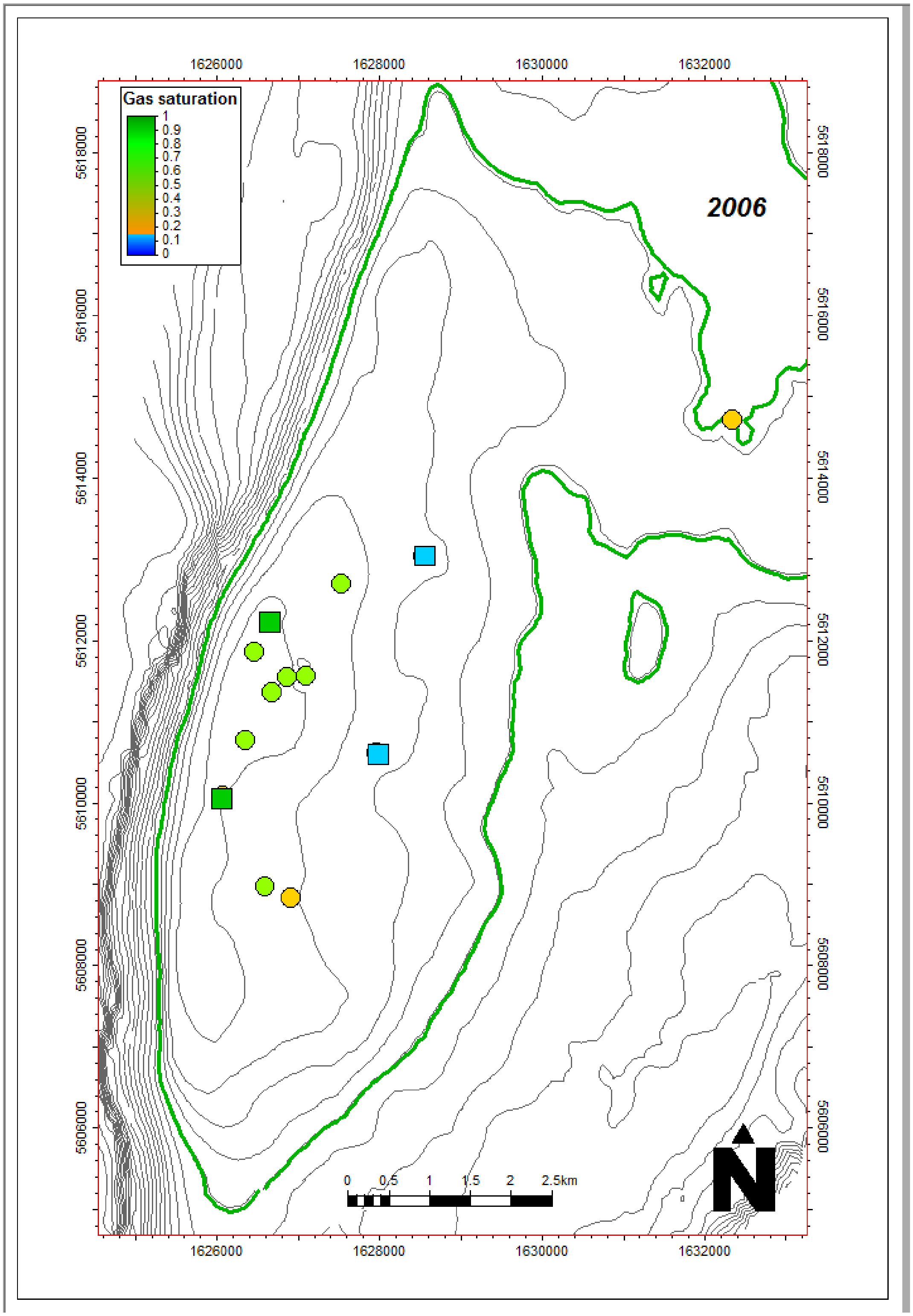

Appendix D. Figure 19. Well Information Map ***(2007)*** (New Zealand Petroleum and Minerals, 2018).

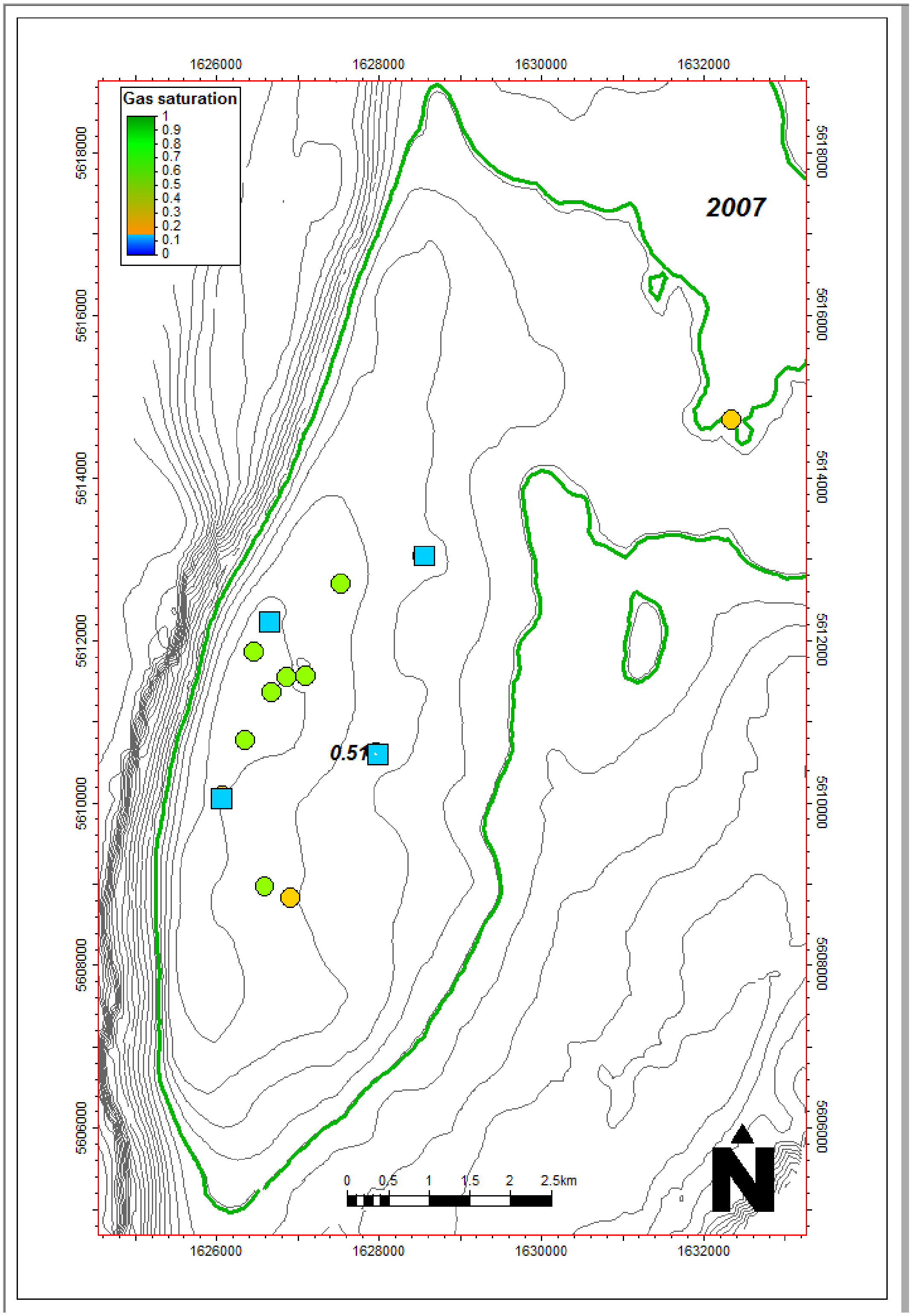

Appendix D. Figure 20. Well Information Map ***(2008)*** (New Zealand Petroleum and Minerals, 2018).

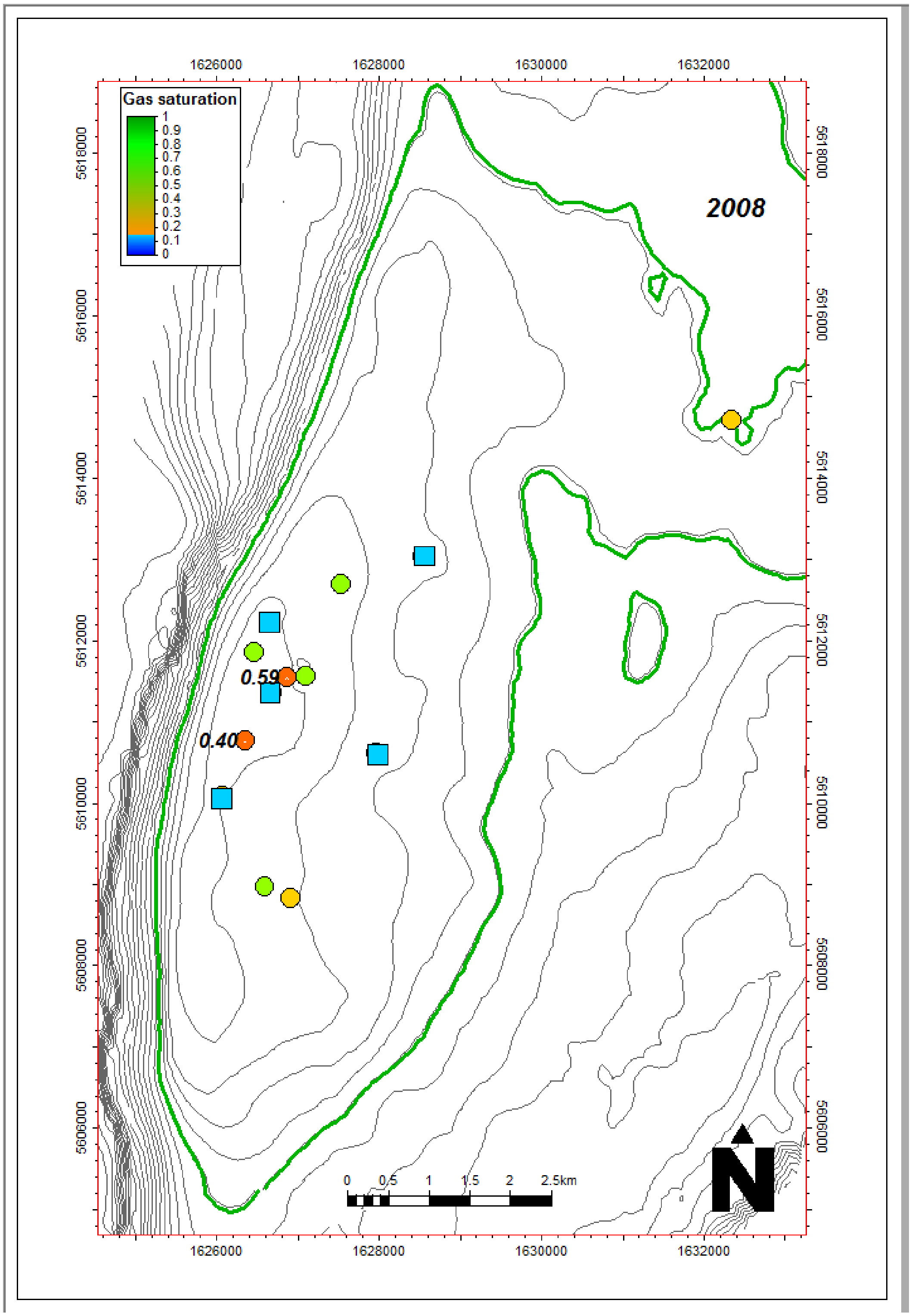

Appendix D. Figure 21. Well Information Map ***(2009)*** (New Zealand Petroleum and Minerals, 2018).

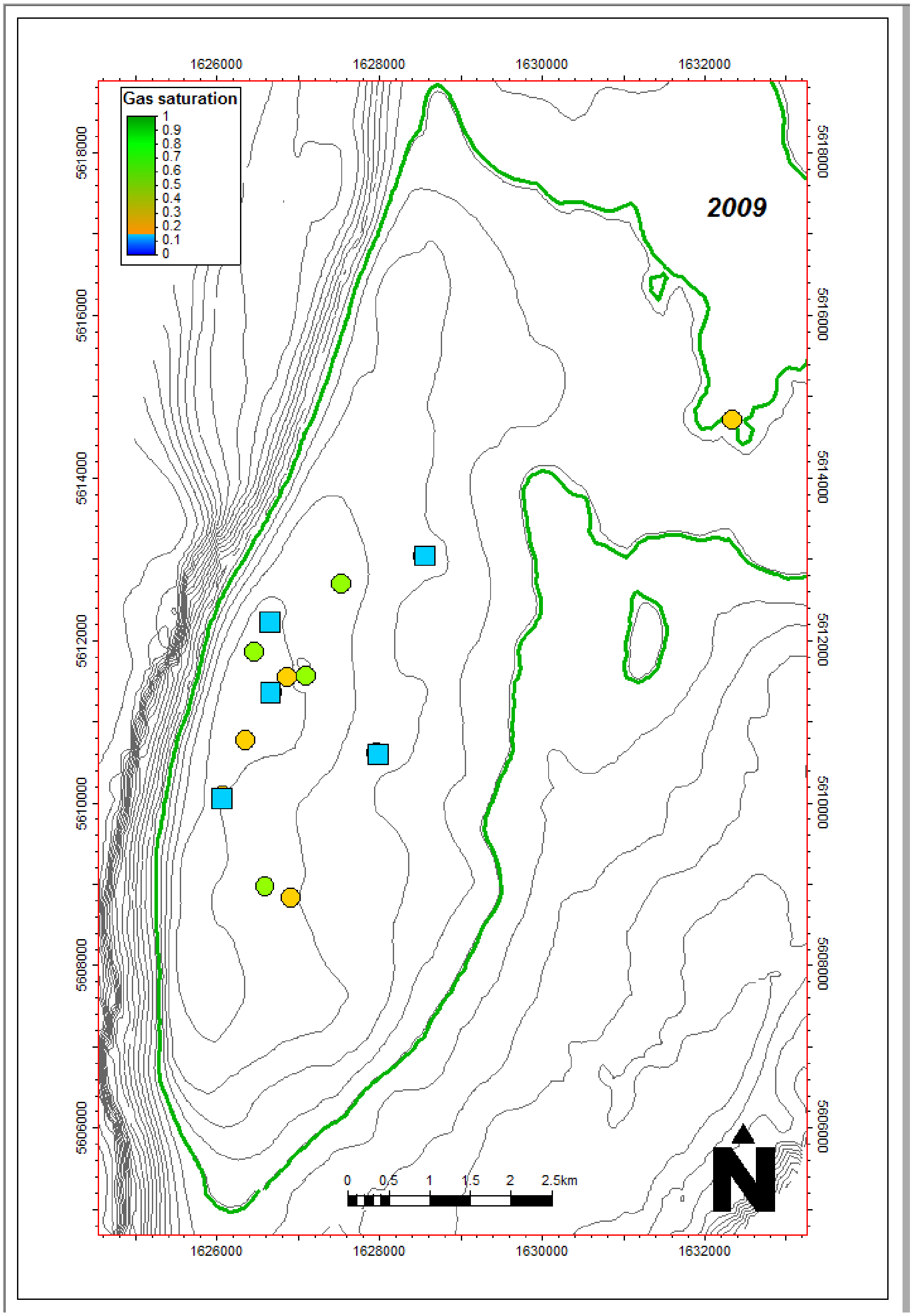

Appendix D. Figure 22. Well Information Map ***(2010)*** (New Zealand Petroleum and Minerals, 2018).

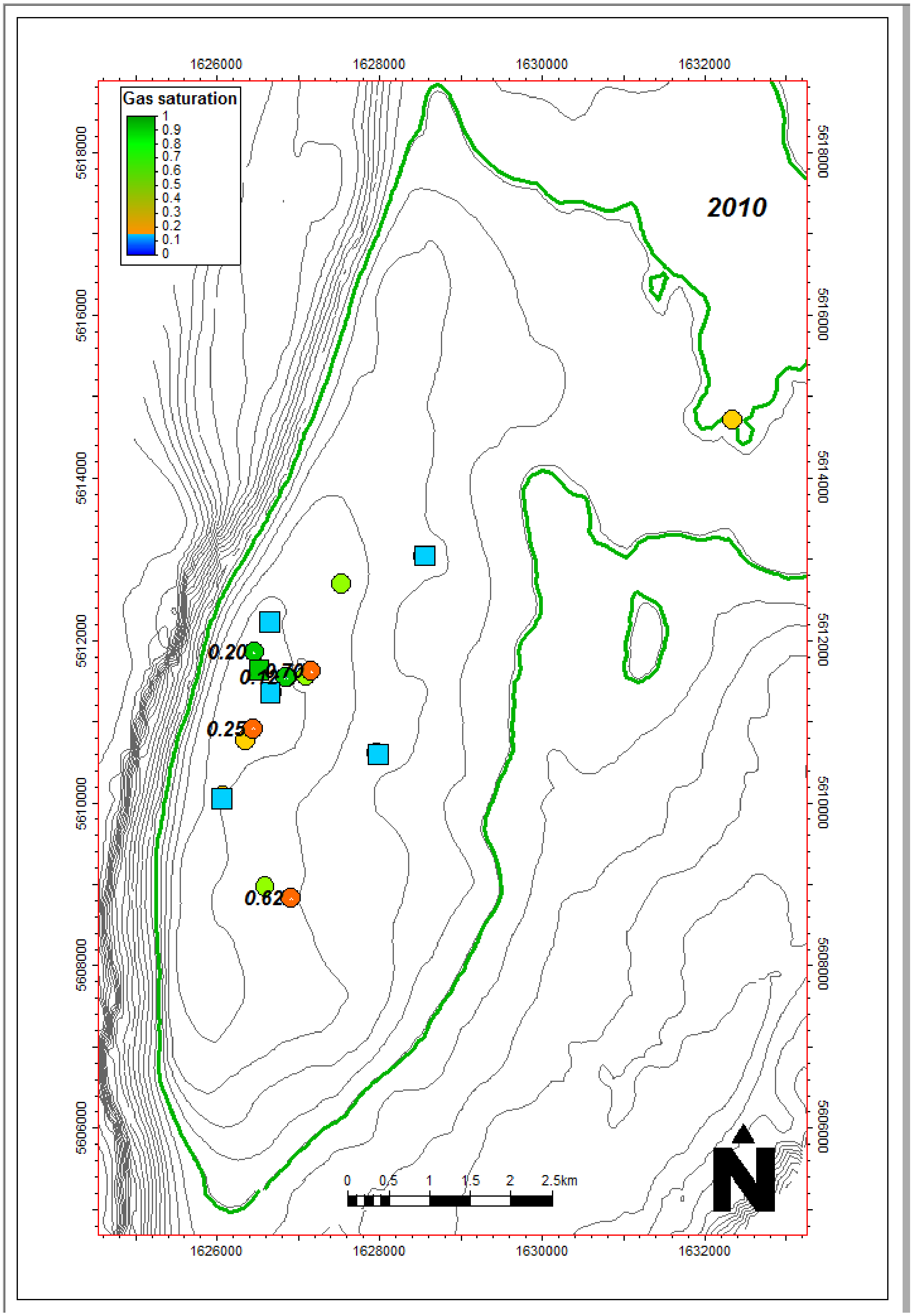

Appendix D. Figure 23. Well Information Map ***(2011)*** (New Zealand Petroleum and Minerals, 2018).

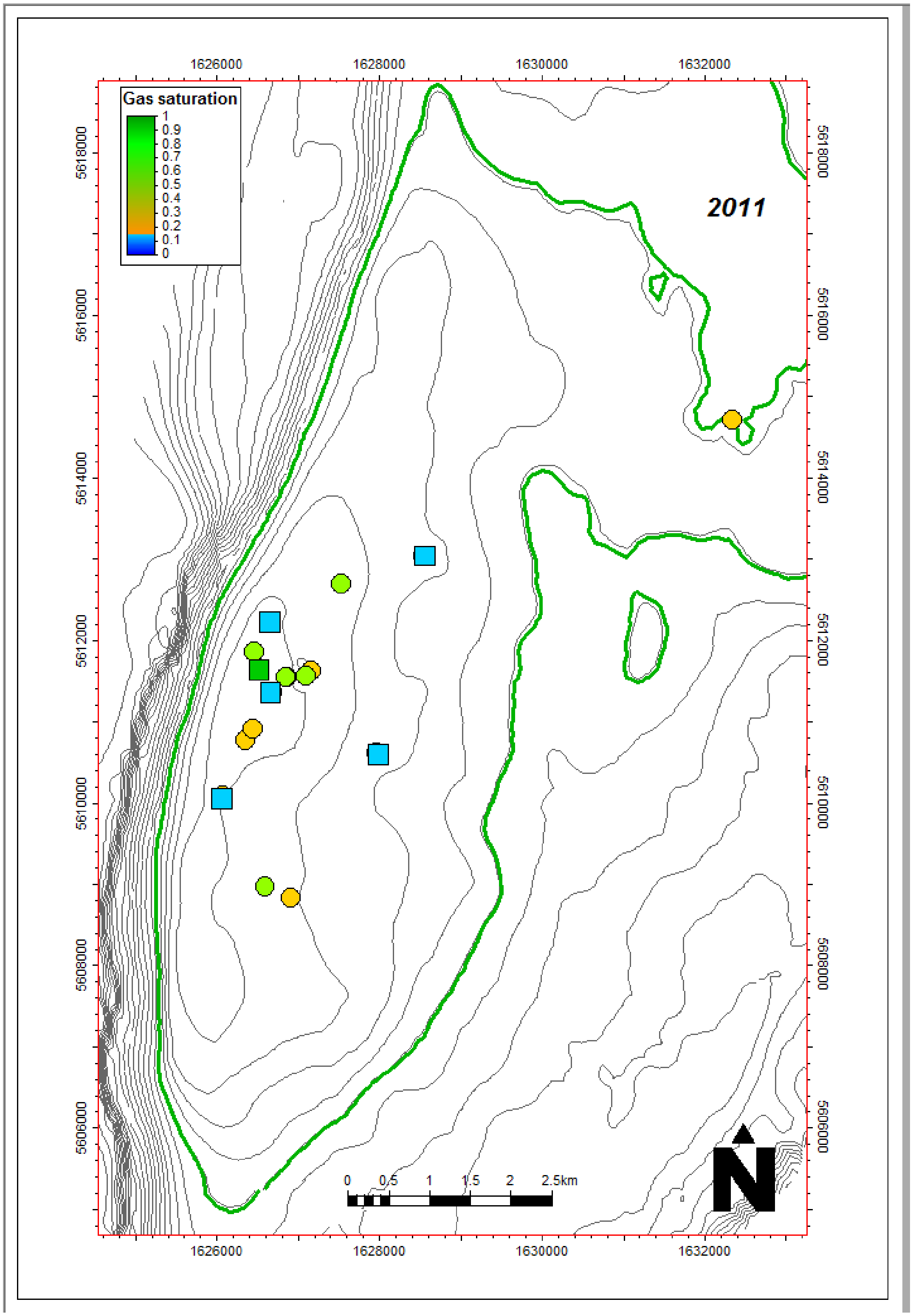

Appendix D. Figure 24. Well Information Map ***(2012)*** (New Zealand Petroleum and Minerals, 2018).

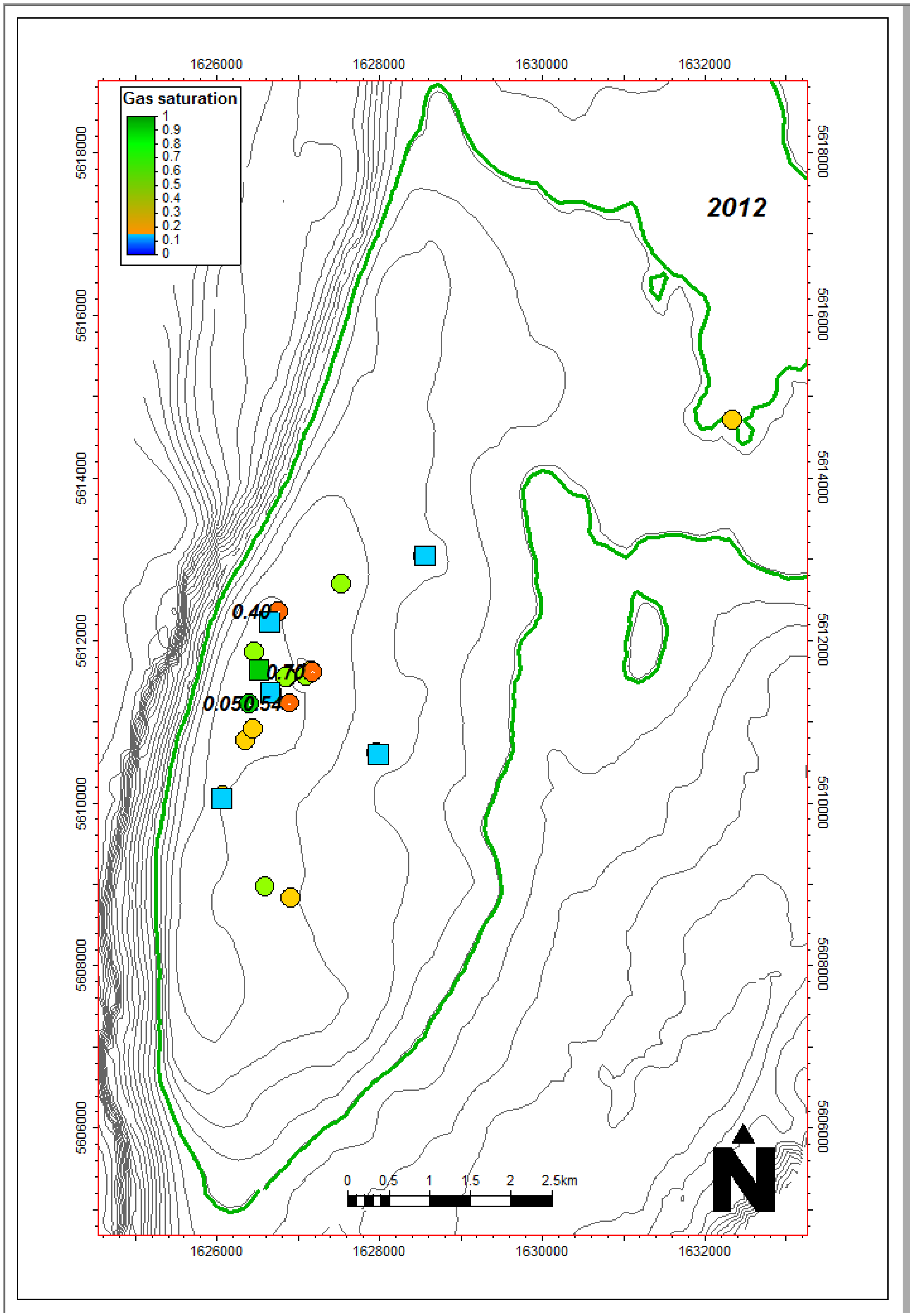

Appendix D. Figure 25. Well Information Map ***(2013)*** (New Zealand Petroleum and Minerals, 2018).

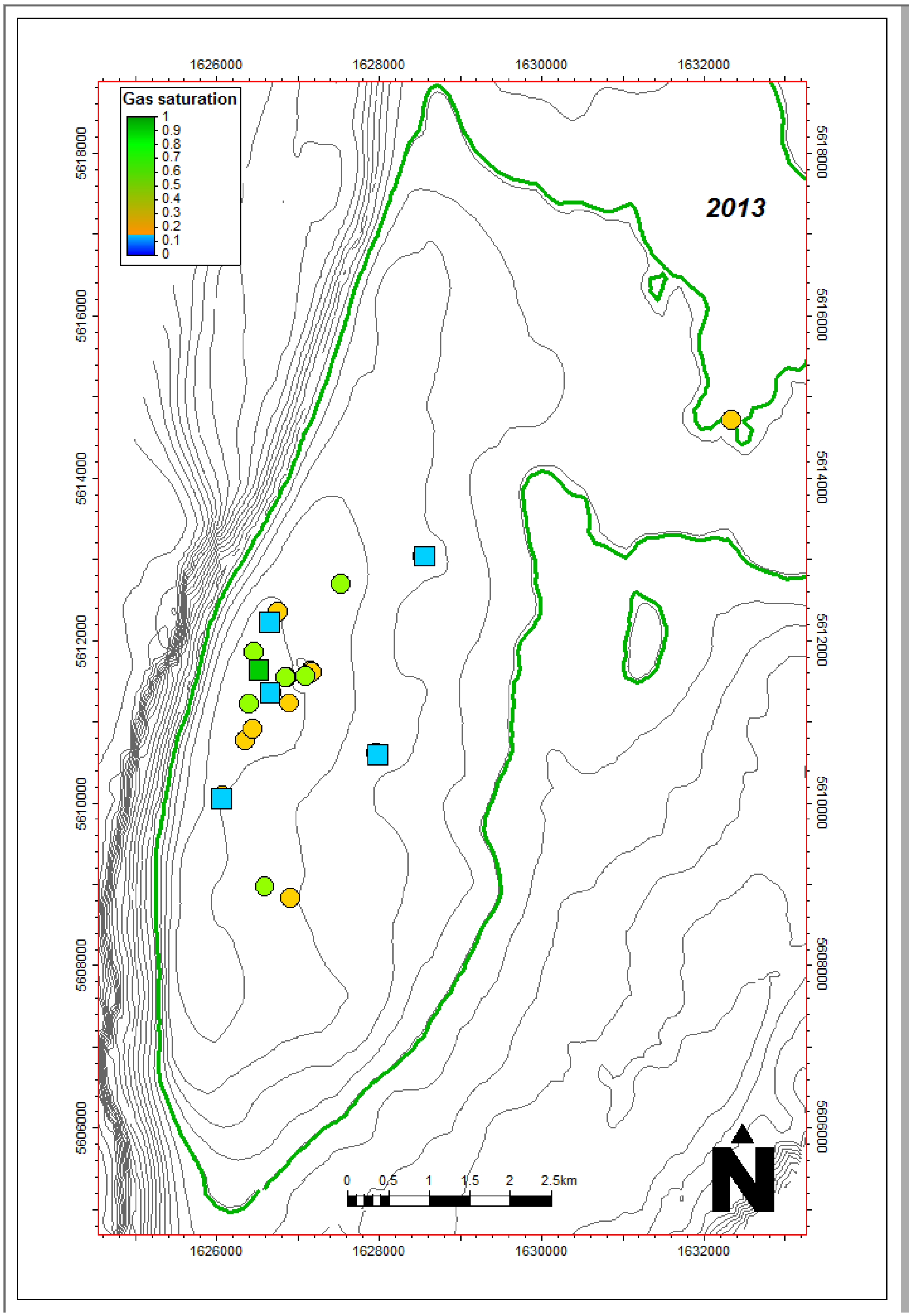

Appendix D. Figure 26. Well Information Map ***(2014)*** (New Zealand Petroleum and Minerals, 2018).